THESIS APPROVAL

GRADUATE SCHOOL, KASETSART UNIVERSITY

Master of Engineering (Chemical Engineering)
DEGREE

Chemical Engineering
FIELD

Chemical Engineering
DEPARTMENT

TITLE: Hydrogen Production via Catalytic Steam Reforming of Acetic Acid and Acetone as Representative Components of Bio-oil by Using Nickel over Calcium Aluminate-Ceria-Titania Catalyst

NAME: Mr. Phusit Saechia

THIS THESIS HAS BEEN ACCEPTED BY

THESIS ADVISOR
(Associate Professor Apinya Duangchan, Ph.D.)

THESIS CO-ADVISOR
(Associate Professor Paisan Kongkachuichay, Ph.D.)

DEPARTMENT HEAD
(Associate Professor Apinya Duangchan, Ph.D.)

APPROVED BY THE GRADUATE SCHOOL ON _____

DEAN
(Associate Professor Gunjana Theeragool, D.Agr.)

THESIS

HYDROGEN PRODUCTION VIA CATALYTIC STEAM REFORMING OF ACETIC ACID AND ACETONE AS REPRESENTATIVE COMPONENTS OF BIO-OIL BY USING NICKEL OVER CALCIUM ALUMINATE-CERIA-TITANIA CATALYST

PHUSIT SAECHIA

A Thesis Submitted in Partial Fulfillment of
the Requirements for the Degree of
Master of Engineering (Chemical Engineering)
Graduate School, Kasetsart University
2011

Phusit Saechia 2011: Hydrogen Production via Catalytic Steam Reforming of Acetic Acid and Acetone as Representative Components of Bio-oil by Using Nickel over Calcium Aluminate-Ceria-Titania Catalyst. Master of Engineering (Chemical Engineering), Major Field: Chemical Engineering, Department of Chemical Engineering. Thesis Advisor: Associate Professor Apinya Duangchan, Ph.D. 112 pages.

Production of hydrogen via catalytic steam reforming by using nickel based catalyst over mixed oxides of calcium aluminate ($12CaO.7Al_2O_3$, denoted as 12C7A), ceria (CeO_2) and titania (TiO_2) from acetic acid and acetone as representative components of bio-oil was investigated**.** The catalysts were prepared by using dry impregnation method and 12C7A, CeO_2, and TiO_2 were mechanically mixed with different molar ratios of 2:1:1 and 1:1:1 used as a support. Catalytic steam reforming reactions were carried out over a catalyst in a fixed bed tube reactor at temperatures between 750 and 900^oC. Effects of reaction temperature, steam to carbon ratio (S/C), and promoted metals over nickel based catalyst (Cu, Co, Cr, and Mg) on H_2 yield and selectivity of gaseous products were studied. The results showed that high temperature and S/C enhanced H_2 generation. The best conditions for producing the highest H_2 yield were operated at 850^oC, S/C of 8, and 1 h. The addition of ceria and titania over 12C7A affected an increase of H_2 yield, selectivity and coke resistance. The Ni-Cu catalyst indicated the highest activity for H_2 production and selectivity of 43.07% and 0.83, respectively, whereas the Ni-Co catalyst is inferior to the Ni-Cu catalyst for acetic acid reforming. Moreover, the bimetallic over 12C7A–CeO_2–TiO_2 catalysts enhanced coke resistance compared to the Ni based catalyst for the same support. The acetone reforming showed a high selectivity of CH_4. It can be attributed to a decrease of H_2 yield. An aqueous phase of bio-oil produced from pyrolysis of coffee bean residue was tested by using 15%Ni-5%Cu /12C7A-CeO_2-TiO_2 and it provided 21.18% of H_2 yield.

_____ _____ ___ / ___ / ___

Student's signature Thesis Advisor's signature

ACKNOWLEDGEMENTS

I am grateful to Associate Professor Apinya Duangchan, my thesis advisor for giving valuable knowledge and suggestions. I would like to give a sincere thank to my co-thesis advisor, Associate Professor Paisan Kongkachuichay, Assistant Professor Attasak Jaree and Dr. Pipat Pichestapong for giving comments and advising my thesis. I would like to sincerely thank to Dr. Thongthai Witoon for giving some ideals about my research. I also thank staff of the Department of Chemical Engineering, Kasetsart University for their support on my work. I would like to thank Ms. Worada Moonsrikaew, Ms. Suchawadee Ratthanaburee, Ms. Sreepair Whungklomklang, Mr. Piriya Pinthong and Mr. Niti Ninchawee for teaching me how to operate and set up the experiment. I am especially appreciated my parents, my sisters, and friends for their continuing encouragements.

I would like to thank National Center of Excellence for Petroleum, Petrochemicals and Advanced Materials (PPAM/PERDO) for financial support.

Phusit Saechia

September 2011

TABLE OF CONTENTS

Page

LIST OF TABLES

LIST OF TABLES (Continued)

LIST OF TABLES (Continued)

LIST OF FIGURES

LIST OF FIGURES (Continued)

LIST OF FIGURES (Continued)

Appendix Figure

LIST OF FIGURES (Continued)

LIST OF FIGURES (Continued)

Appendix Figure **Page**

LIST OF FIGURES (Continued)

Appendix Figure **Page**

LIST OF FIGURES (Continued)

HYDROGEN PRODUCTION VIA CATALYTIC STEAM REFORMING OF ACETIC ACID AND ACETONE AS REPRESENTATIVE COMPONENTS OF BIO-OIL BY USING NICKEL OVER CALCIUM ALUMINATE-CERIA-TITANIA CATALYST

INTRODUCTION

Hydrogen is a clean and sustainable energy which is an important material in many chemical industries. It can be used as fuel for transportation and electricity generation from fuel cell (Larson, 1994; Cox, 1995). Nowadays, various processes for hydrogen production produced from fossil fuel are studied including catalytic steam reforming from natural gas, partial oxidation of heavy oil, and coal gasification etc. However, hydrogen production from petroleum oil provides a large amount of CO_2 releasing to the atmosphere that causes green house effect.

An alternative feedstock for hydrogen production is biomass because it can be renewed. Generally, bio-oil can be produced from pyrolysis of biomass. In Thailand, the quantity of biomass from agricultural waste depends on the quantity of agricultural products that can be produced in the country.

Bio-oil which is derived from pyrolysis of biomass is a mixture of oxygenated organic compounds including acids, alcohols, aldehydes, ketones, substituted phenolics, and derivatives, as well as carbohydrates, and a large proportion of lignin-derived oligomers (Oasmaa and Meier, 2002).

Steam reforming is a high performance process for hydrogen production. This process has been studied in the last decade and used for commercial industry because it is simple and low cost for operation. Catalytic steam reforming can be used to convert the entire bio-oil or each fraction of it to hydrogen rich stream. Famous metals that are used as catalysts for the steam reforming process are Ni, Fe, Co, and

noble metals (Pt, Ru, Ir, and Rh) which are specific and provide a high performance for hydrogen production.

A severe problem of steam reforming process is the formation of carbonaceous substances on the catalyst surface. The main factor that affects coke formation is a steam to carbon in the feed ratio (S/C). The high S/C enhanced hydrogen generation, carbon conversion of feedstock, and improved carbon gasification on the catalyst surface (Wang and Pan, 2007). Noble metals (such as Pt, Ru, Rh) are generally more effective than Ni-based catalysts and cause less coke deposition but they are not used in real applications because of their high cost. Thus, it is very significant to realize non-noble catalysts and decrease carbon deposits during the bio-oil's reforming process.

From various studies, steam reforming reaction of methane, partial oxidation, and dry reforming indicates activities of Ni metal on various types of calcium aluminate catalysts (Yang, 2004). These catalysts have high thermal stability, low carbon deposition on the surface of catalyst, and high hydrogen yield. The molar ratio of CaO to Al_2O_3 of the support and preparation methods could affect activities and formation rate of coke in dry reforming and partial oxidation reactions of methane (Lemonidou, 1998; Goula, 1996).

The steam reforming of model compounds derived from bio-oil (acetic acid, phenol, acetone, and ethanol) using noble metals (Pt, Pd, and Rh) over alumina and ceria-zirconia was studied by Rioche *et al*. (2005). The ceria-zirconia materials showed a higher activity than alumina.

$Ni/Ce_{0.5}Ti_{0.5}O_2$ catalyst is very active, selective and comparatively stable for steam reforming of ethanol reported by Ye *et al*. (2008). Compared with Ni/TiO_2 catalyst, $Ni/Ce_xTi_{1-x}O_2$ catalysts ($x \neq 1$) are more coke-resistant. The formation of Ce–O–Ti improves the oxygen mobility in $Ni/Ce_xTi_{1-x}O_2$ catalysts which is beneficial for eliminating carbon on the catalyst surface; while the TiO_2 component tends to catalyze the carbon deposition formation.

The effects of promoted metals over nickel based catalysts on catalytic steam reforming of bio-oil were investigated by Gacia *et al.* (2000). They found that Ni-Co/MgO-La_2O_3-Al_2O_3 and Ni-Cr/MgO-La_2O_3-Al_2O_3 catalysts showed the best results in the laboratory tests. The catalysts were prepared by impregnation of Al_2O_3 support with Ni and additives. Magnesium (Mg) and lanthanum (La) used as support modifiers enhanced steam adsorption while cobalt (Co) and chromium (Cr) additives reduced coke formation reactions. Moreover, copper-ceria catalysts have been used in a variety of other catalytic reactions. Catalytic steam reforming of ethanol by using Cu-Ni supported catalysts showed high selectivity of hydrogen (Vizcaíno *et al.*, 2007). Two commercial amorphous solids (SiO_2 and γ-Al_2O_3) and three synthesized materials (MCM-41, SBA-15 and ZSM-5 nanocrystalline) were used as supports. The highest hydrogen selectivity was achieved with the Cu–Ni/SBA-15 catalyst, due to a smaller metallic crystallite size.

The objectives for this research are production of hydrogen via catalytic steam reforming by using nickel based catalyst over mixed oxides of calcium aluminate ($12CaO.7Al_2O_3$, denoted as 12C7A), ceria (CeO_2) and titania (TiO_2) from acetic acid and acetone as representative components of bio-oil. Ni based catalysts are more favorable due to their low cost. The mixed oxides of calcium aluminate, ceria and titania are used as a supporting material to reduce coke accumulation on the surface of a catalyst. Moreover, metals (Mg, Co, Cu and Cr) are promoted on Ni/12C7A-CeO_2-TiO_2 catalysts to investigate the effect on performance of steam reforming process.

OBJECTIVES

1. To investigate the performance of nickel over calcium aluminate-ceria-titania catalyst on hydrogen production of representative components of bio-oil via catalytic steam reforming in term of hydrogen yield and selectivity of gaseous products.

2. To study the influence of magnesium (Mg), chromium (Cr), copper (Cu) and cobalt (Co) promoted nickel over calcium aluminate-ceria-titania catalyst on hydrogen yield and selectivity of gaseous products.

Working Scopes

1. Bio-oil's representative components in this study are limited to acetic acid and acetone.

2. The best catalyst providing the highest hydrogen yield from model compound reforming tests is selected to investigate the hydrogen production activity by using a bio-oil's aqueous phase via pyrolysis of coffee bean residue as a reactant.

3. Nickel on calcium aluminate-ceria-titania catalysts performances are tested in a fixed bed tube reactor via steam reforming processes of acetic acid and acetone at temperatures ranging from 750-900^{o}C and atmospheric pressure.

4. Calcium aluminate (12C7A) is prepared by 2 methods. The first one is solid-state reaction at 1,150 and 1,300^{o}C. The other is chemical solution deposition method (CSD method). Ceria (CeO_2) is prepared by using spray pyrolysis technique. 12C7A, CeO_2, and TiO_2 (commercial grade) are mechanically mixed with different mole ratios of 2:1:1 and 1:1:1.

5. Ni/12C7A-CeO_2-TiO_2 catalysts are prepared by an incipient wetness impregnation method with nickel loading of 15wt%.

6. Metals (Mg, Cr, Cu and Co) promoted Ni/12C7A-CeO_2-TiO_2 catalysts are prepared by a co-incipient wetness impregnation method with 5wt% of promoted metals. All the catalysts are tested and compared with 15wt% Ni/Al_2O_3 in term of hydrogen yield and selectivity of gaseous products.

Benefits

This research produces hydrogen which can be used as an alternative energy. The nickel over calcium aluminate-ceria-titania catalysts that were prepared in our laboratory hopefully can improve hydrogen production for steam reforming process. Ceria and titania, which are known as coke prevention catalysts, have not been reported applied to the Ni/12C7A. Expectedly, ceria and titania prolong catalyst life and Mg, Cr, Cu and Co improve activity of the Ni/12C7A-CeO_2-TiO_2 catalyst.

LITERATURE REVIEW

1. Biomass

Biomass refers to living and recently dead biological material. It can be used as a source of energy like petroleum oil or coal but its advantage is renewable energy. Biomass can be directly used as a fuel for heat and electricity generation and a raw material for liquid fuel producing. Biomass is an organic material from both plant and animal such as hazel nut, lemon peel, cattle manure, molass and soybean cake. It contains long chain hydrocarbon which consists of carbon, hydrogen, oxygen, nitrogen and sulfur.

2. Biomass conversion processes

Biomass can be converted to useful products by two main processes:

(a) Thermo-chemical process and

(b) Bio-chemical process

In this work, only thermo-chemical process is focused.

2.1 Thermo-chemical process

The thermo-chemical conversion process has two basic approaches. The first one is the gasification of biomass and its conversion to hydrocarbons. The second one is to liquefy biomass directly by high-temperature pyrolysis, high-pressure liquefaction, ultra-pyrolysis, or supercritical extraction. These processes convert waste biomass into energy rich useful products. Choice of conversion process depends upon the type and quantity of biomass feedstock, the desired form of the energy, i.e., end user requirements, environmental standards, economic conditions and project specific factors.

Different thermo-chemical conversion processes include combustion, gasification, liquefaction, hydrogenation and pyrolysis. Although pyrolysis is still under developing stage but during current energy scenario, pyrolysis has received special attention as it can convert biomass directly into solid, liquid and gaseous products by thermal decomposition of biomass in the absence of oxygen. Pyrolysis offers efficient utilization of particular importance for agriculture countries with vastly available biomass by-products. In this work, the focus has been made on pyrolysis process only.

3. Pyrolysis process

Pyrolysis process is a thermo-chemical conversion process and is found to be best suited for conversion of biomass to liquid fuel. It is a thermal decomposition of biomass in the absence of air or oxygen. Pyrolysis of biomass can be operated at 350–550^{o}C and goes up to 700^{o}C. This technique leads to the production of useful liquid oil, gases and solid products. Different conditions lead to formation of products in different proportions.

Initially pyrolysis was done with slow heating rates. This in turn produces more char. The higher yield of desirable liquid product can be obtained by fast pyrolysis. It involves rapid heating of biomass but not as fast as flash pyrolysis. Heating rate is somewhere about 300^{o}C/min. Generally, fast pyrolysis is used to obtain high-grade bio-oil. Fast pyrolysis is successful with most of fluidized-bed reactors as it offers high heating rates, rapid de-volatilization, easy control, easy product collection, etc. (Lou, 2004).

Cao *et al.* (2004) produced bio-oil from pyrolysis process of corn cob in a tube-typed stainless steel reactor at 350-600^{o}C with the heating rate of 30 K/min. The results showed that as pyrolytic temperature increased the yields of solid and the liquid products decreased (31.60-23.60% and 40.96-34.00%, respectively), but the yield of gas products increased (27.00-40.96%). The gas products were analyzed by gas chromatograph (GC). It was found that components of the gas products were CO_2,

CO, H_2, CH_4, C_2H_4, C_3H_6, C_3H_8, etc. At the temperature range of 350-400^oC, the gas products had CO_2 and CO 80-85% (v/v). For further increase of temperature, the yields of H_2, CH_4, C_2H_4, C_3H_6 and C_3H_8 gradually increased. The liquid products were analyzed by gas chromatograph-mass spectrometer (GC-MS) as phenols, 2-furanmethanol, 2-cyclopentanedione, etc. The heating rate affects not only the activation energy of decomposition reaction, but also the path of the reaction.

Zhang *et al.* (2009) studied fast pyrolysis of corn cob in a fluidized-bed reactor using HZSM-5 zeolite as a catalyst. The pyrolysis results showed that the amount of liquid products increased at the beginning and gradually decreased as the temperature increased from 400 to 700^oC. The optimum conditions which provided the highest liquid products of 56.8% were at catalytic pyrolytic temperature of 550^oC with the gas flow rate of 3.4 L/min and the material particle size of 1-2 mm.

Bio-oil that is produced from pyrolysis process can be fractionated into 2 phases. Yanik *et al.* (2007) produced bio-oil from pyrolysis process of 3 wastes from agricultural industry including corn cob, rice straw, and oreganum stalks at 500^oC. The desired liquid product was separated into aqueous and oil phases. The oil phase could be fractionated as water soluble (including water, volatile acids, alcohols, sugars) and water insoluble parts (lignin derivative). As a result, corn cob is the biomass that provides the highest amount of bio-oil followed by oreganum stalks and rice straw, respectively.

4. Pyrolysis product composition

4.1. Pyrolysis oil composition

Oil obtained from pyrolysis of biomass contains several organic as well as inorganic species. Some of the organic groups presence in the bio-oil are acids, esters, alcohols, ketones, aldehydes, phenols, alkenes, aromatics, nitrogen compounds, furans, sugars and miscellaneous oxygenated compounds.

Moreover, inorganic species are present in the following forms in the bio-oil: (i) associated with counter ions, (ii) connected to organic acids, (iii) related to various enzymatic compounds. Inorganic compounds present in the bio oil comprises Ca, Si, K, Fe, Al, Na, S, P, Mg, Ni, Cr, Zn, Li, Ti, Mn, Ln, Ba, V, Cl, etc. (Goyal, 2008).

4.2. Pyrolysis gas composition

Pyrolysis gas comprises CO, CO_2 and CH_4. The other components present are H_2, propane, propylene, butane, butene, C_5, ethane, etc.

4.3. Pyrolysis char composition

Char contains elemental carbon along with hydrogen. In addition, char also comprises various inorganic species.

This bio-oil can be reformed as an entire or separated by water extraction into 2 fractions; an organic fraction with lignin derived materials that can be used for the production of more valuable products, and a water soluble fraction or aqueous phase that can be catalytically steam reformed.

5. Model compounds derived from bio-oil

Model compounds derived from pyrolysis oil have been used as representative components of bio-oil or a reactant for various reactions including steam reforming reaction. As mentioned in the previous section, the main components of bio-oil are oxygenated compounds such as alcohols, acids, aldehydes, and ketones.

In addition, numerous studies on steam reforming of a model compound (acetic acid, m-cresol, phenol, acetone and ethanol) of bio-oil have been reported using steam reforming for hydrogen production (Wu *et al.*, 2008: Rioche *et al.*, 2005). They reported that the bio-oil steam reforming for hydrogen production would seem

to be a promising route. However, research conducted on steam reforming of actual bio-oil instead of a model compound of bio-oil is limited.

6. Hydrogen production processes

Generally, processes for hydrogen production are catalytic steam reforming of methane, light hydrocarbons, and naphtha, partial oxidation of heavy oil residues, and coal gasification (Garcia *et al.*, 2000).

The limitation of current hydrogen generation is based on natural gas and naphtha catalytic steam reforming, or coal gasification, as its main sources. These well established industrial processes release large amount of carbon dioxide into the atmosphere as the direct combustion of fossil fuels, with a net production of greenhouse gas. An alternative approach to the production of hydrogen from biomass may be steam reforming of bio-oil from biomass. Moreover, an integrated process, in which biomass is partially used to produce more valuable materials or chemicals, while the residual fractions are utilized for the generation of hydrogen, may be economically viable in energy market (Czernik *et al.*, 2002).

7. Catalytic steam reforming

Catalytic steam reforming reaction is the exothermic reaction that uses catalyst and steam to decompose oxygenated compounds ($C_mH_nO_k$). Oxygenated compounds are converted to carbon monoxide and hydrogen via this process. The temperature range of 600-700^oC is required for this process. The range may be different depends on types of catalyst (Domine *et al*., 2008).

$$C_nH_mO_k + (n-k)H_2O \xrightarrow{\Delta} nCO + (n+\frac{m}{2}-k)H_2 \qquad (1)$$

The process undergoes reforming conditions, a water gas shift reaction which is an exothermic reaction can occur as a side reaction at high temperature region.

$$nCO + nH_2O \overset{\Delta}{\leftrightarrow} nCO_2 + nH_2 \quad (2)$$

The overall process as shown in reaction (3), oxygenated compounds react with water to produce CO_2 and H_2.

$$C_nH_mO_k + (2n - k)H_2O \overset{\Delta}{\rightarrow} nCO_2 + (2n + \frac{m}{2} - k)H_2 \quad (3)$$

This is the complete steam reforming reaction. The products are CO_2 and H_2 compared with the first reaction that the products are CO and H_2.

The thermodynamic and kinetic considerations of steam reforming process were discussed by Davda *et al.* (2005) and the data was collected. Figure 1 shows the changes in the standard Gibbs free energy ($\Delta G^0/RT$) associated with reaction (4) for a series of alkanes (CH_4, C_2H_6, C_3H_8, C_6H_{14}). It can be indicated that the steam reforming of alkanes is thermodynamically favorable due to negative values of $\Delta G^0/RT$ only at temperatures higher than 675 K. If the number of carbon atoms increases (increasing of molecular weight), the Gibbs free energy decreases. The reaction (5) shows a production of CO and H_2 from oxygenated hydrocarbons which have a C:O ratio of 1:1 such as carbohydrates.

$$C_nH_{2n+2} + nH_2O \leftrightarrow nCO + (2n+1)H_2 \quad (4)$$

$$C_nH_{2y}O_n \leftrightarrow nCO + yH_2 \quad (5)$$

The oxygenated hydrocarbons that have C:O ratio of 1:1 include methanol (CH_3OH), ethylene glycol ($C_2H_4(OH)_2$), glycerol ($C_3H_5(OH)_3$), and sorbitol ($C_6H_8(OH)_6$). Importantly, sorbitol is produced via the hydrogenation of glucose. Figure 1 shows the steam reforming of these oxygenated hydrocarbons that it produces CO and H_2 and is thermodynamically favorable at significantly lower temperatures than those required for alkanes with similar number of carbon atoms.

Accordingly, the steam reforming of oxygenated hydrocarbons having a C:O ratio of 1:1 would offer a low-temperature route for the formation of CO and H_2. Figure 1 also shows that the value of $\Delta G^0/RT$ for water-gas shift of CO to CO_2 and H_2 (reaction 2) is more favorable at lower temperatures. Therefore, it might be possible to produce H_2 and CO_2 from steam reforming of oxygenated compounds utilizing a single-step catalytic process, since the water-gas shift reaction is favorable at the same low temperatures at which steam reforming of carbohydrates is possible.

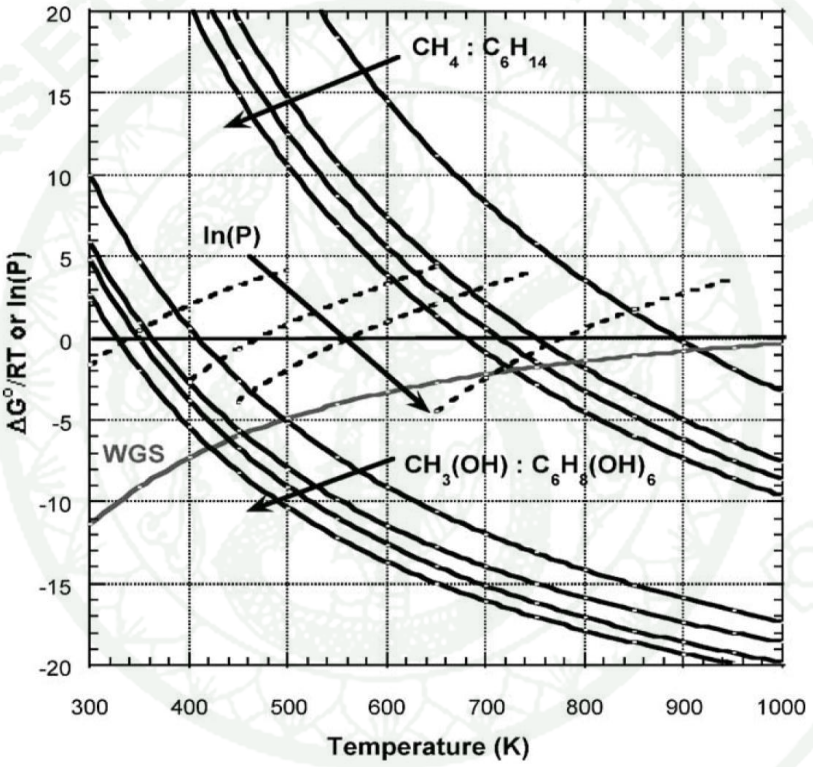

Figure 1 Temperature affects on the standard Gibbs free energy ($\Delta G^o/RT$) for production of CO and H_2 from vapor phase reforming of alkanes (CH_4, C_2H_6, C_3H_8, C_6H_{14}), oxygenated hydrocarbons ($CH_3(OH)$, $C_2H_4(OH)_2$, $C_3H_5(OH)_3$, $C_6H_8(OH)_6$) and water-gas shift. Dotted lines show the values of the vapor pressure in atm (ln(P)) of oxygenated hydrocarbons.

Source: Davda *et al*. (2005)

The steam reforming reaction is endothermic and is favored by high temperature, leading to high hydrogen yield and carbon conversion. In contrast, the water-gas shift reaction is exothermic and favors lower temperature. Thus, the increase of steam content and temperature are in favor of both reactions, resulting in an increase of the hydrogen yield at higher temperature and higher steam to carbon in the feed ratio (S/C).

For the kinetic considerations, hydrogen production via oxygenated hydrocarbons reforming process would require an efficient catalyst that promotes reforming reactions, which is C-C bond breaking followed by water-gas shift reaction, and inhibits alkane formation reactions, C-O bond breaking followed by hydrogenation. Moreover, Davda *et al*. (2005) concluded the data from other researches about the catalytic activities of different metals for C-C bond breaking reaction. They informed that in order to obtain a high selectivity for hydrogen production, the catalysts must not easily conduct undesired side reactions, such as methanation of CO and Fischer-Tropsch synthesis. Therefore Pt and Pd indicated suitable catalytic activity and selectivity for hydrogen production by oxygenated hydrocarbons' reforming, which requires high activity for C-C bond breaking and water-gas shift reaction, and low activity for methanation. Whereas Cu shows the highest water-gas shift rates, although it does not show activity for C-C bond breaking. The summary of thermodynamic and kinetic considerations of the aqueous phase reforming process is shown in Figure 2.

Hu and Lu (2009) informed that many compositions in bio-oil are thermally unstable. The various reactions such as decomposition (reaction 6) and dehydration (reaction 7) may occur before reacting or on catalyst bed. As a result, undesired by-products are produced and reduce hydrogen yield.

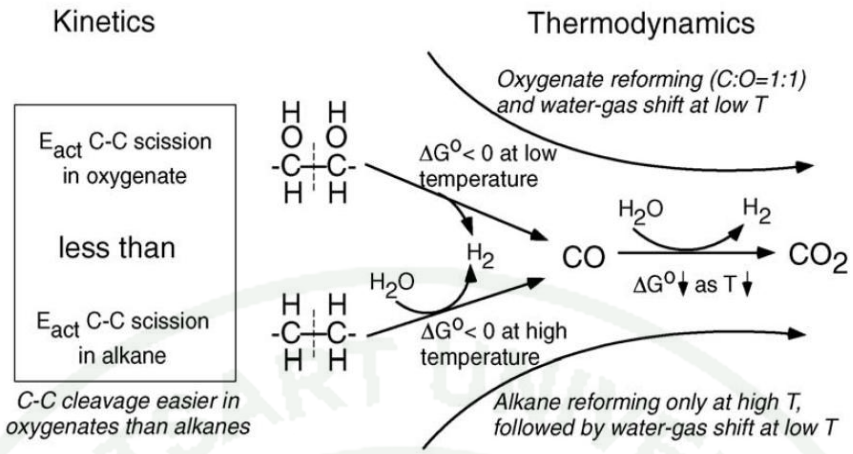

Figure 2 Summary of thermodynamic and kinetic considerations of the aqueous phase reforming process

Source : Davda *et al*. (2005)

$$C_nH_mO_k \rightarrow C_xH_yO_z + \text{gases } (H_2, CO, CO_2, CH_4 \ \ldots) \quad (6)$$

$$C_nH_mO_k \rightarrow C_xH_yO_z + H_2O \quad (7)$$

Methane (CH_4) is another by-product in steam reforming that greatly reduces hydrogen yield. Decomposition of the organic compounds and methanation of carbon oxide (CO and CO_2) in the reactions (8) and (9) are main routes for methane generation at low temperature regime (around 300-400^oC).

$$CO + 3H_2 \rightarrow CH_4 + H_2O \quad (8)$$

$$CO_2 + 4H_2 \rightarrow CH_4 + 2H_2O \quad (9)$$

Carbon formation, which causes loss of effective surface area of the catalyst and performance of reforming process, may occur due to decomposition of oxygenated compounds (reaction 10), methane (reaction 11), and disproportion of CO

(reaction 12) as well as the reaction of CO or CO_2 with H_2 (reactions 13 and 14) are the main routes for its formation.

.

$$C_nH_mO_k \rightarrow C_xH_yO_z + \text{coke} \quad (10)$$

$$CH_4 \rightarrow C + 2H_2 \quad (11)$$

$$2CO \rightarrow C + CO_2 \quad (12)$$

$$CO + H_2 \rightarrow C + H_2O \quad (13)$$

$$CO_2 + 2H_2 \rightarrow C + 2H_2O \quad (14)$$

Wang *et al.* (2007) used various types of metal coating on a calcium aluminate (C12A7-O^-, $[Ca_{24}Al_{28}O_{64}]^{4+}.4O^-$/M, M=Mg, K, Ce) as catalysts for steam reforming reaction of bio-oil with temperature range of 250-750^{o}C. The C12A7-O^-/18%Mg catalyst shows high activity for steam reforming which provided the highest hydrogen yield and carbon conversion, 80% and 96% respectively, at 750^{o}C and S/C of 9. For catalyst deactivation test, the C12A7-O^-/18%Mg catalyst can be affected by carbon formation on the catalyst surface. The results showed that hydrogen yield increased during the first 20 min and then decreased from 80 to 50% after 3.5 h and dropped to 21% after 5 h.

The catalytic steam reforming of model compounds derived from bio-oil, acetic acid and acetone, over calcium aluminate supported Ni and noble metal (0.5 wt% Rh or Ir) catalysts were studied by Vagia and Lemonidou (2008). The results showed that hydrogen yields depend on the metal types, metal loading, and the ratio of CaO to Al_2O_3 of the support ($CaO.2Al_2O_3$ and $12CaO.7Al_2O_3$). The 5 wt% Ni/$CaO.2Al_2O_3$ catalyst showed high performance for hydrogen production at 750^{o}C and S/C of 3, while the 0.5 wt% Rh/$CaO.2Al_2O_3$ catalyst showed the highest resistant to coking.

Some additives can be added into catalysts for catalytic steam reforming process to diminish catalyst deactivation. Gacia *et al.* (2000) studied the effects of catalyst composition on the performance of the catalysts in terms of hydrogen yield and catalyst deactivation caused by carbon deposition. The catalysts were prepared by impregnation of Al_2O_3 support with Ni and additives. Magnesium (Mg) and lanthanum (La) used as support modifiers enhanced steam adsorption while cobalt (Co) and chromium (Cr) additives reduced coke formation reactions. They found that Ni-Co/MgO-La_2O_3-Al_2O_3 and Ni-Cr/MgO-La_2O_3-Al_2O_3 catalysts showed the best results in the laboratory tests. Ni-Cu catalysts promoted on different materials (α-Al_2O_3, $Ce_{0.6}Zr_{0.4}O_2$, ZnO and Nb_2O_5) were investigated in ethanol steam reforming reaction (Furtado, 2009). Analysis of the ethanol conversion indicated that Ni-Cu/$Ce_{0.6}Zr_{0.4}O_2$ catalyst was the most appropriate one for the ethanol steam reforming under investigated reaction conditions. During 8 h of reaction, this catalyst presented an average ethanol conversion of 43%, producing a high amount of H_2 around 60 mol% by steam reforming, ethanol decomposition, and dehydrogenation parallel reactions.

Noble metals (Pt, Ru, and Ir) promoted Co/$MgAl_2O_4$ catalysts (Profeti *et al.*, 2009) showed high performance on hydrogen production for steam reforming process. The results showed that CoRu/$MgAl_2O_4$ catalyst provided the highest activity for hydrogen production, high carbon conversion of 98% at 500^{o}C.

Singhto *et al.* (2006) studied steam reforming of ethanol by using Ni/Ce-ZrO_2 catalyst. The results showed that Ni/Ce-ZrO_2 catalyst provided high performance for hydrogen production from steam reforming process and high coke formation resistance when compared with Ni/Al_2O_3 catalyst at the same conditions. At high temperature of 800^{o}C, products were H_2, CO, CO_2, and small amounts of CH_4.

8. Calcium aluminate

The microporous crystal of calcium aluminate ($12CaO{\cdot}7Al_2O_3$), which has been known as the mayenite mineral, has a cubic structure. The unit cell contains 2

molecules which can be expressed as $[Ca_{24}Al_{28}O_{64}]^{4+}$ consisting of 12 cages with a free vacancy of about 0.4 nm in diameter as shown in Figure 3. The two remaining ions, $2O^{2-}$, are stored in the cages of the $[Ca_{24}Al_{28}O_{64}]^{4+}$ (Hosono *et al.*, 2007).

Moreover, the O^{2-} anions can be released into the gas phase by the applying an extraction field under suitable temperature. Active O^{2-} is key intermediate in low temperature oxidation or dissociation of hydrocarbons. Because $12CaO{\cdot}7Al_2O_3$ has the particular O^{2-} storage and emission behavior, therefore this material may be used as a good catalyst for oxidizing or decomposing of some chemicals (Wang *et al.*, 2007).

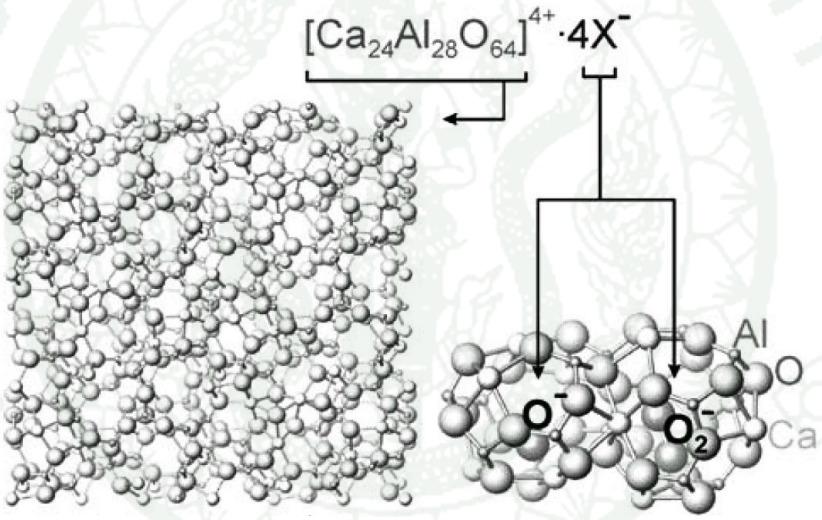

Figure 3 Crystal structure of $12CaO{\cdot}7Al_2O_3$

Source : Hosono *et al.*, (2007)

9. Ceria

Ceria or cerium oxide (CeO_2) has the molecular weight of 172.12. The lattice structure of cerium oxide is a face centered cubic structure (FCC) as depicted in Figure 4.

Several techniques have been developed for the synthesis of CeO_2 including hydrothermal synthesis, urea-based homogeneous precipitation, decomposition of oxalate precursor, force hydrolysis, and electrochemical synthesis. However, these techniques provide the particles which are agglomerated, impure, and irregular shaped. Thus, the technique has been studied as an alternative powder formation is spray pyrolysis applied to synthesize micro spherical ceramic powders with narrow size distribution, uniform shapes, and controlled purities (Xu *et al.*, 2002).

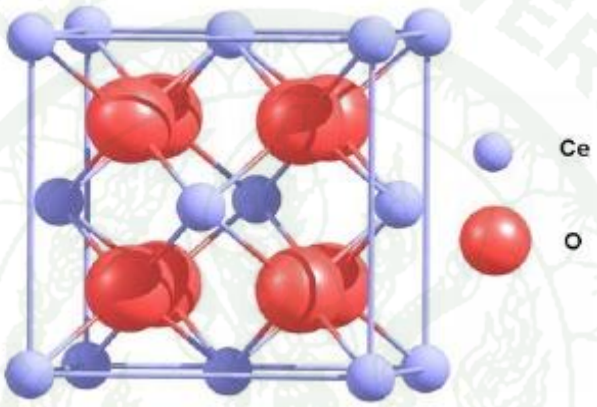

Figure 4 Crystal structure of cerium oxide

Source : Xu (2007)

CeO_2 is considered a useful material in various applications for glasses, ceramics, catalytic supports for automotive exhaust system, etc. In addition, it has been widely used as support due to a good oxygen storage capacity. Besides, some researches informed that an addition of Ti in CeO_2 improved the redox capacity of CeO_2 (Ye *et al.*, 2008).

10. Titania

Titania or titanium dioxide (TiO_2) has been found in nature which has 3 types of crystal structure including anatase, rutile, and brookite. The anatase phase can be formed by calcination of a titanium salt at mild temperature. For further increasing of

calcined temperature, the crystal structure of TiO_2 changes from anatase to rutile structure. In both structures as depicted in Figure 5, slightly distorted octahedral are the basic building units. The bond lengths and angles of octahedrally coordinated Ti atoms are indicated and stacking of the octahedral in both structures is shown on the right side (Ulrike, 2003).

TiO_2 is used in heterogeneous catalysis, as a photocatalysts, in solar cells for the production of hydrogen and electric energy, as gas sensor, white pigments, a corrosive protective coating, in ceramics, and in electronic devices. The anatase is a famous to use as a support of catalysts because surface area of anatase is higher than that for rutile phase (Wittayakun and Grisdanurak, 2004).

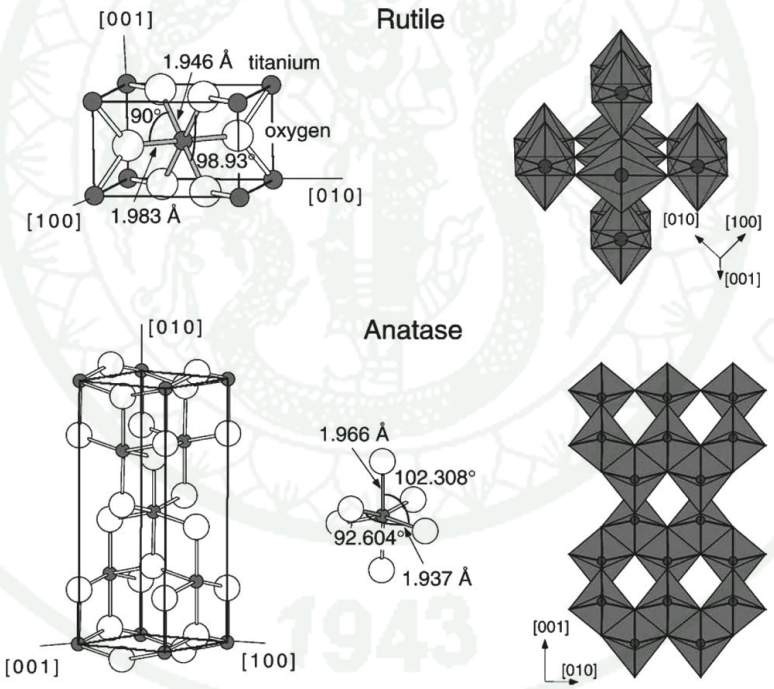

Figure 5 Crystal structures of rutile and anatase

Source : Ulrike (2003)

MATERIALS AND METHODS

Materials

Acetic acid (assay 99.8% glacial CH_3COOH, AR grade) and acetone (assay 99.5% CH_3COCH_3, AR grade) were used as a representative component of bio-oil and a reactant for steam reforming process which were obtained from QRëc (imported by Roongsarp Chemical Ltd., part.). The aqueous phase of bio-oil produced from pyrolysis process of coffee bean residue at 500^oC was also used as a raw material.

Methods

1. Catalyst preparation

The catalyst Ni/Al_2O_3 of 15wt% was prepared by incipient wetness impregnation method using $Ni(NO_3)_2.6H_2O$ as a precursor. After impregnation, the catalyst was dried at 110^oC overnight. Finally, it was calcined at 500^oC for 4 h (Hu and Lu, 2009).

Ceria or cerium oxide (CeO_2) was synthesized by spray pyrolysis technique using $Ce(NO_3)_3.6H_2O$ (assay 99%, Aldric Chemmistry) as a precursor. The solution of 0.05 M of $Ce(NO_3)_3$ (150 mL) was contained in an ultrasonic nebulizer with a resonant frequency of 1.7 MHz for generation of sprays (atomized precursor). As shown in Figure 6, the air flow of 300 mL/min carries the atomized precursor passing through a tubular quartz reactor at 650^oC. The resulting product particles are collected in the cold traps and on the filter positioned between the cold traps and the vacuum pump.

Calcium aluminate, $CaO:Al_2O_3$ with mole ratio of 12:7, was prepared by solid-state reaction between $CaCO_3$ and γ-Al_2O_3 (the BET surface area of 120-190 m^2/g, MERCK). The mixture was mixed with a small amount of 10% nitric acid to convert carbonates to nitrates. After aging and drying for 24 h, the mixture was

calcined at 650°C to decompose $Ca(NO_3)_2$ to CaO. After that, it was calcined at 1,150°C or (1,300°C) for 20 h in order to form the crystal phase between 2 oxides (Lemonidou and Vasalos, 1989).

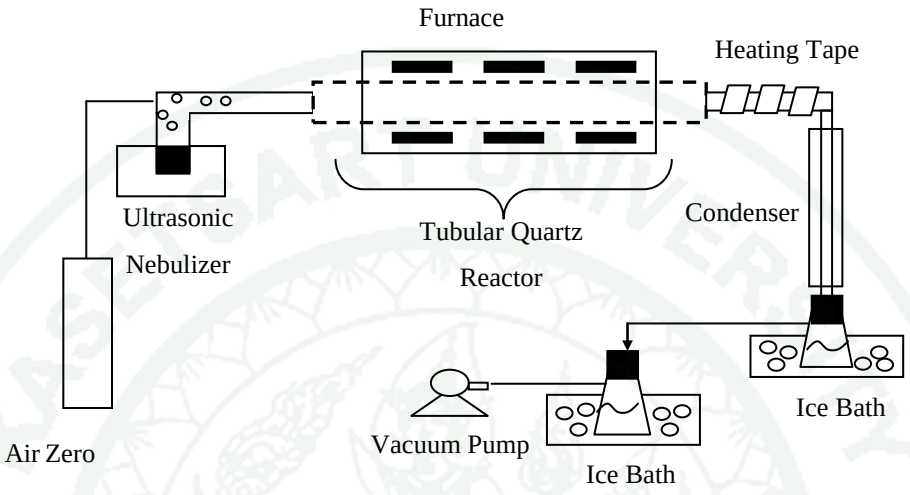

Figure 6 Schematic diagram of spray pyrolysis technique.

The calcium aluminate can be prepared by the other technique which is called chemical solution deposition (CSD). Aluminium sec-butoxide ($Al(OBu^2)_3$, assay 95%, Fluka Chemika, Sigma-Aldrich Chemical) and calcium nitrate tetrahydrate ($Ca(NO_3)_2.4H_2O$, assay 99%, Analytical Rasayan, Sd Fine-Chem Limited) were used as a precursor of Al and Ca, respectively. Acetylacetone ($CH_3COCH_2COCH_3$, assay 99%, QRëc) of 0.014 mol was dissolved in 0.52 mol of 2-methoxy ethanol solution ($CH_3OCH_2CH_2OH$, assay 99%, UNIVAR, Ajax Fine Chem Pty. Ltd.) and 1 mL of nitric acid, used as a deflocculant, was added in it. The $Al(OBu^2)_3$ of 0.007 mol was added in the solvent and this solution was agitated for 15 min in order to mix the Al source and the solvent. After that the $Ca(NO_3)_2.4H_2O$ of 0.006 mol was added in the solution. For dissolving the the Ca source, the solution was refluxed at 125°C for 2 h. The precursor solution was dried at 150°C for 1 h and the dried gel obtained from the solution was calcined at 900°C for 2 h in air atmosphere (Sakamoto *et al.*, 2009).

The support, 12C7A-CeO_2-TiO_2, was prepared by mechanically mixed of $12CaO.7Al_2O_3$, CeO_2, and TiO_2 (assay 99.5%, UNILAB, APS Chemicals limited) with different mole ratios of 2:1:1 (12C7A = 91.70 wt%, CeO_2 = 5.68 wt%, TiO_2 = 2.61 wt%) and 1:1:1 (12C7A = 84.60 wt%, CeO_2 = 10.49 wt%, TiO_2 = 4.86 wt%).

Co-incipient wetness impregnation method was applied for loading metals on the 12C7A-CeO_2-TiO_2. The precursors used for Ni, Cu, Mg, Co, and Cr metals were $Ni(NO_3)_2.6H_2O$ (assay 97%, UNILAB,), $Cu(NO_3)_2.3H_2O$ (assay 99%, UNIVAR) , $Mg(NO_3)_2.6H_2O$ (assay 99%, UNILAB), which were obtained from Ajax Fine Chem Pty. Ltd., $Co(NO_3)_2.6H_2O$ (assay 98-102%, UNIVAR, APS Chemicals limited), and $Cr(NO_3)_3$. $6H_2O$ (assay 99%, ACRŌS Oganics), respectively. After that the precursors were calcined at 650^oC for 2 h.

2. Characterization of catalysts

The catalysts (before reduction) and the support (before metal loading) were characterized by the X-ray diffractrometer (D8 Advance, Bruker axs) to identify the lattice structure of the catalysts and support. The Brunauer-Emmett-Teller (BET) surface area was evaluated from autosorb instrument (AUTOSORB®-1-C/MS, Quantachorme instruments) using the N_2 adsorption-desorption isotherms. The samples were outgassed at 300^oC while reduction temperature of loaded metal catalysts can be determined by using hydrogen temperature-programme reduction (H_2-TPR) operated by autosorb instrument equipped with a mass spectrometer (MS) as the same apparatus described for evaluation of the BET surface area.

In order to investigate coke formation on a surface of the catalysts (after steam reforming process), thermogravimetric analysis (TG-DTA, model SDT 2960 PN 925605.001, Perkin Elmer) were performed in air flow (50 mL/min) with a heating rate of 15^oC/min up to 1,000^oC.

3. Hydrogen production from catalytic steam reforming process

The system of steam reforming process (Figure 7) consists of N_2 as a carrier gas with 200 mL/min to lead acetic acid and acetone, which were firstly dissolved in water with a given S/C to an evaporator by syringe pumps (model A-99.FZ and R-99.EZ) in order to vaporize all the feeds. The vapor of the feeds passed through a fixed bed tube reactor at 750-900^{o}C which contained 0.150 g of a catalyst with space velocity of 80,000 mL/g_{Cat}/h at 25^{o}C. Before reforming tests, all the catalysts were reduced in situ at a specific temperature for each catalyst (reduction temperature obtained from H_2-TPR measurement) for 2 h with hydrogen flow.

Finally, water and condensable products were trapped in an ice bath and the gaseous products were collected by gas sampling, then compositions of gaseous products were analyzed by a gas chromatograph, GC.

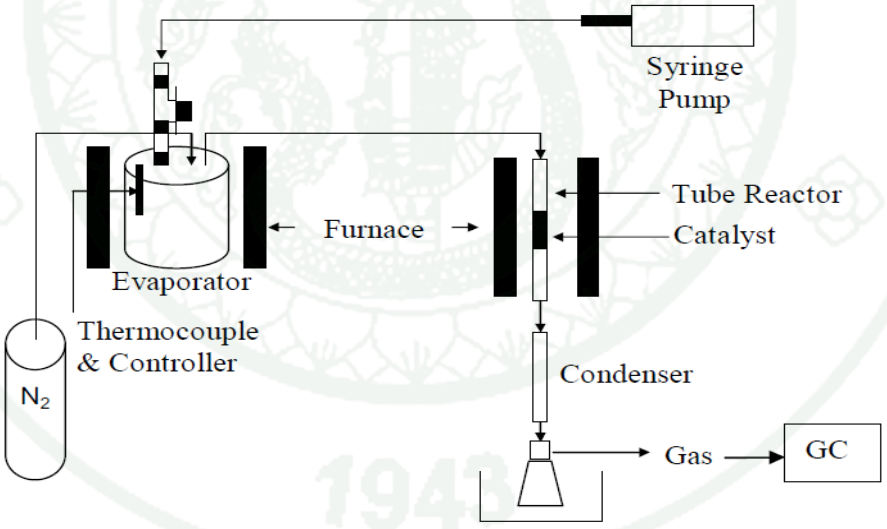

Figure 7 Schematic diagram of the steam reforming process.

4. Products analysis

The gaseous products from steam reforming process are commonly reported in term of hydrogen yield and selectivity. The quantitative analysis of gaseous products can be determined by using GC (Varian, model CP3800) with a capillary column

(Carboxen-1010 plot column) in the length of 30 cm and diameter of 0.53 mm and using a thermal conductivity detector (TCD). The injection port temperature was 200°C. The column temperature was initially at 35°C and increased at a rate of 10°C/min to temperature of 230°C, whereas the liquid products were analyzed via Rt®-Q-bond capillary column and a flame ionized detector (FID).

Hydrogen yield, selectivity, and conversion can be calculated as following equations.

$$\text{Hydrogen yield (\%)} = \frac{\text{moles of hydrogen produced}}{\left(2n + \frac{m}{2} - k\right) \times \text{moles of carbon in feed}} \times 100$$

. Where n, m, and k defined as moles of carbon, hydrogen, and oxygen in the feed ($C_nH_mO_k$), respectively

The moles of hydrogen and other gases produced are obtained from the calibration curve of peak area.

$$\text{Selectivity of gaseous product}_i = \frac{\text{moles of gaseous product}_i}{\sum \text{moles of gaseous products}}$$

$$\text{Conversion of reactant (\%)} = \frac{\text{moles of reactant}_{in} - \text{moles of reactant}_{out}}{\text{moles of reactant}_{in}} \times 100$$

RESULTS AND DISCUSSION

1. Characterization of prepared catalysts and supports

1.1 Calcium aluminate

The X-ray diffractograms of calcium aluminate ($12CaO.7Al_2O_3$) is illustrated in Figure 8. The calcium aluminate prepared by solid-state reaction with a molar ratio of 12:7 ($CaO:Al_2O_3$) appears to be a mixture of 3 crystal phases: $Ca_{12}Al_{14}O_{33}$ (12C7A), $CaAl_4O_7$ (1C2A), and $CaAl_2O_4$ (1C1A). The existent peaks of more than one phases of calcium aluminate can be attributed to mild conditions for the solid- state reaction at 1,150°C for 20 h [Figure 8 (a)]. For higher temperature at

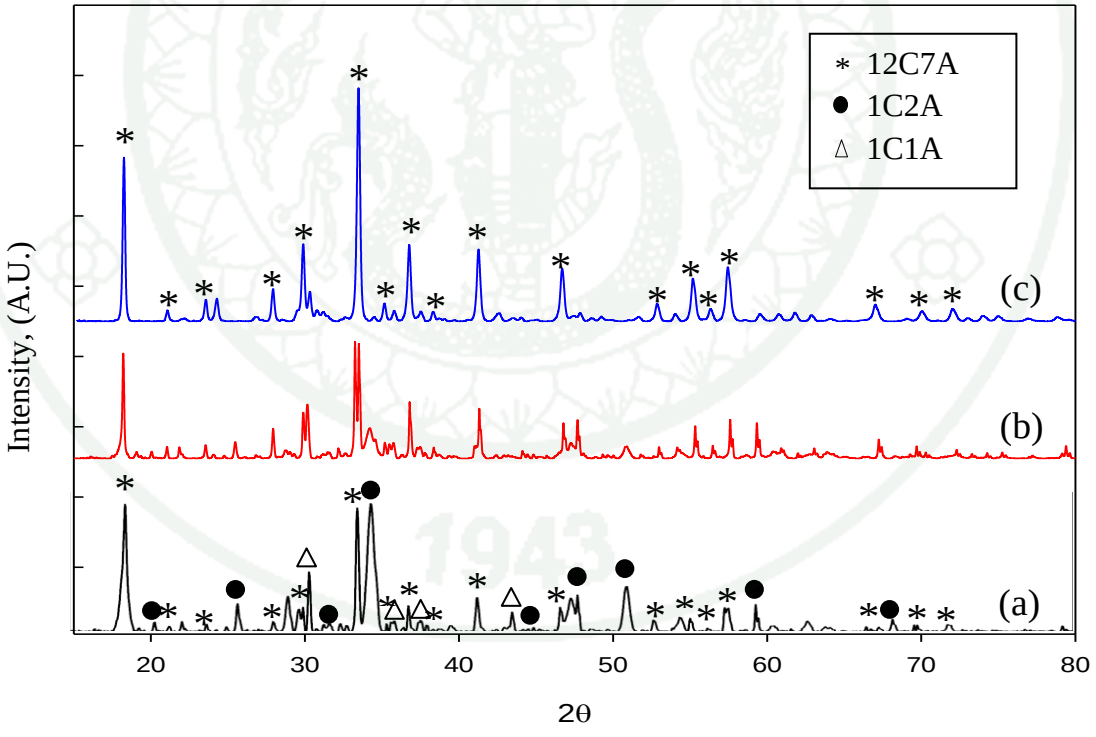

Figure 8 XRD patterns of calcium aluminate (before metal loading) were prepared by solid-state reaction calcined at (a) 1,150°C, (b) 1,300°C for 20 h. and (c) prepared by chemical solution deposition method (CSD) at 900°C.

1,300^{o}C [Figure 8 (b)], the solid-state reaction provided a lower interference peaks of another calcium alminate phases (1C2A or 1C1A). the XRD pattern of the calcium aluminate [Figure 8 (c)] prepared by using the CSD method at 900^{o}C illustrates dominant peaks of the calcium aluminate with molar ratio of 12:7 (12C7A) and provides the other phases less than that prepared by solid-state reaction. It is shown that solid-state reaction of the two species of solid is difficult to give a homogeneous mixture.

The surface area of the prepared calcium aluminates is reported in Table 1. The prepared 12C7A from both techniques showed higher surface area than those from previous studies. Besides, the prepared 12C7A materials from both techniques showed a close value of surface area, the surface area of 12C7A obtained from solid-state reaction was slightly greater than that from CSD method.

Table 1 The BET surface areas (m^2/g) of the prepared calcium aluminate

Preparation method	BET surface area (m^2/g)	
	This research	Previous researches
Solid-state reaction at 1,300^{o}C	17.49	0.24 (Lemonidou and Vasalos, 1989)
CSD method at 900^{o}C	14.80	4.20 (Sakamoto *et al.,* 2009)

From previous research, Vagia and Lemonidou (2008) studied an activity of noble and non noble metals over calcium aluminate catalysts with different $CaO:Al_2O_3$ molar ratios (1:2 and 12:7). They reported that the calcium aluminate with a ratio of 12:7 provides both component elements Ca and Al which were uniformly distributed in the pellet. In addition, Lemonidou and Vasalos (1989) studied the effect of preparation of catalysts for ethylene production via steam cracking. They prepared several calcium aluminate phases to investigate the activity for steam cracking of n-hexane. The results also indicated that the calcium aluminate with a ratio of 12:7 is the most suitable one for steam cracking due to high yields of ethylene and propylene

but low yield of carbon dioxide obtained. The 12C7A was recommended to use as a strong oxidizing catalyst due to the oxygen radicals, O^{2-}, in the 12C7A cage which is known to have a high oxidative power (Sakamoto *et al.*, 2009).

As already mentioned, the calcium aluminate with a molar ratio between CaO and Al_2O_3 of 12:7 (12C7A) is suitable for using as a catalyst support due to especial active anions within the structure, high metal dispersion on a surface of the calcium aluminate, high activity for steam cracking, and high thermal stability. For synthesis of 12C7A, in order to provide a uniform distribution of 12C7A phase, the CSD technique is recommended as a preparation method of the 12C7A because this technique gives more homogeneous mixture than the solid-state reaction method. Moreover, the CSD method not only provides a uniform product but also helps saving energy consumption. Since this method operates at lower temperature of 900^{o}C and the duration time is only 2 h whereas the solid-state reaction method operates at above 1,100^{o}C for 20 h.

1.2 Ceria or cerium oxide

A cerium oxide (CeO_2) prepared by spray pyrolysis technique at 650^{o}C was identified a structure by XRD analysis as show in Figure 9. From the result, the XRD pattern shows dominant peaks at 28, 33, 47, and 56^{o} which correspond to the data base of reference pattern for ceria. Therefore, this technique is proposed for synthesis of pure ceria with fine particles.

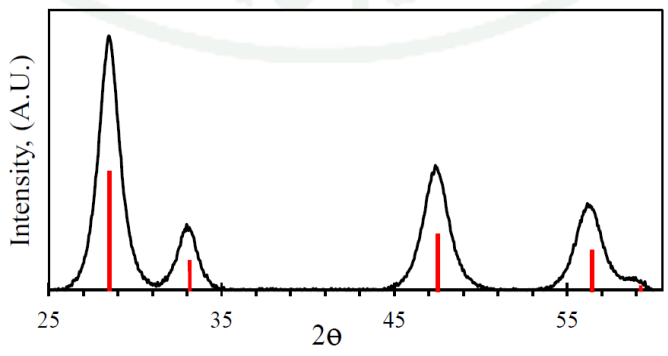

Figure 9 XRD pattern of ceria prepared by spray pyrolysis technique.

1.3 Loaded metal catalysts

Figure 10 illustrates the XRD patterns of loaded metals over 12C7A-CeO_2-TiO_2 support, molar ratio of 2:1:1, before reduction. From Figure 10 (a), the XRD patterns dominantly depicts nickel oxide (NiO) crystal phase (∗). Lattice framework peaks of CeO_2 (●) and TiO_2 (♦) do not clearly appear due to a small amount of the metal oxides added and the hindrance of calcium aluminate peaks. For the XRD patterns of promoted metal catalysts (Cu, Cr, Co, and Mg) on the Ni based catalyst as shown in Figure 10 (b) to (e), the characteristic peaks of NiO are still clearly exist on the XRD patterns of the bimetallic catalysts. Conversely, the charac-

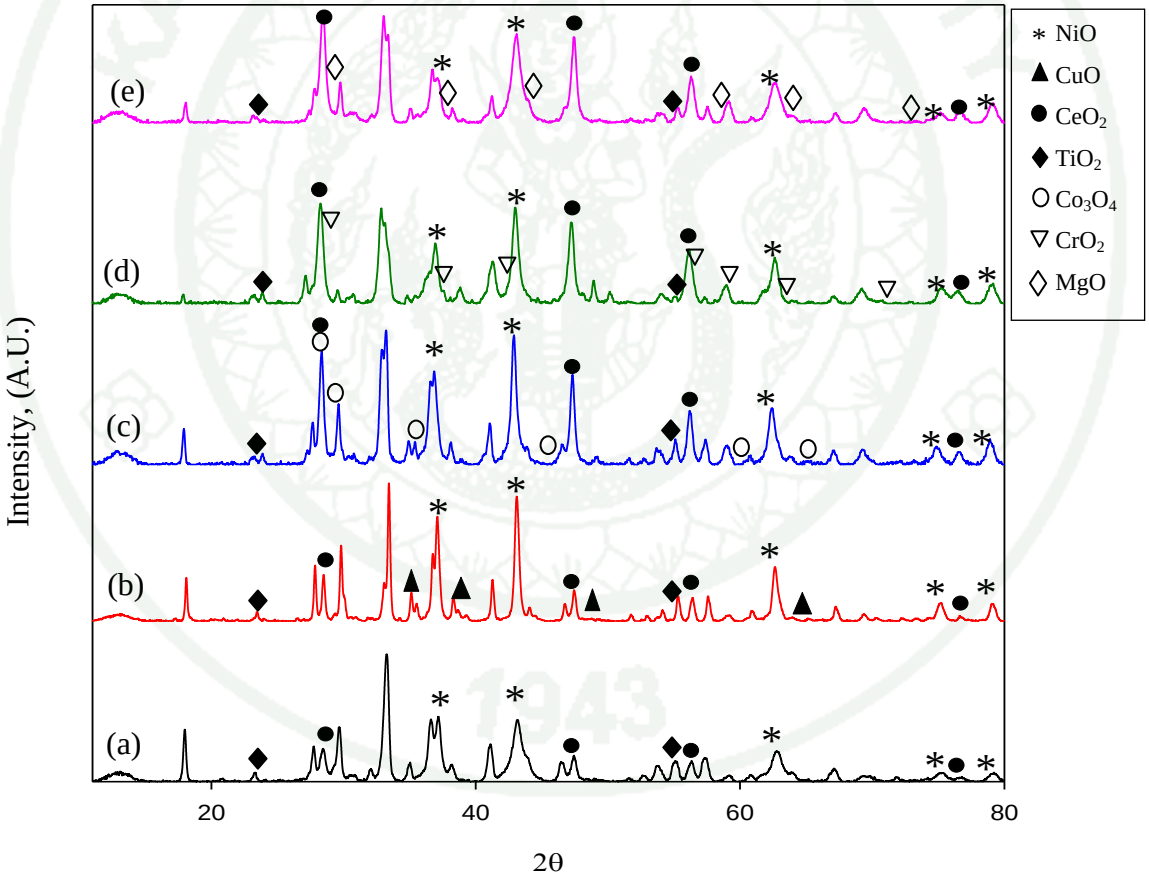

Figure 10 XRD patterns of loaded metal catalysts (before reduction): (a) 15%Ni/12C7A-CeO_2-TiO_2, (b) 15%Ni-5%Cu/12C7A-CeO_2-TiO_2, (c) 15%Ni-5%Co/12C7A-CeO_2-TiO_2, (d) 15%Ni-5%Cr/12C7A-CeO_2-TiO_2 and (e) 15%Ni-5%Mg/12C7A-CeO_2-TiO_2.

teristic peaks of the promoted metal oxides are quite difficult to observe in the XRD patterns, consistent with CeO_2 and TiO_2 cases. Moreover, some characteristic peaks of CeO_2 and TiO_2 as well as the other loaded metals disappear.

Reduction temperatures can be specified via temperature program reduction (TPR) whereas TPR profiles of loaded metal catalysts are illustrated in Figure 11. Reduction of the Ni based catalyst [Figure 11 (a)] shows a broad peak at high temperature about 700 to 800^{o}C.

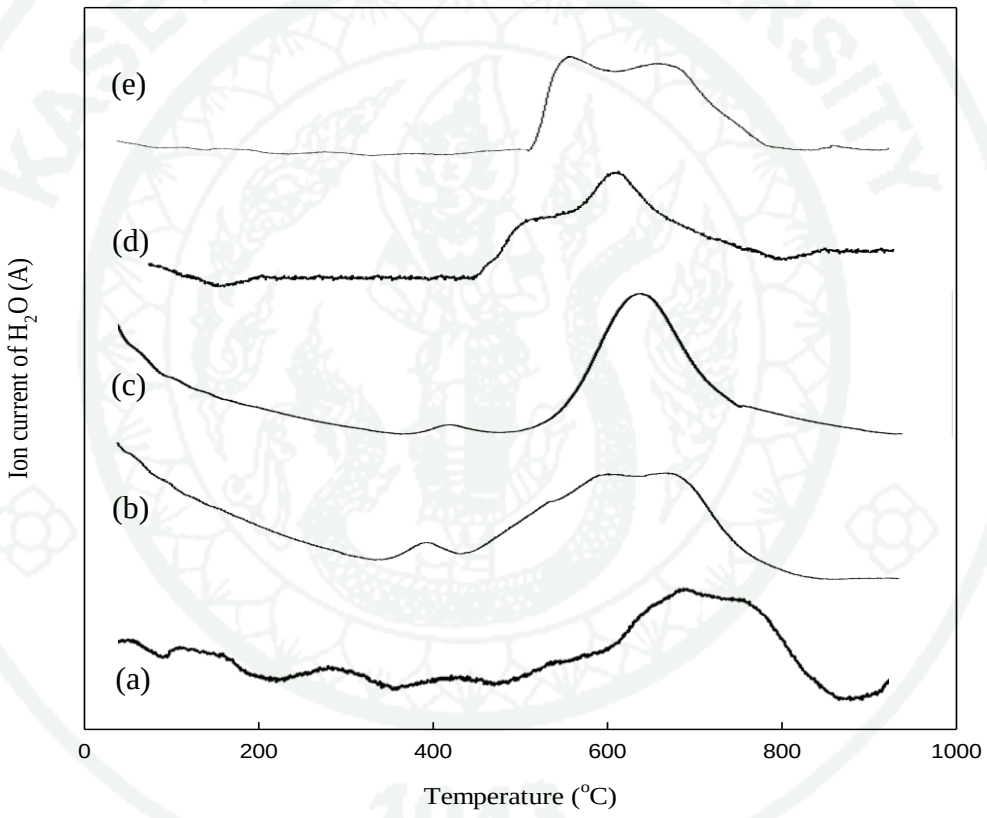

Figure 11 TPR profiles of loaded metal catalysts: (a) 15%Ni/12C7A-CeO_2-TiO_2, (b) 15%Ni-5%Cu/12C7A-CeO_2-TiO_2, (c) 15%Ni-5%Mg/12C7A-CeO_2-TiO_2, (d) 15%Ni-5%Cr/12C7A-CeO_2-TiO_2 and (e) 15%Ni-5%Co/12C7A-CeO_2-TiO_2.

According to Profeti *et al.* (2009), 3 peaks of NiO dispersed on an oxide support (CeO_2-Al_2O_3) were observed. The first peak was the reduction of NiO at low temperature (200 to 400^oC). The second peak was attributed to the reduction of highly dispersed non-crystalline NiO species (705^oC) and the last peak was attributed to the reduction of both, Ni^{2+} in intimate contact with CeO_2 and Ni^{2+} into the alumina lattice forming $NiAl_2O_4$ at 840^oC. Pure NiO generally shows a single definite peak at 360^oC due to the reduction of species Ni^{2+} to Ni^0. Accordingly, the broad peak at high temperature depicted in TPR profile of 15%Ni/12C7A-CeO_2-TiO_2 [Figure 11 (a)] may be attributed to the reduction of NiO or Ni^{2+} with strong interaction between the support and metal oxides.

For bimetallic catalysts as shown in Figure 11 (b) to (e), TPR profiles almost depict broad peak and some shoulder at high temperature (600 to 750^oC) are attributed to a strong interaction between metal oxides and support. Comparison between Ni based catalyst and promoted metal on Ni based catalysts it is shown that the promoted metal catalysts improve reducibility of NiO due to a migration of the broad peak to lower temperature. A small peak around 400^oC as shown in Figure 11 (b) and (c) is attributed to the reduction of NiO on a surface of the catalyst. It seems that the main NiO added into the 12C7A-CeO_2-TiO_2 may form a strong interaction with the support or the reduction of Ni^{2+} in the support structure might occur.

The promotion of catalyst activity by the promoted metal was also reported by Vizcaíno *et al.* (2007). The TPR profiles of Cu and/or Ni over silica catalysts were investigated in their study. Monometallic Cu catalyst is characterized by the peak at 210 and 280^oC corresponding to the reduction of Cu^{2+} and CuO interacting with support to Cu^0, respectively. Moreover, monometallic Ni catalyst shows a reduction peak of Ni^{2+} to Ni^0 around 310^oC as well as a broad shoulder at 420^oC, which is attributed to the formation of $NiSiO_3$ by a strong interaction between metal and support. On the other hand, bimetallic Cu-Ni catalyst show reduction peak between 200 and 260^oC, the first one is CuO reduction, while the other at higher temperature is NiO reduction. The improvement of the reducibility of NiO when CuO

is present in the catalyst is owing to a synergistic interaction between the metal oxides.

While the reduction peak of surface Ce–O–Ti cannot be observed due to the hindrance of the broad reduction peak of NiO at high temperature around 500°C and a trace amount of added CeO_2 and TiO_2 (Ye *et al.*, 2008).

2. Effects of reaction temperature & S/C ratio

The H_2 yield was measured as a function of reforming temperature ranging from 750 to 900°C at S/C of 4 by using 15%Ni-5%Cu/12C7A-CeO_2-TiO_2. Figure 12 shows the effect of temperature on the H_2 yield for the catalytic steam reforming process. The results show that H_2 yields increase linearly with the increasing temperature and reach the maximum at 850°C (35.63%). Further increasing reaction temperature results in the decrease of H_2 yield to 31.13% at 900°C.

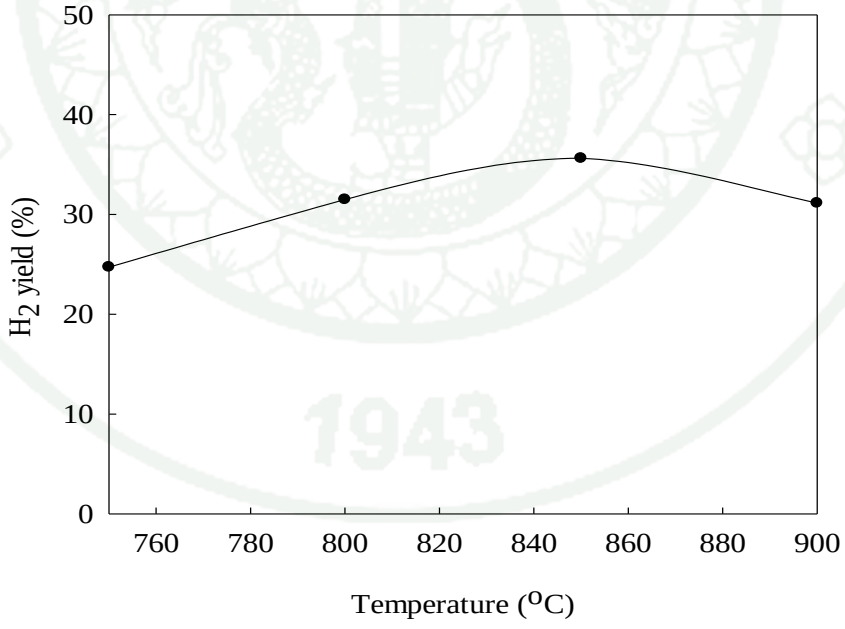

Figure 12 Effect of reaction temperature on the H_2 yield for steam reforming of acetic acid by using 15%Ni-5%Cu/12C7A-CeO_2-TiO_2 as a catalyst at S/C of 4 for 1 h.

The steam reforming reaction of oxygenated compound ($C_nH_mO_k + (n-k)H_2O \xrightarrow{\Delta} nCO + (n+\frac{m}{2}-k)H_2$) is endothermic and is favored by high temperature, leading to high H_2 yield. The water gas shift reaction ($nCO + nH_2O \overset{\Delta}{\leftrightarrow} nCO_2 + nH_2$) is exothermic (favors at lower temperature) and reversible reaction. Therefore, there is an optimum temperature providing the highest H_2 yield. At the reforming temperature of 900°C, the H_2 yield decreases because the undesired reverse water gas shift (as in reaction 15) which is endothermic initiates (Hu and Lu, 2009). Thus, in this study 850°C was chosen.

$$CO_2 + H_2 \rightarrow CO + H_2O \qquad (15)$$

The effect of S/C ratio on hydrogen yield was investigated by using 15%Ni-5%Cu/12C7A-CeO_2-TiO_2 catalysts at 850°C with various S/C ratios between 4 and 10. For increasing S/C ratio, H_2 yield increases when the increasing of S/C and leads to maximum at S/C of 8 (43.51%). Further increasing S/C ratio results in the decrease of H_2 yield to 39.71% as shown in Figure 13. Thus, the increase of steam amount S/C

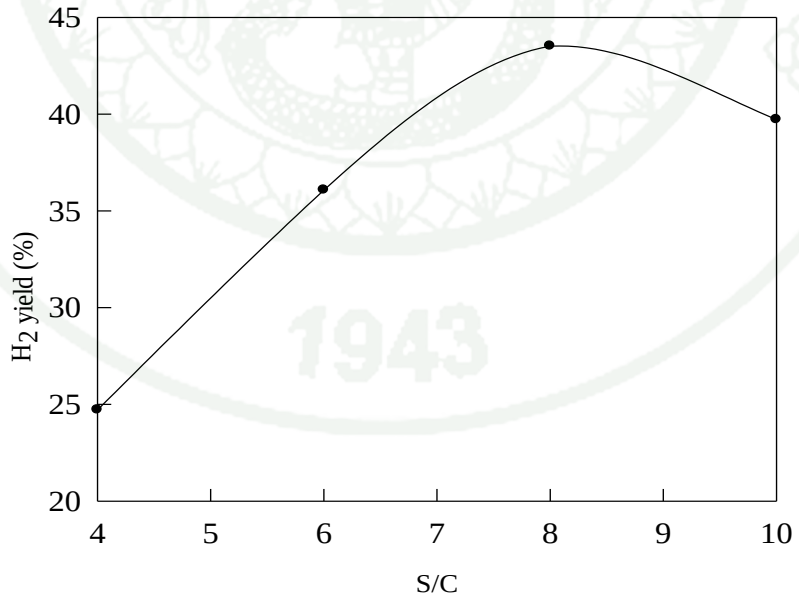

Figure 13 Effect of S/C on the H_2 yield for steam reforming process of acetic acid by using 15%Ni-5%Cu/12C7A-CeO_2-TiO_2 as catalyst at 850°C for 1 h.

ratio at a certain range promotes the forward reaction to obtain hydrogen and carbon dioxide. Moreover, the high partial pressure of steam promotes the adsorption of steam on the active sites thus the decomposition of the feedstocks is reduced (Hu and Lu, 2009), resulting in an increase of the H_2 yield at higher S/C ratio.

Thus, the operating conditions for steam reforming process were performed at 850^{o}C and S/C of 8 in order to obtain the highest hydrogen production.

3. Catalyst tests

3.1 Addition of supporting materials (CeO_2 and TiO_2) on the 12C7A

In order to study the effects of supporting materials on H_2 yield and product distribution (in term of selectivity), ceria and titania were added into the 12C7A. The tests were carried out at 850^{o}C, S/C of 8, and 1 h by using acetic acid as a representative component of bio-oil. The molar ratio between the 12C7A to CeO_2 or TiO_2 (supporting materials) investigated in this section was 2, whereas molar ratio of 12C7A:CeO_2:TiO_2 was 2:1:1.

The addition of CeO_2 or TiO_2 to 12C7A affects on H_2 yield and conversion of acetic acid as shown in Figure 14. The 12C7A provided H_2 yield of 22.53%, whereas the 12C7A:CeO_2 = 2 and 12C7A:TiO_2 = 2 increased the H_2 yields to 28.58 and 25.64%, respecttively. The 12C7A:CeO_2:TiO_2 of 2:1:1 provided the highest yield of H_2 gas about 30.28%. The conversions of acetic acid when using all types of supporting materials approached a maximum conversion about 100%.

The gaseous product distribution is reported in term of selectivity. Figure 15 shows the effect of supporting materials on selectivity of gaseous products (H_2, CO, CH_4, and CO_2). It can be seen that the 12C7A-CeO_2-TiO_2 provided the highest selectivity of H_2 about 0.85 but selectivities of CO, CH_4, and CO_2 were very low. The 12C7A-TiO_2 provided the lowest H_2 selectivity about 0.36. However, it provided the highest selectivities of CH_4 and CO_2, 0.037 and 0.48, respectively.

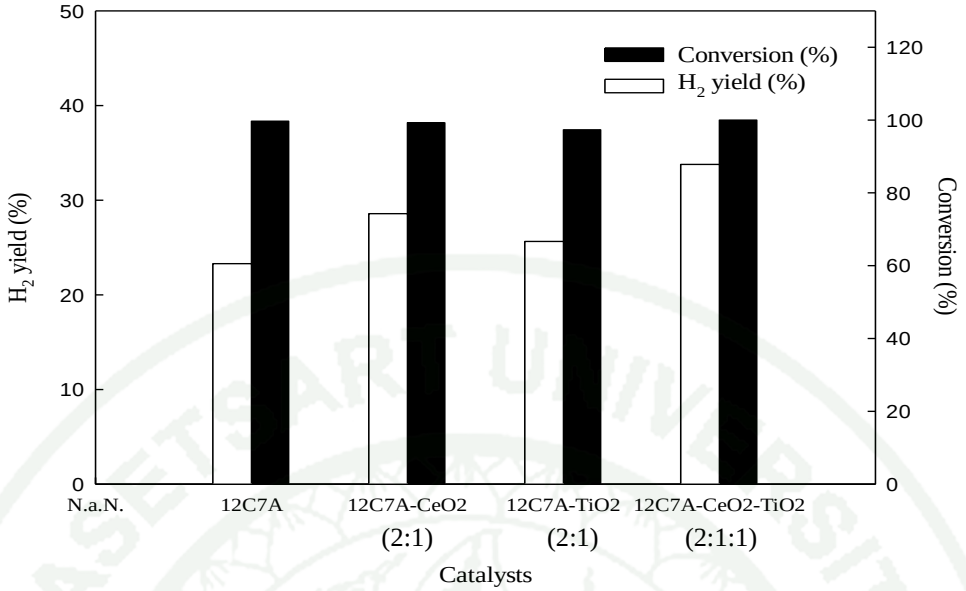

Figure 14 The effects of supporting materials (CeO_2 and TiO_2) on H_2 yield and conversion from steam reforming process of acetic acid at 850°C, S/C of 8, and 1 h.

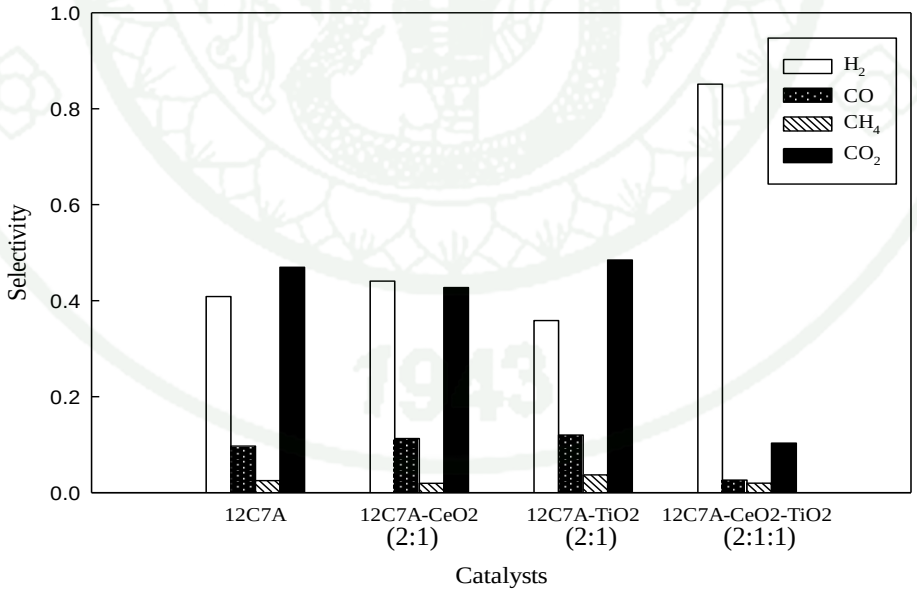

Figure 15 Effect of supporting materials (CeO_2 and TiO_2) on selectivity of gaseous products from steam reforming process of acetic acid at 850°C, S/C of 8, and 1 h.

Amount of coke formation on the catalyst was measured by TG-DTA and verified by quantity of weight loss in thermograms due to elimination of carbonaceous species on the catalyst surface corresponding to exothermic peaks as shown in Appendix E. The coke formation rates for 12C7A and the modified supports decreased in the order: 12C7A > 12C7A-CeO_2 > 12C7A-CeO_2-TiO_2 (1:1:1) > 12C7A-CeO_2-TiO_2 (2:1:1) > 12C7A-TiO_2 as shown in Figure 16. This indicated that CeO_2 and/or TiO_2 improved coke resistance on the support surface as these supporting materials have good oxygen storage capacity, which is beneficial for the elimination of coke deposited on the catalyst surface. Some researchers reported that addition of Ti in CeO_2 could form Ce–O–Ti solid solution, which improved the redox capacity of CeO_2.

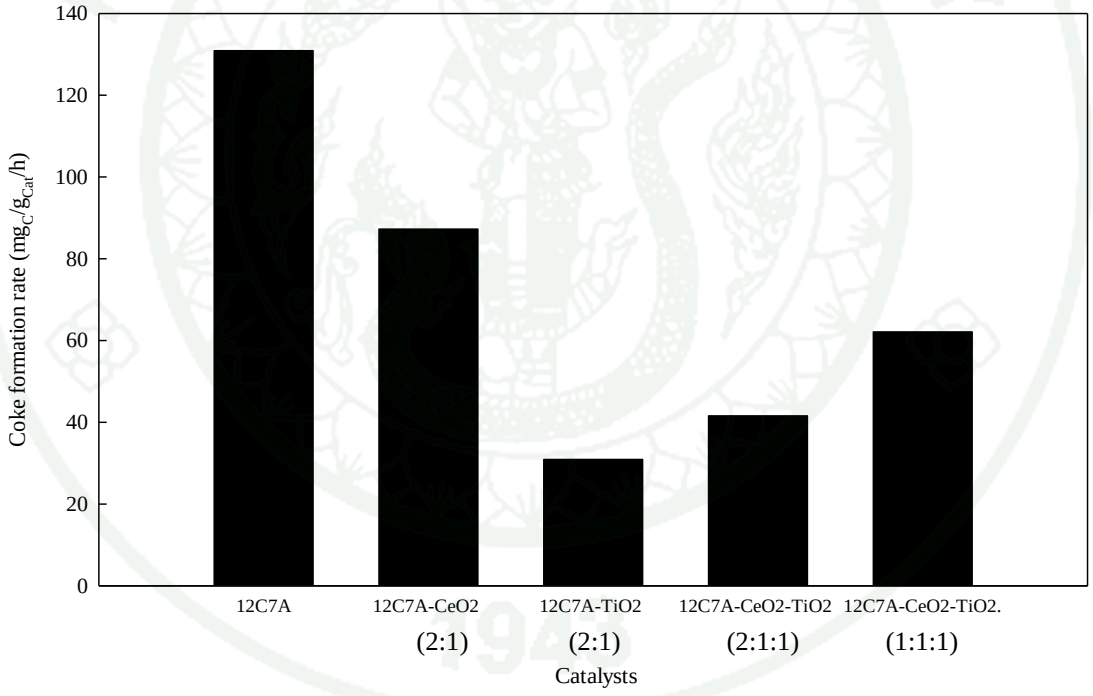

Figure 16 The supporting materials affect on coke formation during steam reforming of acetic acid at 850°C, S/C of 8, and 1 h.

According to Ye *et al*. (2008), Ni over Ce–O–Ti catalysts showed the high hydrogen selectivity and the molar ratios of Ce/Ti had obvious effect on products selectivity. The addition of Ce effectively improved the coke resistance of Ni/TiO_2

catalyst. They concluded that the amount of coke deposited due to TiO_2 is much higher than that of CeO_2. Moreover, the size of Ti^{4+} is smaller than Ce^{4+}, so that Ti^{4+} can substitute into the CeO_2 lattice structure and forms Ce–O–Ti solid solution. It was reported that the formation of Ce–O–Ti improved the oxygen mobility in catalysts for eliminating carbon on the catalyst surface.

Thus, the addition of an equimolar of ceria and titania can attribute to the improvement of activities for hydrogen production and coke resistance of calcium aluminate. The formation of Ce-O-Ti solid solution enhances oxygen radicals, O^{2-}, which are stored in the lattice structure of calcium aluminate.

Furthermore, effect of different molar ratios of 12C7A:CeO_2:TiO_2 (2:1:1 and 1:1:1) on hydrogen yield, selectivity of gaseous products, and coke formation rate were investigated via steam reforming of acetic acid at 850°C, S/C of 8, and 1 h. Figure 17 shows that different molar ratios of 12C7A:CeO_2:TiO_2 do not clearly affect the hydrogen yield and conversion of acetic acid.

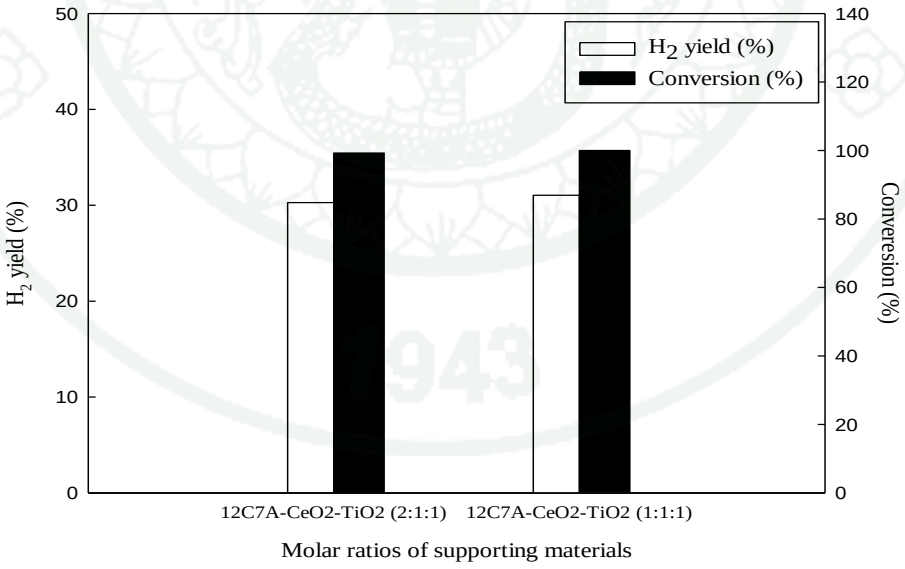

Figure 17 Effect of different molar ratios of supporting materials (12C7A:CeO_2: TiO_2) on H_2 yield and conversion of gaseous products from steam reforming process of acetic acid at 850°C, S/C of 8, and 1 h.

On the other hand, the gaseous product distribution indicated the altering of product selectivity as shown in Figure 18. The molar ratio of 12C7A:CeO_2:TiO_2 was varied from 2:1:1 to 1:1:1 led to a decrease of H_2 selectivity from 0.85 to 0.56 whereas the selectivity of CO_2 increased from 0.10 to 0.40. The selectivities of CO and CH_4 were similar in both ratios. Therefore, the 12C7A:CeO_2:TiO_2 molar ratio of 2:1:1 was selected because it provided higher H_2 selectivity and coke resistance as shown in Figure 16, coke formation rates dropped from 62 (1:1:1) to 42 (2:1:1) $mg_C/g_{Cat}/h$.

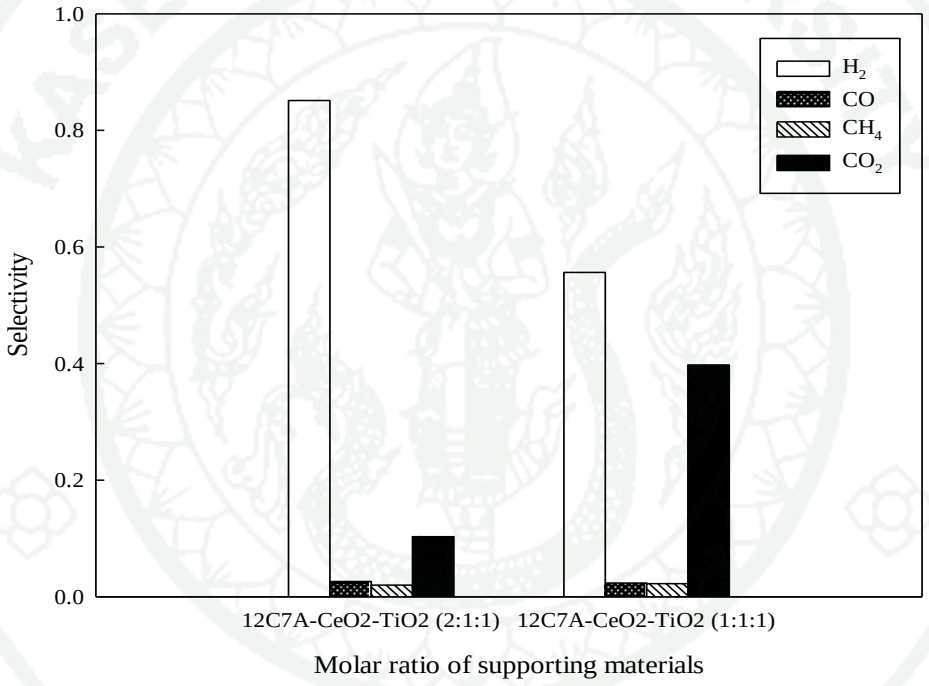

Figure 18 The effect of molar ratios of supporting materials on selectivity of gaseous products from steam reforming process of acetic acid at 850°C, S/C of 8 and 1 h.

3.2 Steam reforming of acetic acid by using promoted metals on Ni based catalyst

Acetic acid reforming tests were performed at 850°C, S/C of 8, and 1 h by using the Ni based catalyst or promoted metals (Cu, Co, Cr, and Mg) on Ni based

catalysts. As illustrated in Figure 19, the bimetallic Ni-Cu catalyst indicated the highest activity for hydrogen production providing 43.07% of H_2 yield and the second is the Ni-Co catalyst, which shows H_2 yield of 42.37%. The monometallic Ni catalyst shows higher activity for hydrogen production than that for some bimetallic catalysts including Ni-Cr and Ni-Mg catalysts. The Ni based catalyst provided 37.51% of H_2 yield compared to the Ni-Cr and Ni-Mg catalysts which provided H_2 yields of 25.18 and 23.58%, respectively.

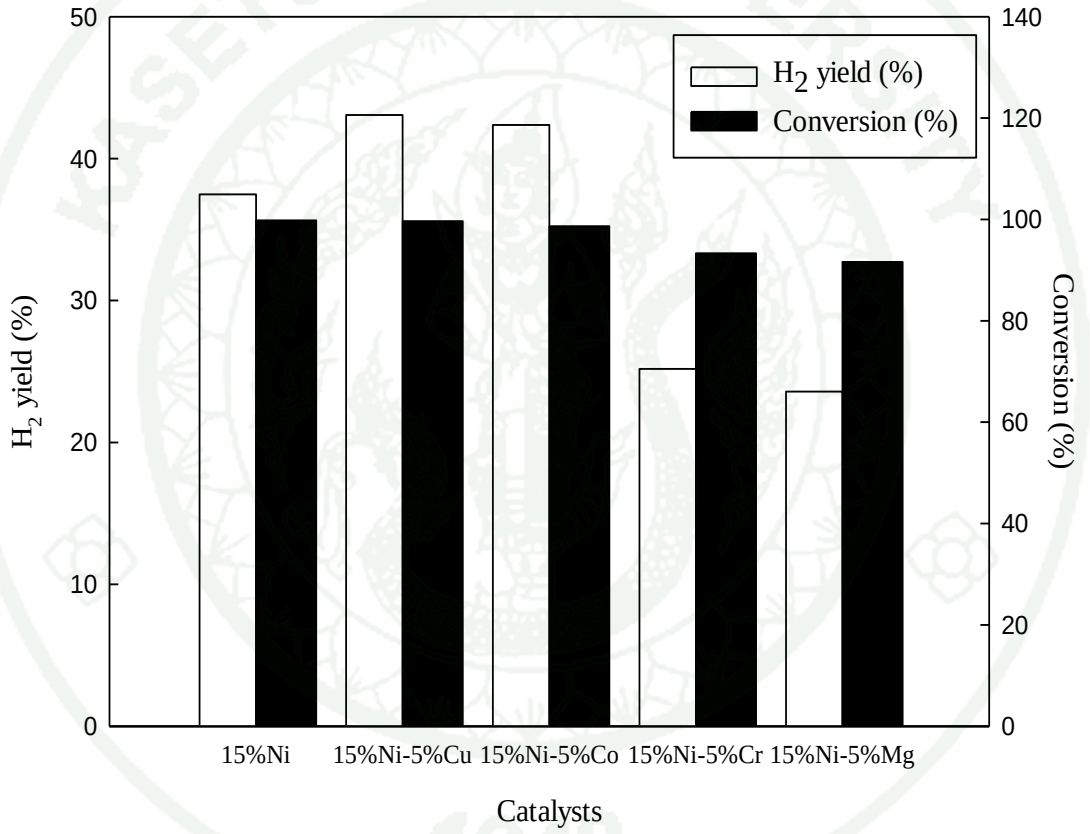

Figure 19 Effect of promoted metals over 15%Ni/12C7A–CeO_2–TiO_2 (2:1:1) on H_2 yield and acetic acid conversion from steam reforming process of acetic acid at 850^{o}C, S/C of 8, and 1 h.

The selectivities of gaseous products are depicted in Figure 20. The Ni-Cu catalyst indicated the highest selectivity of H_2 about 0.83 and provided a very low selectivity of CH_4 and CO of 0.014 and 0.018, respectively, which may attribute to a

poor activity for methanation reaction. The Ni, Ni-Co, and Ni-Mg catalysts provided H_2 selectivity of 0.49, 0.48, and 0.50, respectively. The Ni-Co catalyst provided the H_2 selectivity of 0.48 and provided the highest CO selectivity of 0.097 among all the promoted metals. The highest CO_2 selectivity of 0.69 was the Ni-Cr catalyst. In contrast, it provided the lowest H_2 yield of 0.29.

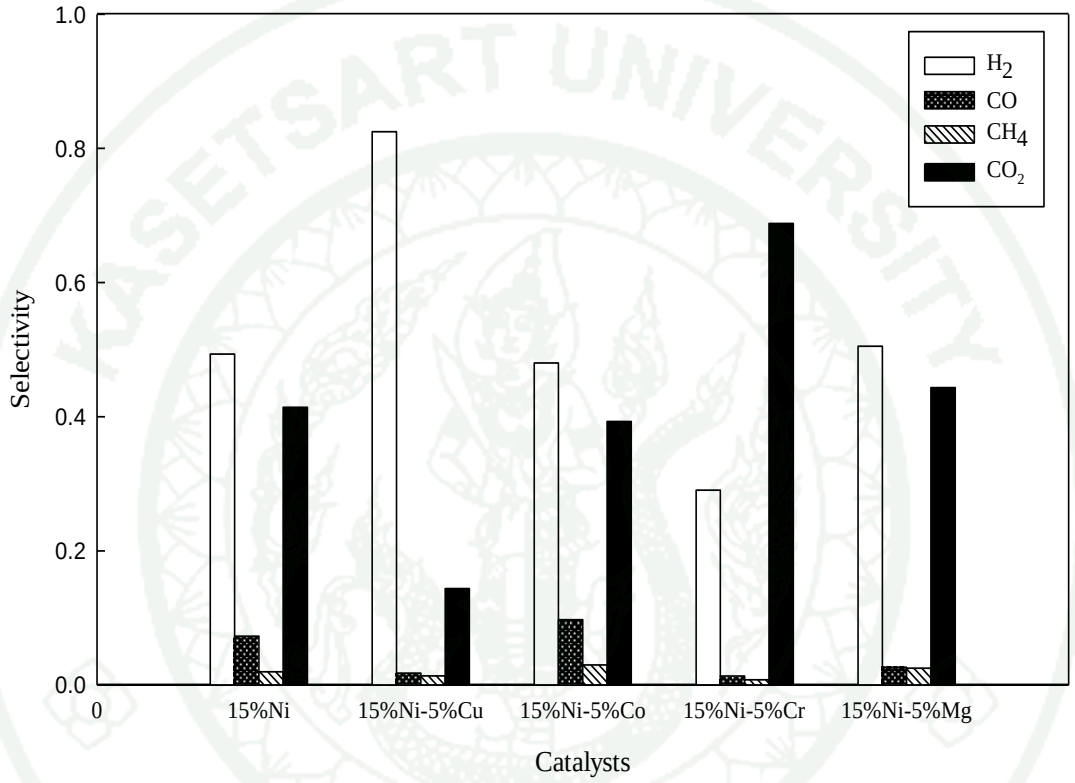

Figure 20 Effect of promoted metals over 15%Ni/12C7A–CeO_2–TiO_2 (2:1:1) on selectivity of gaseous products from steam reforming process of acetic acid at 850°C, S/C of 8, and 1 h.

In addition, comparison of the activity for hydrogen production between Ni based catalyst with different supports, 12C7A–CeO_2–TiO_2 (2:1:1) and Al_2O_3, was investigated. From the results, the Ni/12C7A–CeO_2–TiO_2 showed a higher activity for hydrogen production of 37.48%, whereas 32.41% of H_2 yield was obtained from the Ni/Al_2O_3 support as shown in Figure 21. Similar trend to H_2 yield, the acetic acid conversion of the Ni/12C7A–CeO_2–TiO_2 catalyst (99.8%) was higher than that for the Ni/Al_2O_3 catalysts (93.7%).

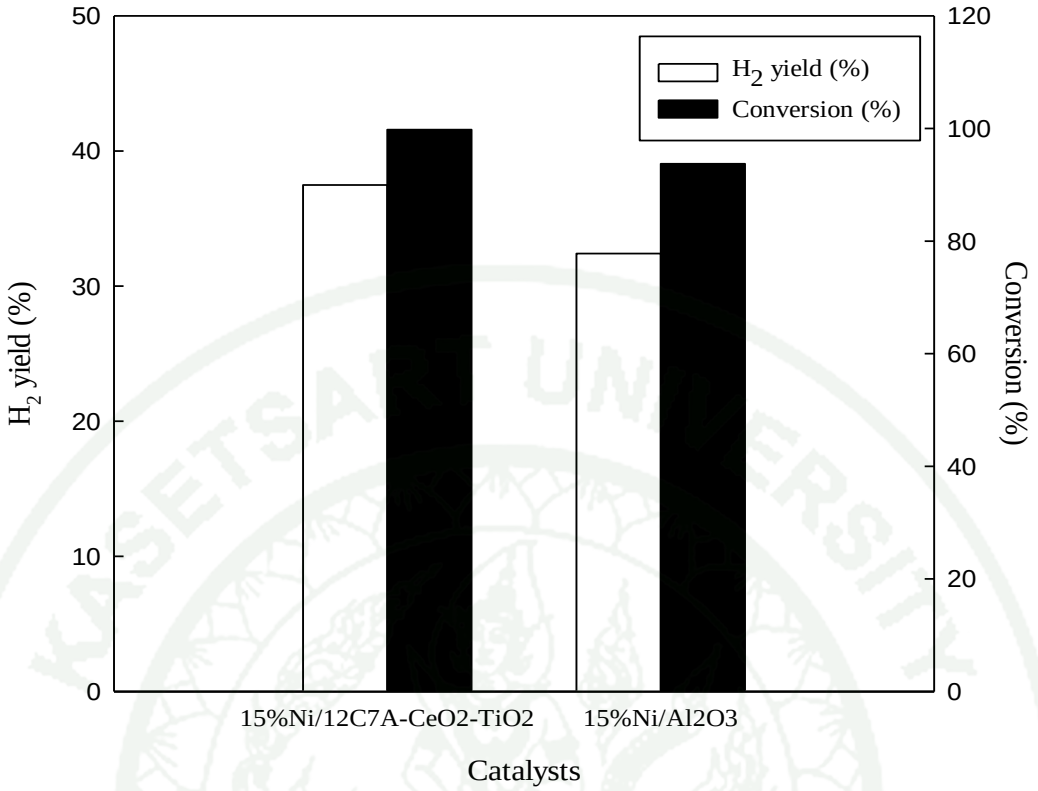

Figure 21 The effect of Ni based catalysts over 12C7A–CeO_2–TiO_2 (2:1:1) and Al_2O_3 on H_2 yield and acetic conversion from steam reforming process of acetic acid at 850^{o}C, S/C of 8, and 1 h.

Effect of different types of support on the selectivity of gaseous products is shown in Figure 22. The H_2 selectivity of Ni/12C7A–CeO_2–TiO_2 catalyst was higher than that for the Ni/Al_2O_3. Furthermore, the enhancement of CO_2 selectivity was observed for the Ni/Al_2O_3 catalyst by 0.54. While the CO selectivities showed a similar value about 0.73.

The data of coke deposited on the surface of the catalysts is summarized in Figure 23. The catalysts after reforming process during 1 h showed a weight loss due to elimination of carbonaceous species in thermograms obtained from TG-DTA technique. The bimetallic over 12C7A–CeO_2–TiO_2 catalysts enhanced a coke resistance compared to the Ni based catalyst for the same support. This refers to the promoted metals can prolong the catalyst life. While Cr and Mg metals dominantly

enhanced the coke resistance compared to Cu and Co metals. However, the Ni supported on alumina provided the lowest coke formation rate among all the catalyst tests.

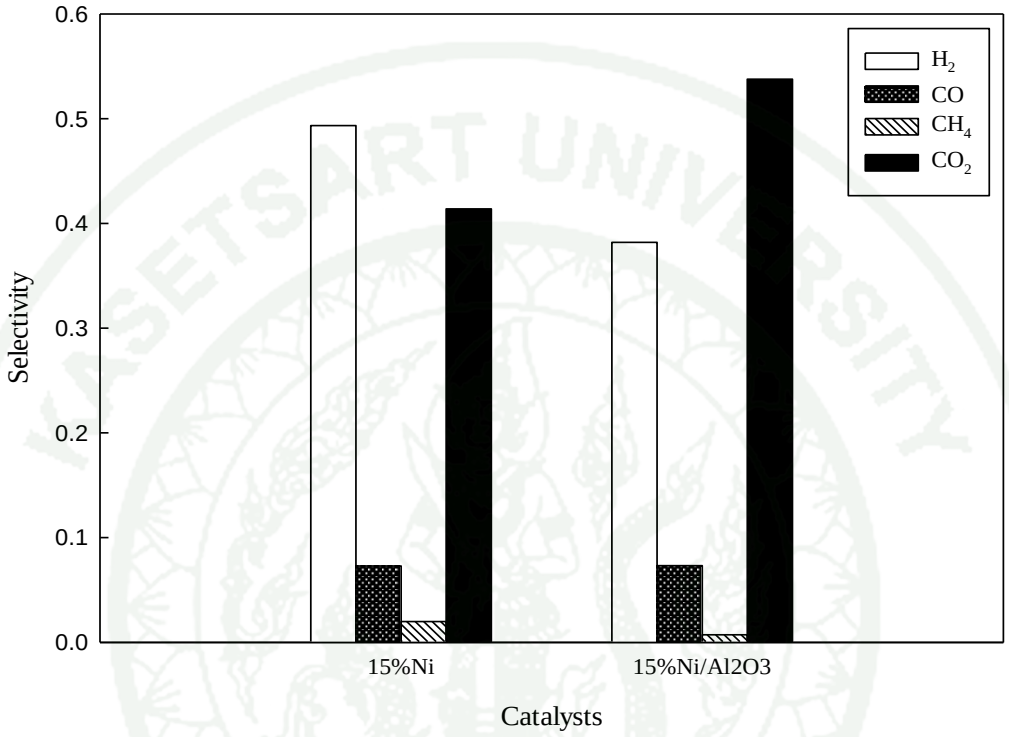

Figure 22 Comparison the effect of Ni based catalysts over 12C7A–CeO_2–TiO_2 (2:1:1) and Al_2O_3 on selectivity of gaseous products from steam reforming process of acetic acid at 850^{o}C, S/C of 8, and 1 h.

Sayed and Matin (2011) studied a deactivation and regeneration of Ni based catalysts via steam reforming of methane. This research used a commercial 18wt% Ni coated on calcium aluminate as the catalysts. They informed that the causes of a Ni based catalyst deactivation are coking, sintering, and poisoning. The deactivated catalyst was regenerated by using CO_2 as an oxidative atmosphere at 700^{o}C. The regenerated catalyst showed increment of methane conversion and H_2 yield up to 73% and 82%, respectively. Moreover, they concluded that the key factor to improve the catalytic performance of the Ni based catalyst is the decrement of sintered Ni particle size.

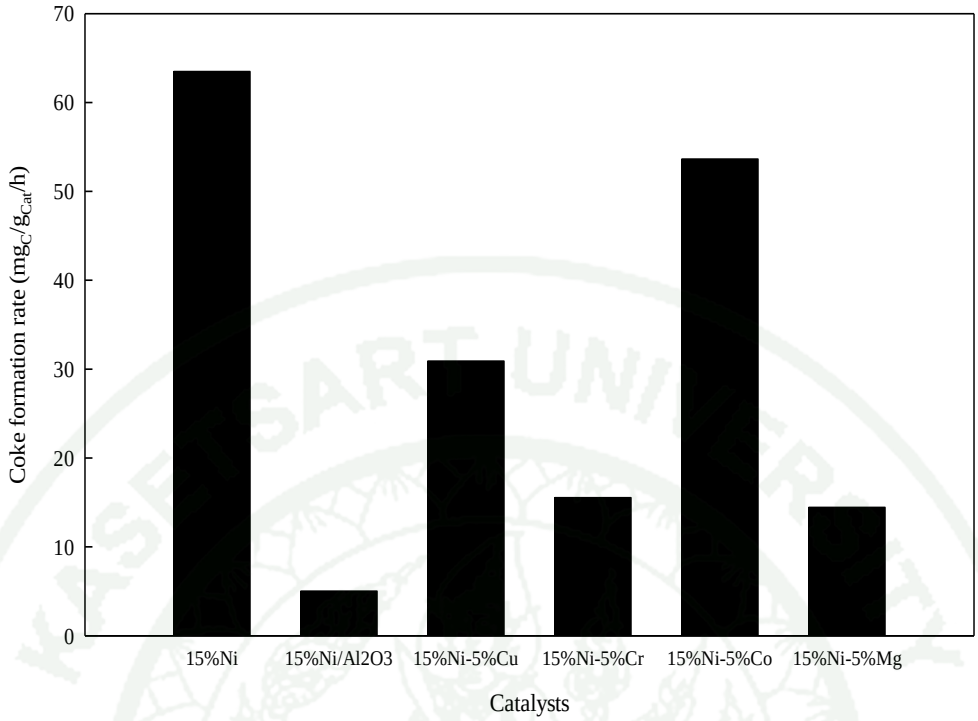

Figure 23 Coke formation during steam reforming of acetic acid at 850°C, S/C of 8, and 1 h.

According to Davda *et al*. (2005), Ni is well known that it promotes C-C bond cleavage. Furthermore they informed that Cu exhibits high activity for water-gas shift reaction resulting in improvement of steam reforming reaction to provide the highest H_2 yield.

Garcia *et al.* (2000) investigated the effects of catalyst composition for steam reforming of bio-oil at 825 to 875°C and S/C of 4.9 to 11.0 by using Ni over α-Al_2O_3 with some additives, MgO and La_2O_3 were used as support modifiers while Co and Cr additives were applied as a promoted metal. They concluded that Co and Cr metals modified the metal sites to form alloys with Ni metal and reducing the crystalline size. Mg and La enhanced steam adsorption facilitating the gasification of carbonaceous species on catalyst surface.

3.3 Steam reforming of acetone reforming by using promoted metals on Ni based catalyst

Acetone reforming was performed under the same experimental conditions as the acetic acid reforming. The activity for hydrogen production in term of H_2 yield is altered by the effect of loaded metals as shown in Figure 24. The yield of hydrogen trend is similar to the acetic acid reforming. The H_2 yield for the Ni based catalyst and promoted metals over Ni based catalysts decreased in the order: Ni-Cu > Ni-Co > Ni-Mg > Ni ≈ Ni-Cr catalysts. The Ni-Cu catalyst still showed a high hydrogen production activity for both acetic acid and acetone reforming reactions.

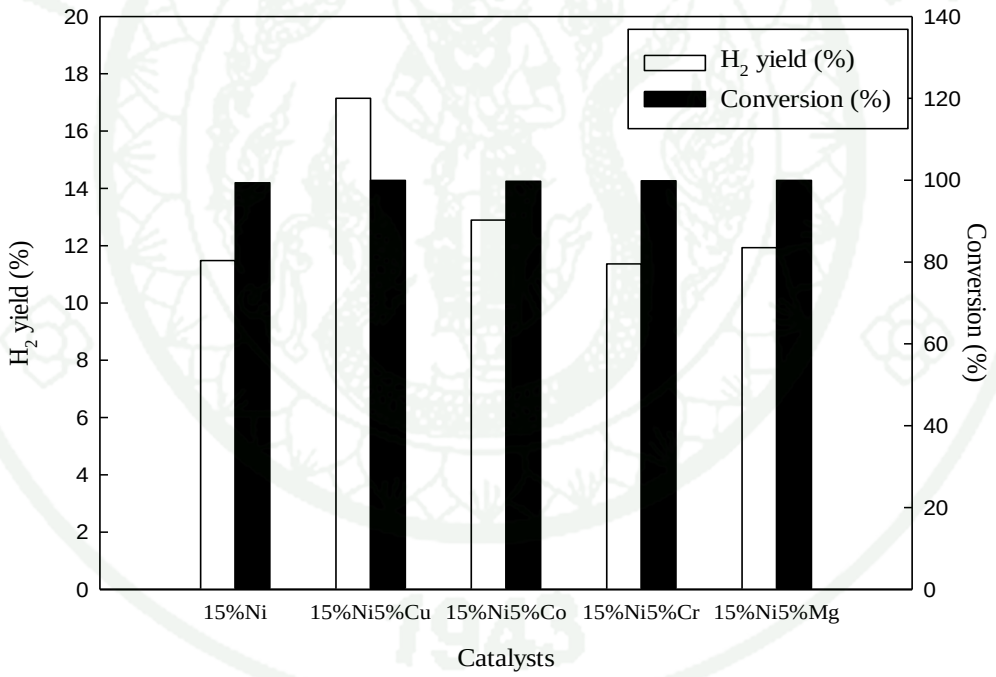

Figure 24 Effect of metal loading over 12C7A–CeO_2–TiO_2 (2:1:1) on H_2 yield and conversion from steam reforming process of acetone at 850°C, S/C of 8, and 1 h.

The distribution of the products from acetone and acetic acid reforming reactions are quite different. The H_2 selectivities of acetone reforming are lower than

that for acetic acid reforming among all catalyst tests as in illustrated in Figure 25. Moreover, the Ni-Cu catalyst also showed the highest selectivity of H_2 about 0.42 and the lowest selectivity of CH_4 about 0.024. In contrast, the high selectivity of CH_4 was observed from the Ni-Cr catalyst with the value of 0.24.

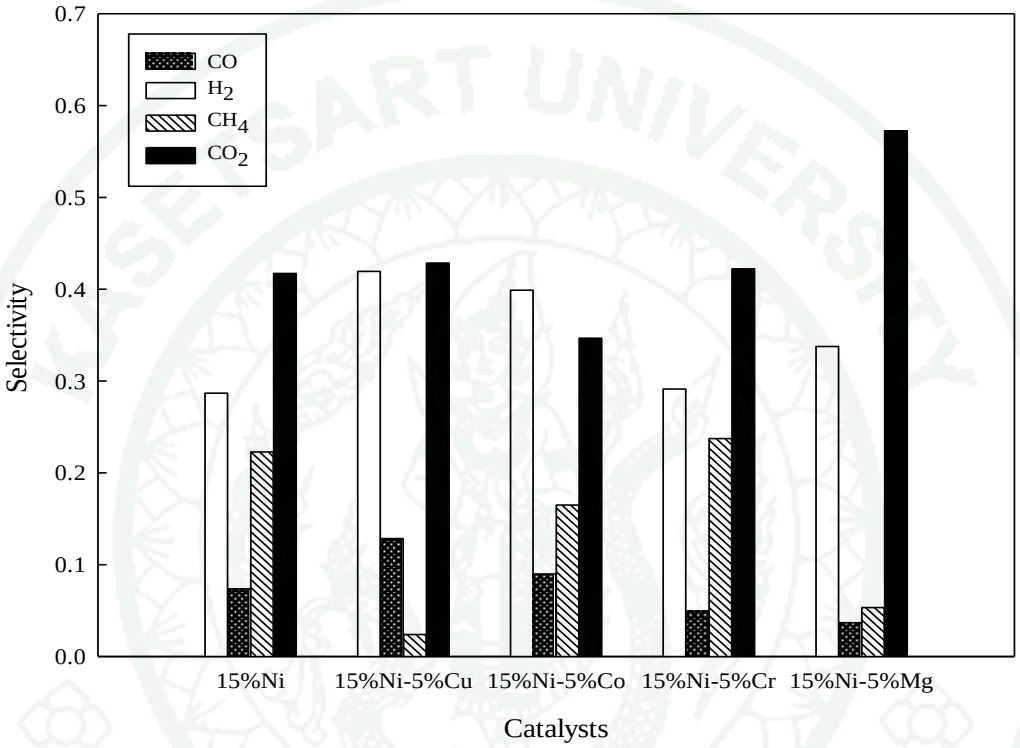

Figure 25 Effect of metal loading over 12C7A–CeO_2–TiO_2 (2:1:1) on selectivity of gaseous products from steam reforming process of acetone at 850°C, S/C of 8, and 1 h.

The main pathway of the products is the decomposition of acetone to ketene following reaction (16). The ketene intermediate may be reformed to CH_4 and CO_2 via hydration reaction following reaction (17) (Vagia and Lemonidou, 2008). This may attribute to the enhancement of CH_4 in the gaseous product resulting in the decreasing of hydrogen yield as described in the previous reaction of methanation (8) and (9).

$$CH_3COCH_3 \rightarrow CH_2CO + CH_4 \quad (16)$$

$$CH_2CO + H_2O \rightarrow CH_4 + CO_2 \quad (17)$$

Coke formation on surface of the catalysts via acetone reforming process is shown in Figure 23. When the promoted metals, Cu, Co, Cr, and Mg, were added into the Ni based catalyst, a decrease of coke formation rate was observed. In this case, the Ni-Cu catalyst showed the highest coke resistance due to providing the lowest coke formation rate (about 19.3 $mg_C/g_{Cat}/h$) which is quite different from the case of acetic acid reforming. The Ni-Cr catalyst provided high carbon deposit next to the Ni based catalyst, followed by the Ni-Mg catalyst. It should be noted that both Ni-Cr and Ni-Mg catalysts showed high coke resistance for acetic acid reforming. In contrast, the Ni-Co catalyst provided lower coke resistance compared to the acetic acid reforming.

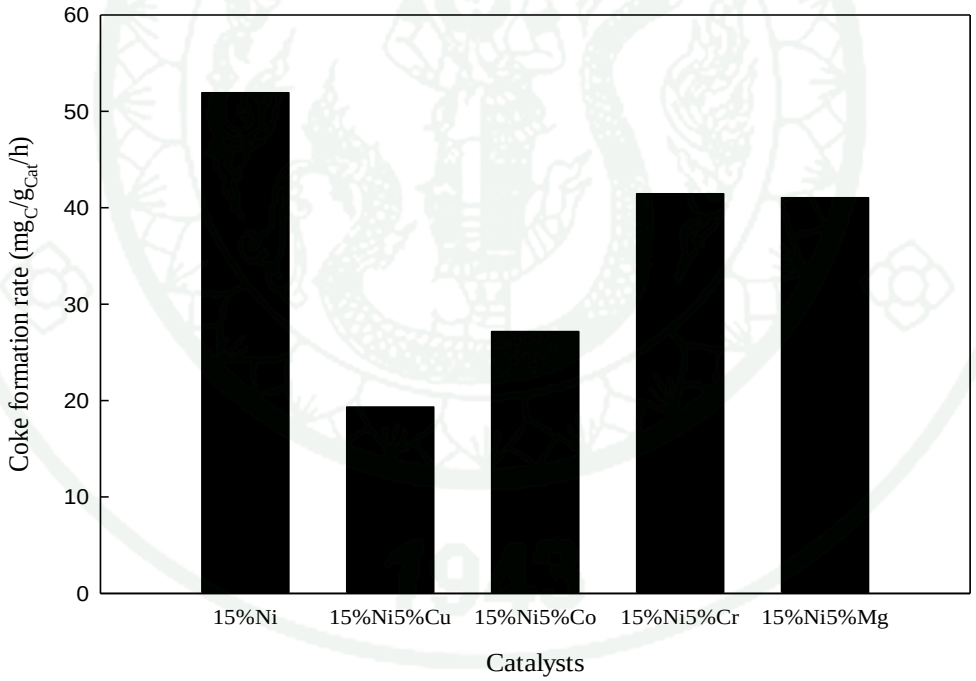

Figure 26 Coke formation during steam reforming of acetone at 850°C, S/C of 8, and 1 h.

4. Endurance test of the promoted Cu on Ni based catalyst

The stability of the promoted Cu on Ni based catalyst was tested for 12 h via steam reforming of acetic acid at 850°C and S/C of 8. As shown in Figure 22, the hydrogen yield over the 15%Ni-5%Cu/12C7A-CeO_2-TiO_2 (2:1:1) was 43% during the first 1 h. After that the hydrogen yield gradually decreased to 20% of the initial value after 10 to 12 h of reforming. Decrement of the hydrogen yield was observed for the longer term observation, indicating a gradual deactivation of the catalyst during the steam reforming of acetic acid. The catalyst's deactivation, occurring in the process of the steam reforming, may be caused mainly by the deposition of coke on the catalyst and sintering of the catalyst. The carbon deposited during reforming process for 12 h was reported as the coke formation on surface of the catalysts and it was 59.90 mg_C/g_{Cat}.

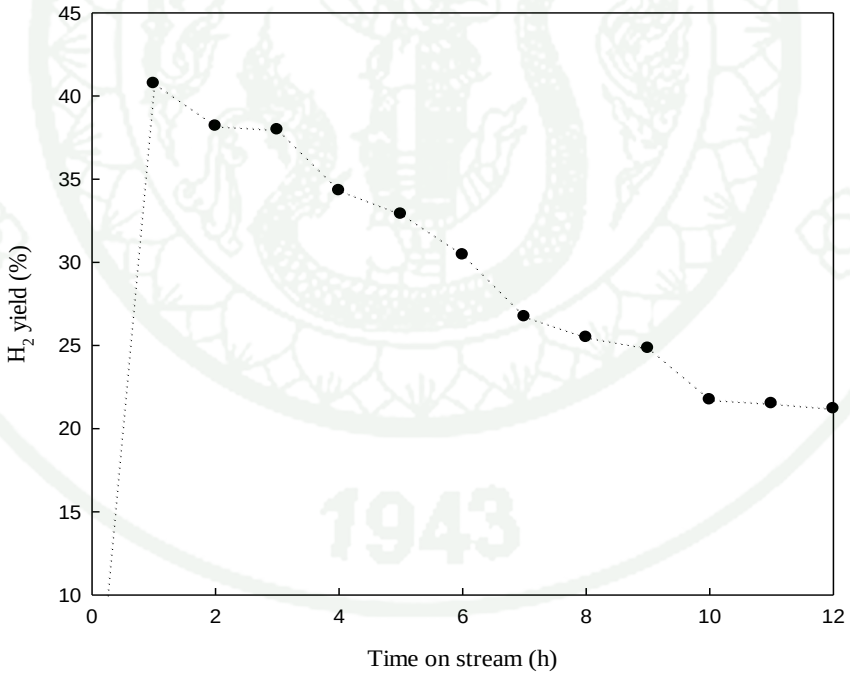

Figure 27 Stability test of 15%Ni-5%Cu/12C7A-CeO_2-TiO_2 catalyst via steam reforming of acetic acid at 850°C, S/C of 8, and 12 h.

5. Steam reforming process of the aqueous phase of bio-oil

The components of the aqueous phase of bio-oil obtained from pyrolysis process of coffee bean residue were analyzed by the gas chromatograph and mass spectrometer (GC-MS). Elemental components in the aqueous phase of bio-oil consist of carbon (C), hydrogen (H), nitrogen (N), and oxygen (O) shown in Table 2. From the results, carbon atom of 67.84 wt% was found as a main component in the aqueous phase of the bio-oil followed by oxygen (11.72 wt%), hydrogen (10.15 wt%), and nitrogen (5.35 wt%), respectively.

Table 2 Elemental components and a heating value of the aqueous of bio-oil from coffee beam residue.

Elemental components	Percent by weight (wt.%)
C	67.84
H	10.15
N	5.35
O	11.72
Empirical formula	$CH_{1.795}O_{0.171}N_{0.083}$
Heating value (MJ/kg)	3.60

Chemical components of the aqueous phase are listed in Table 3. The majority functional group is ketone compounds. Moreover, carboxylic acids, amines, esters and some derivative of heterocyclic compounds were found. The aqueous phase of bio-oil obtained from the coffee bean residue can be expressed in an empirical formula as $CH_{1.795}O_{0.171}N_{0.083}$.

According to the low heating value and compositions of the aqueous phase of bio-oil, it should be used in other applications rather than for upgrading or a direct fuel for engines. Therefore, previous reports often used the aqueous phase of bio-oil as a substance for hydrogen production via steam reforming or cracking process (Domine *et al.*, 2008).

Table 3 Chemical compositions of bio-oil produced from pyrolysis process of a coffee bean residue.

Compositions	Percent by weight (wt.%)	Molecular formula
Propanoic acid	1.22	$C_3H_6O_2$
1,3-Cyclopentanedione	3.65	$C_5H_6O_2$
3-Penten-2-one, 4-methyl-	7.43	$C_6H_{10}O$
2-Pentanone, 4-hydroxy-4-methyl-	7.26	$C_6H_{12}O_2$
2-Pyrrolidinone,1-methyl-	2.60	C_5H_9NO
N,N-Diethylacetamide	7.17	$C_6H_{13}NO$
Methylphenidyl acetate	10.95	$C_{14}H_{19}NO_2$
2-Cyclohexen-1-one, 6-[(dimethylamino)methylene]-	6.66	$C_9H_{13}NO$
4-Piperidinone,2 ,2, 6, 6-tetramethyl-	40.85	$C_9H_{17}NO$
Ethylcyclopentenolone	7.35	$C_7H_{10}O_2$
Phenol,2,4-bis(1,1-dimethylethyl)-	1.64	$C_{14}H_{22}O$
Caffeine	3.22	$C_8H_{10}N_4O_2$

The aqueous phase of bio-oil obtained from pyrolysis process of coffee bean residue was tested for steam reforming process at 850^{o}C, S/C of 8, and 1 h. The 15%Ni-5%Cu over 12C7A-CeO_2-TiO_2 catalyst was chosen for the aqueous phase of bio-oil reforming because it provided the highest activity for hydrogen production as mentioned in previous section for the reforming of model compounds, acetic acid and acetone.

The results show that the aqueous phase of bio-oil reforming provided H_2 yield of 21.18% while the selectivity of gaseous products is reported in Figure 28. Compared to the acetic reforming, the selectivity of H_2 in bio-oil was lower but was close to that from the acetone reforming. The trend of gaseous products distribution of the aqueous phase's bio-oil reforming is also close to the acetone reforming test.

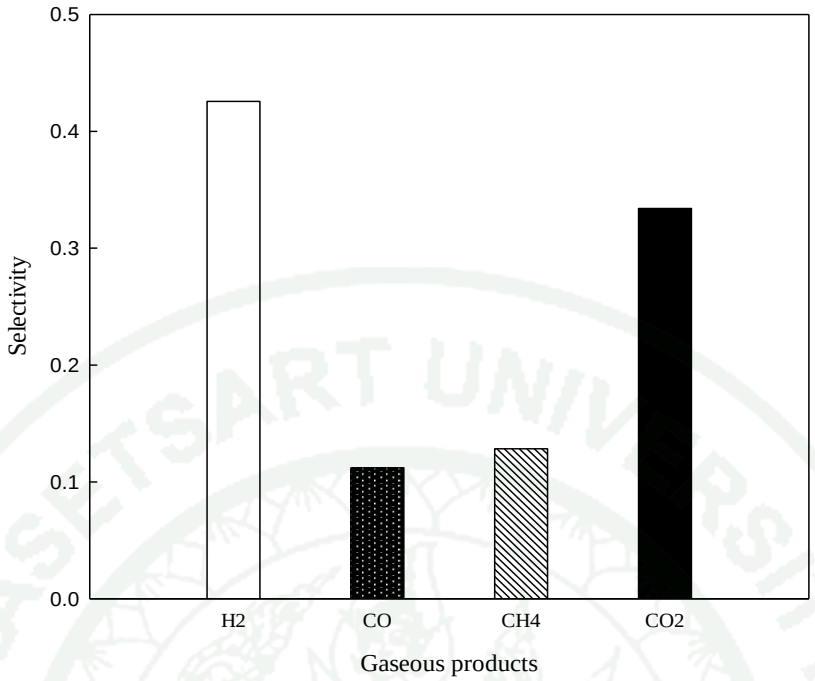

Figure 28 Selectivity of gaseous products from steam reforming of the aqueous phase of bio-oil by using 15%Ni-5%Cu/12C7A-CeO_2-TiO_2 as a catalyst at 850^{o}C, S/C of 8, and 1 h.

Since the major chemical composition of aqueous phase of bio-oil consisting of ketone group as shown in the GC-MS results, acetone can be attributed to a good representative component of the aqueous oil for explanation the reforming behavior of the aqueous phase of bio-oil. The catalyst after 1 h reaction was determined for the amount of coke deposited on a catalysts surface and showed 47.04 $mg_C/g_{Cat}/h$ of coke formation rate.

CONCLUSION AND RECOMMENDATION

Conclusion

Catalytic steam reforming of representative components of bio-oil, acetic acid and acetone, by using Ni/12CaO.7Al_2O_3-CeO_2-TiO_2 catalysts is favored by increasing the reaction temperature and S/C ratio. The hydrogen yield of 43% was obtained under the optimum steam reforming conditions; reforming temperature at 850^oC, S/C ratio of 8, using the 15%Ni-5%Cu/12C7A-CeO_2-TiO_2 as a catalyst for 1 h.

The effects of supporting materials, ceria and titania, on 12C7A were carried out at 850^oC, S/C of 8, 1 h, and using acetic acid as a representative component of bio-oil. Addition of CeO_2 and TiO_2 into the 12C7A provided the highest yield and selectivity of hydrogen. The coke formation rates for the 12C7A and modified supports decreased in the order: 12C7A > 12C7A-CeO_2 > 12C7A-CeO_2-TiO_2 (1:1:1) > 12C7A-CeO_2-TiO_2 (2:1:1) > 12C7A-TiO_2. Different molar ratios of 12C7A:CeO_2:TiO_2 (2:1:1 and 1:1:1) affected the activity for hydrogen production and coke formation rate. The results showed higher H_2 selectivity and coke resistance at the ratio of 2:1:1

Acetic acid reforming tests were performed at 850^oC, S/C of 8, 1 h, using the Ni based catalyst or promoted metals (Cu, Co, Cr, and Mg) on Ni based catalysts. The results show that the bimetallic Ni-Cu catalyst indicated the highest activity for hydrogen production and selectivity providing 43.07% of H_2 yield and 0.83 of selectivity, whereas the Ni-Co catalyst is inferior to the Ni-Cu catalyst. The monometallic Ni catalyst shows higher yield of hydrogen than that for some bimetallic catalysts including Ni-Cr and Ni-Mg catalysts. Moreover, the bimetallic over 12C7A–CeO_2–TiO_2 catalysts enhanced coke resistance compared to the Ni based catalyst for the same support. This means the promoted metals can prolong the catalyst life.

Acetone reforming was performed under the same experimental conditions as the acetic acid reforming. The gaseous products distribution between the acetone and acetic acid reforming are quite different. The acetone reforming showed the high selectivity of CH_4. It can be attributed to a decrease of hydrogen yield and selectivity.

The stability of promoted Cu on Ni based catalyst was tested for 12 h via steam reforming of acetic acid. The result indicated that after 1 h the hydrogen yield gradually dropped from 43 to 20% for about 10 to 12 h during reforming. An aqueous phase of bio-oil produced from pyrolysis of coffee bean residue was tested by using 15%Ni-5%Cu/12C7A-CeO_2-TiO_2 and provided 21.18% of hydrogen yield.

Recommendation

The mixed oxide of ceria and titania with an equimolar amount of Ce/Ti may be prepared by co-precipitation method to improve homogeneity of the mixed oxide catalyst. The effect of calcium aluminate preparation techniques to the results including hydrogen yield, conversion, and product distribution should be investigated. Moreover, the amounts of promoted metals and nickel metal should be varied to provide a suitable quantity to enhance the activity of hydrogen production.

From the TPR results, classification of each peak in the profiles may be performed by additional TPR data of the monometallic of promoted metals (Cu, Co, Cr, and Mg) over 12C7A-CeO_2-TiO_2.

For a gas collecting step, the online GC and mass flow control are required for the gaseous product analysis in order to diminish some errors in this process due to leakage of products and unstable flow rate of gas outlet.

LITERATURE CITED

Cao, Q., K.C. Xie, W.R. Bao and S.G. Shen. 2004. Pyrolytic behavior of waste corn cob. **Bioresource Technology**. 94: 83-89.

Cox, J.L., A.Y. Tonkovich, D.C. Eilliott, E.G. Baker and E.J. Hoffman**.** 1995. **Proceeding of Second Biomass Conference of the Americas**. Portland, p.657.

Czernik, S., R. French, C. Feik and E. Chornet. 2002. Hydrogen by catalytic steam reforming of liquid byproducts from biomass thermoconversion processes. **Industrial and Engineering Chemistry Research**. 41 (17): 4209-4215.

Davda, R.R., J.W. Shabaker, G.W. Huber, R.D. Cortright and J.A. Dumesic, 2005. A review of catalytic issue and process conditions for renewable hydrogen and alkanes by aqueous-phase reforming of oxygenated hydrocarbons over supported metal catalysts. **Applied Catalysis B: Environmental**. 56: 171-186.

Domine, M. E., E. E. Jojiu, T. Davidian, N. Guilhaume and C. Mirodatos, 2008. Hydrogen production from biomass-derived oil over monolithic Pt- and Rh-based catalysts using steam reforming and sequential cracking process. **Catalysis Today**. 133-135: 565-573.

Furtado, A. C., C. G. Alonso, M. P. Cantão, and N. R. C. Fernandes-Machado. 2009. Bimetallic catalysts performance during ethanol steam reforming: Influence of support materials. **International Journal of Hydrogen Energy**. 34: 7189-7196.

Garcia, L., R. French, S. Czernik and E. Chornet. 2000. Catalytic steam reforming of bio-oils for the production of hydrogen: effects of catalyst composition. **Applied Catalysis A: General**. 201: 225-239.

Goula, M. A., A. A. Lemonidou and A. M. Efstathiou. 1996. Characterization of carbonaceous species formed during reforming of CH_4 with CO_2 over Ni/CaO-Al_2O_3 catalysts studied by various transient techniques**. Journal of Catalysis.** 161 (2): 626-640**.**

Goyal, H.B., D. Seal and R.C. Saxena. 2008. Bio-fuels from thermochemical conversion of renewable resources: A review. **Renewable and Sustainable Energy Reviews**. 12: 504–517.

Hosono, H., K. Hayashi and M. Hirano. 2007. Active anion manipulation for emergence of active functions in the nanoporous crystal $12CaO{\cdot}7Al_2O_3$: a case study of abundant element strategy. **Journal of Materials Science**. 42: 1872-1883.

Hu, X. and G. Lu. 2009. Investigation of the steam reforming of a series of model compounds derived from bio-oil for hydrogen production. **Applied Catalysis B: Environmental**. 88: 376-385.

Larson, E.D., R.E. Katofsky and A.V. Bridgwater. **Advances in Thermochemical Biomass Conversion**, Blackie, London, 1994, p.495.

Lemonidou, A. A., and I. A. Vasalos. 1989. Preparation and evaluation of catalysts for the production of ethylene via steam cracking: Effect of operating condition on the performance of $12CaO\text{-}7Al_2O_3$ catalyst. **Applied Catalysis**. 54: 119-138.

Lemonidou, A. A., M. A. Goula and I. A. Vasalos. 1998. Carbon dioxide reforming of methane over 5 wt.% nickel calcium aluminate catalysts Effect of preparation method**. Catalysis Today**. 46 (2-3): 175-183.

Luo, Z., S. Wang, Y. Liao, J. Zhou, Y. Gu and K. Cen. 2004. Research on biomass fast pyrolysis for liquid fuel. **Biomass Bioenergy.** 26: 455–62.

Oasmaa, A., and D. Meier. **Fast Pyrolysis of Biomass: A Handbook**, vol. 2, Newbury, UK, 2002, p. 41-58.

Profeti, Luciene P.R., E. A. Ticianelli and E. M. Assaf. 2009. Ethanol steam reforming for production of hydrogen on magnesium aluminate-supported cobalt catalysts promoted by noble metals. **Applied Catalysis A: General.** 360: 17-25.

Rioche, C., S. Kulkarni, F. C. Meunier, J. P. Breen and R. Burch. 2005. Steam reforming of model compounds and fast pyrolysis bio-oil on supported noble metal catalysts. **Applied Catalysis B: Environmental**. 61: 130-139.

Sakamoto, N., M. Hori, Y. Matsuyama, N. Wakiya and H. Suzuki. 2009. Oxygen-enhanced crystallization of solution-derived $12CaO.7Al_2O_3$. **Journal of American Ceramic Society**. 92: 189-191.

Sayed, S. M. and P. Matin. 2011. Deactivation of nickel-based catalysts for steam-methane reforming. **Chinese Journal of Catalysis**. 32:273-279.

Singhto, W., N. Laosiripojana, S. Assabumrungrat and S. Charojrochkul. 2006. Steam reforming of bio-ethanol over Ni on Ce-ZrO_2 support: Influence of redox properties on the catalyst reactivity. **Songklanakarin Journal of Science and Technology**. 28(6): 1251-1264.

Ulrike, D. 2003. The surface science of titanium dioxide. **Surface Science Reports**. 48: 53-229.

Vagia, E.C. and A. A. Lemonidou. 2008. Hydrogen production via steam reforming of bio-oil components over calcium aluminate supported nickel and noble metal catalysts. **Applied Catalysis**. 351: 111–121.

Vizcaíno, A.J., A. Carrero and J.A. Calles. 2007. Hydrogen production by ethanol steam reforming over Cu–Ni supported catalysts. **International Journal of Hydrogen Energy**. 32: 1450–1461.

Wang, Z., Y. Pan, T. Dong, X. Zhu, T. Kan, L. Yuan, Y. Torimoto, M. Sadakata and Q. Li. 2007. Production of hydrogen catalytic reforming of bio-oil using C12A7-O^--based catalysts. **Applied Catalysis**. 320:24-34.

Wittayakun, J. and N. Grisdanurak. 2004. **Catalysis: Fundamentals and applications**. 1st ed. Thammasat University Publisher, Bangkok.

Wu, C., Q. Huang, M. Sui, Y. Yan and F. Wang. 2008. Hydrogen production via catalytic steam reforming of fast pyrolysis bio-oil in a two-stage fixed bed reactor system. **Fuel Processing Technology**. 89: 1306-1316.

Xu, H., L. Gao, H. Gu, J. Gao and D. Yan. 2002. Synthesis of solid, spherical CeO_2 particles prepared by the spray hydrolysis reaction method. **Journal of the American Ceramic Society**. 85: 139-144.

Xu, S. 2007. **Electrolyte and electrode in slid oxide fuel cell (SOFC).** University of Florida, Florida.

Yang, S., J.N. Kondo, K. Hayashi, M. Hirano, K. Domen and H. Hosono. 2004. Partial oxidation of methane to syngas over promoted C12A7. **Applied Catalysis A: General.** 277 (1-2): 239-246.

Yanik, J., C. Kornmayer, M. Saglam and M. Yüksel. 2007. Fast pyrolysis of agricultural wastes: Characterization of pyrolysis products. **Fuel Processing Technology**. 88 (10): 942-947.

Ye, J. L., Y.Q. Wang, Y. Liu and H. Wang. 2008. Steam reforming of ethanol over Ni/ $Ce_xTi_{1-x}O_2$ catalysts. **International Journal of Hydrogen Energy**. 33: 6602–6611.

Zhang, H., R. Xiao, H. Huang and G. Xiao. 2009. Comparison of non-catalytic and catalytic fast pyrolysis of corncob in a fluidized bed reactor. **Bioresource Technology**. 100:1428-1434.

APPENDICES

Appendix A

Chromatograms and peak areas of standard gases obtained from gas chromatography

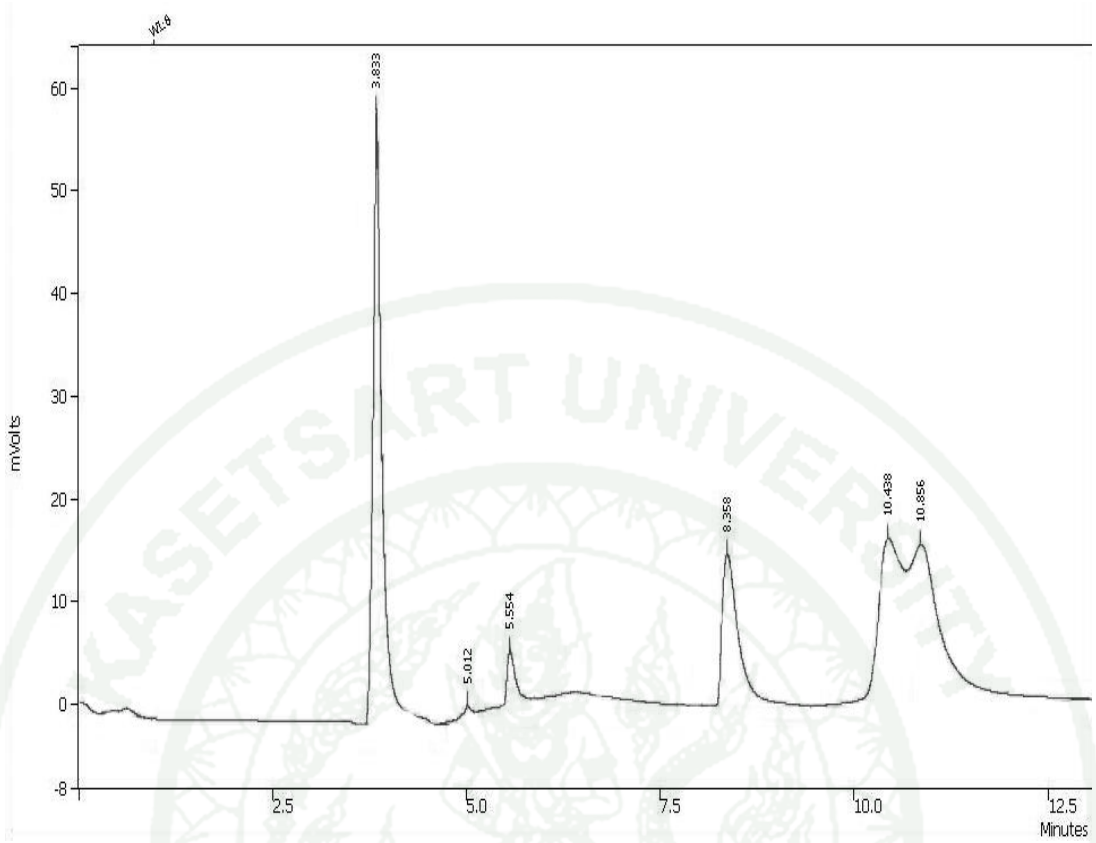

Appendix Figure A1 Chromatogram of 0.2 mL standard mixed gas.

Appendix Table A1 Peak area and retention time of 0.2 mL standard mixed gas from chromatogram Appendix Figure A1

Peak No.	Gasses	Result	Ret. Time (min)	Area (counts)	Width ½ (sec)
1	H_2	24.6250	3.833	492838	6.4
2	N_2	0.9151	5.012	18314	0.0
3	CO	5.3715	5.554	107503	9.2
4	CH_4	13.1551	8.358	263283	13.7
5	CO_2	18.7651	10.438	375560	17.6
		24.4621	10.856	489579	42.8
Total		100.0000		2001375	

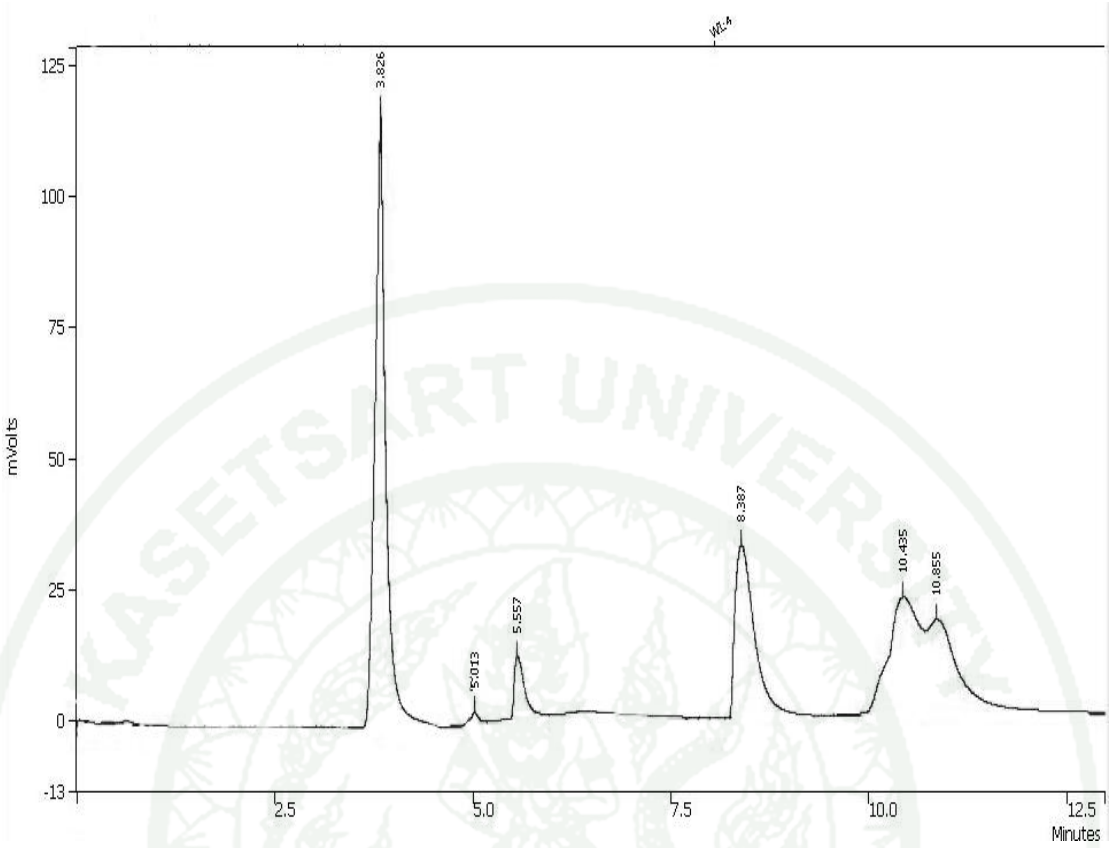

Appendix Figure A2 Chromatogram of 0.4 mL standard mixed gas.

Appendix Table A2 Peak area and retention time of 0.4 mL standard mixed gas from chromatogram Appendix Figure A2

Peak No.	Gasses	Result	Ret. Time (min)	Area (counts)	Width ½ (sec)
1	H_2	34.7596	3.826	1118313	7.7
2	N_2	0.1677	5.013	19462	0.0
3	CO	4.9861	5.557	160418	8.9
4	CH_4	17.7466	8.387	570957	0.0
5	CO_2	19.6870	10.435	633385	22.2
		17.5004	10.855	563035	36.3
Total		100.0000		3217277	

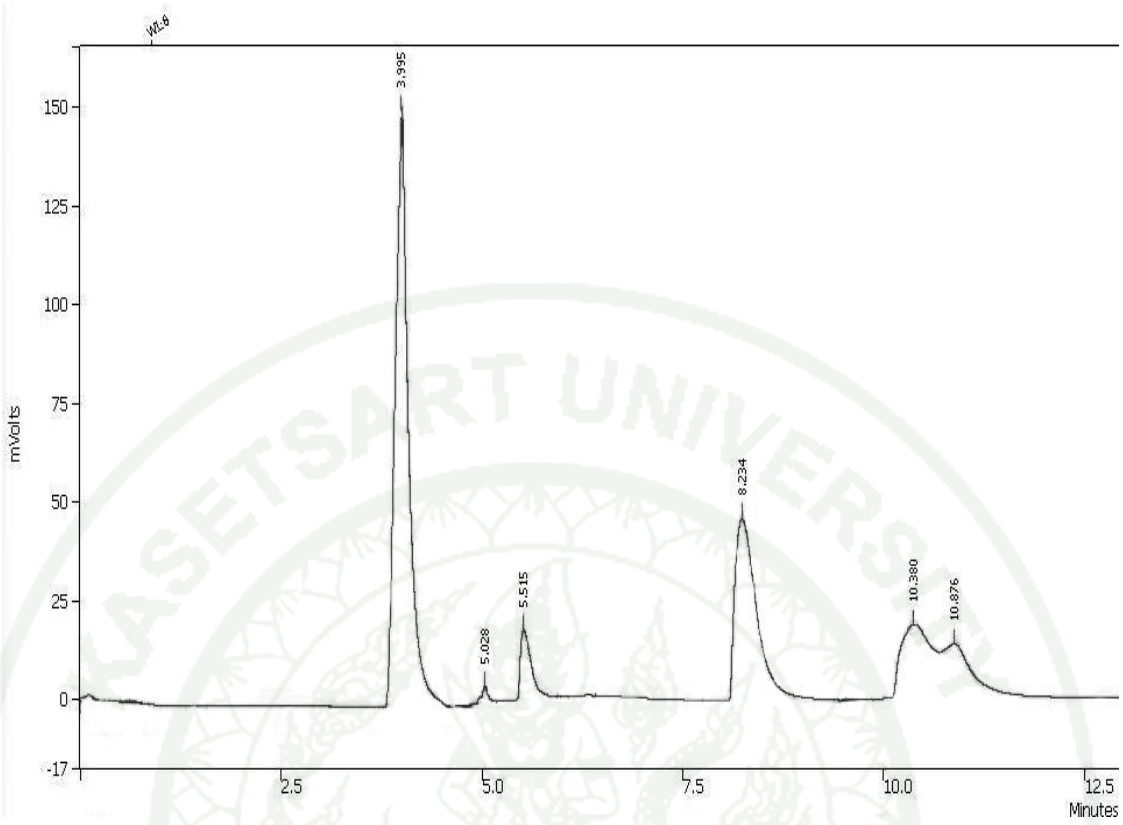

Appendix Figure A3 Chromatogram of 0.6 mL standard mixed gas.

Appendix Table A3 Peak area and retention time of 0.6 mL standard mixed gas from chromatogram Appendix Figure A3

Peak No.	Gasses	Result	Ret. Time (min)	Area (counts)	Width ½ (sec)
1	H_2	39.5993	3.995	1766295	10.0
2	N_2	0.4380	5.028	19538	0.0
3	CO	5.5196	5.515	246197	9.2
4	CH_4	22.2234	8.234	991254	17.5
5	CO_2	12.5468	10.380	559639	25.7
		12.1723	10.876	542934	44.9
Total		100.0000		4460413	

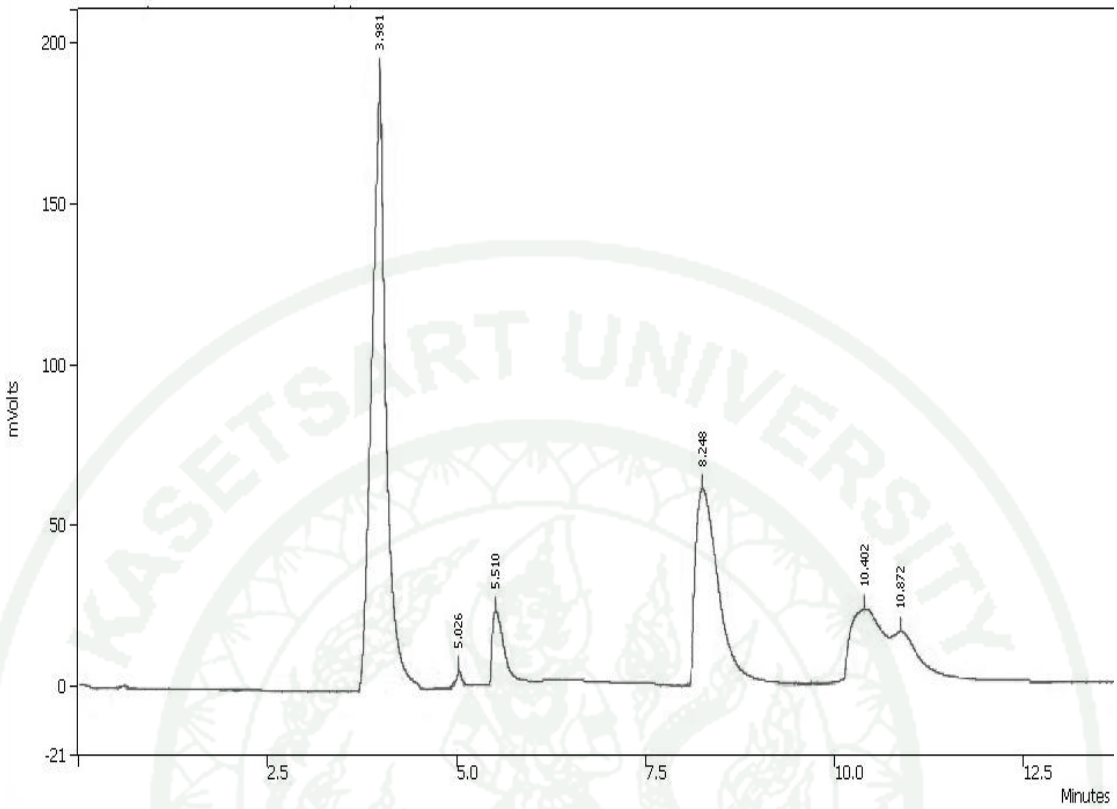

Appendix Figure A4 Chromatogram of 0.8 mL standard mixed gas.

Appendix Table A4 Peak area and retention time of 0.8 mL standard mixed gas from chromatogram Appendix Figure A4

Peak No.	Gasses	Result	Ret. Time (min)	Area (counts)	Width ½ (sec)
1	H_2	44.1429	3.981	2530835	11.3
2	N_2	0.4132	5.026	23689	0.0
3	CO	5.7456	5.510	329409	10.5
4	CH_4	23.8705	8.248	1368564	20.7
5	CO_2	12.1251	10.402	695163	0.0
		9.1307	10.872	523488	45.0
Total		100.0000		5733276	

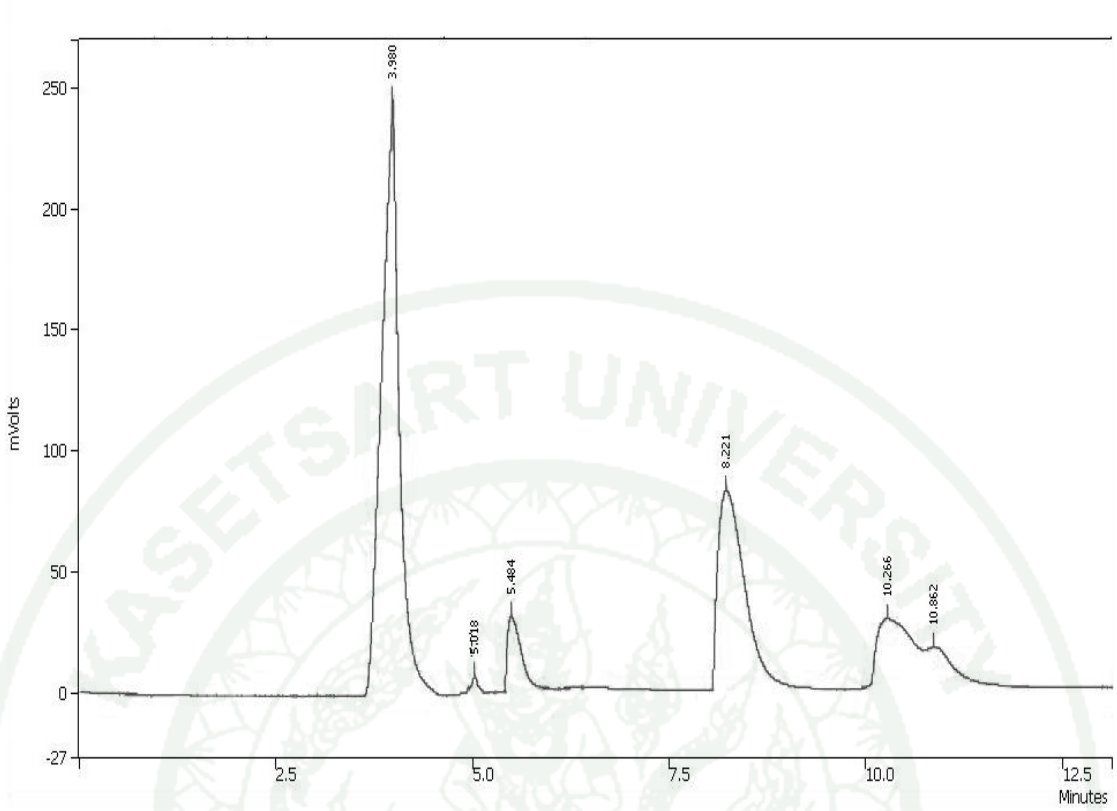

Appendix Figure A5 Chromatogram of 1.0 mL standard mixed gas.

Appendix Table A5 Peak area and retention time of 1.0 mL standard mixed gas from chromatogram Appendix Figure A5

Peak No.	Gasses	Result	Ret. Time (min)	Area (counts)	Width ½ (sec)
1	H_2	49.7570	3.980	3318924	12.4
2	N_2	0.4886	5.018	37598	4.9
3	CO	4.9531	5.484	381155	12.4
4	CH_4	26.0268	8.221	1812825	24.0
5	CO_2	12.0071	10.266	923979	0.0
		6.5491	10.862	503965	37.8
Total		100.0000		7695241	

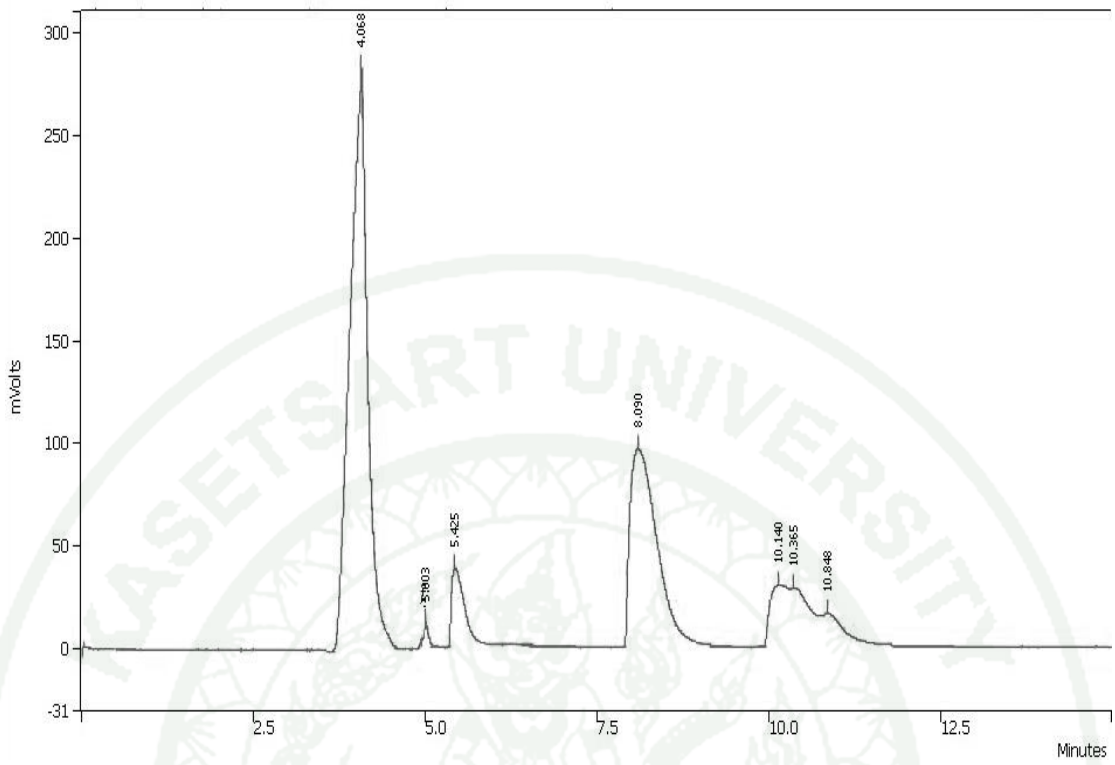

Appendix Figure A6 Chromatogram of 1.5 mL standard mixed gas.

Appendix Table A6 Peak area and retention time of 1.5 mL standard mixed gas from chromatogram Appendix Figure A6

Peak No.	Gasses	Result	Ret. Time (min)	Area (counts)	Width ½ (sec)
1	H_2	50.4685	4.068	5068369	0.0
2	N_2	0.5960	5.003	59854	0.0
3	CO	5.6901	5.425	571435	12.2
4	CH_4	26.8480	8.090	2696251	26.0
5	CO_2	5.5928	10.140	561668	19.1
		5.7349	10.365	575940	0.0
		4.7070	10.848	472707	39.5
Total		100.0000		10042644	

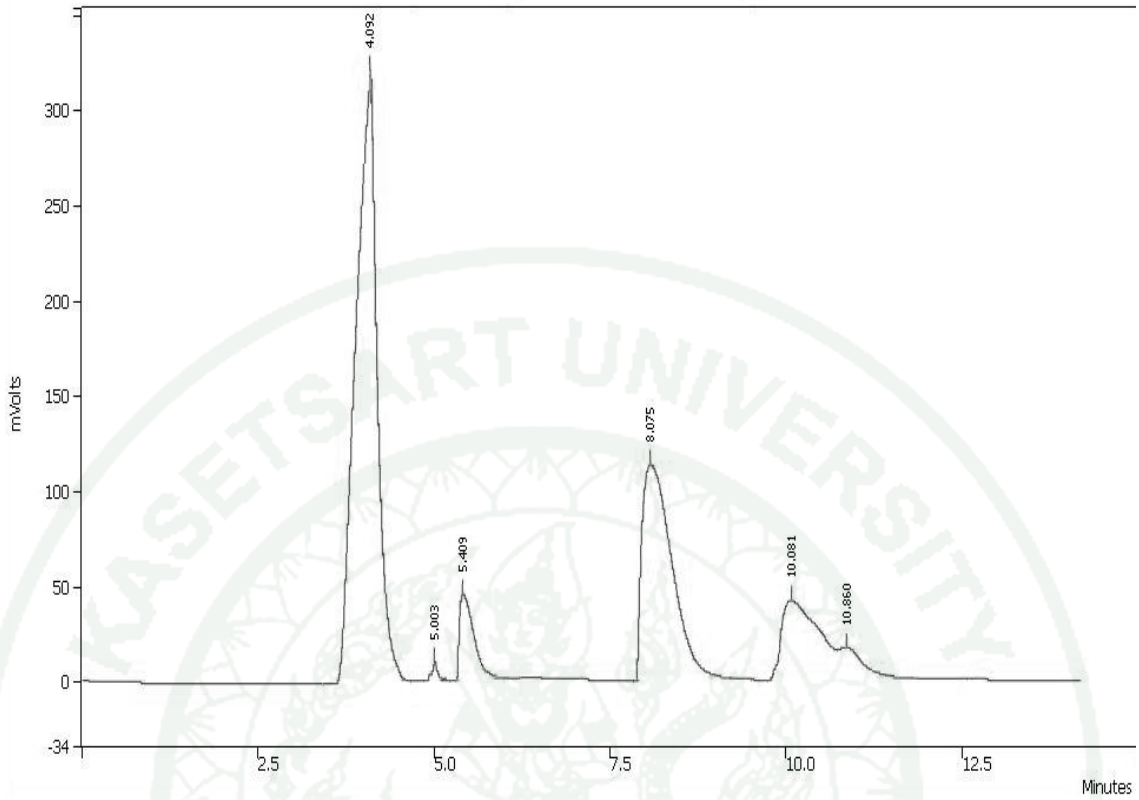

Appendix Figure A7 Chromatogram of 2.0 mL standard mixed gas.

Appendix Table A7 Peak area and retention time of 2.0 mL standard mixed gas from chromatogram Appendix Figure A7

Peak No.	Gasses	Result	Ret. Time (min)	Area (counts)	Width ½ (sec)
1	H_2	52.6839	4.092	6753910	20.8
2	N_2	0.4286	5.003	54951	4.3
3	CO	4.9206	5.409	630806	13.3
4	CH_4	26.4936	8.075	3396401	28.5
5	CO_2	12.0212	10.438	1541085	39.5
		3.4520	10.860	442540	0.0
Total		100.0000		12819693	

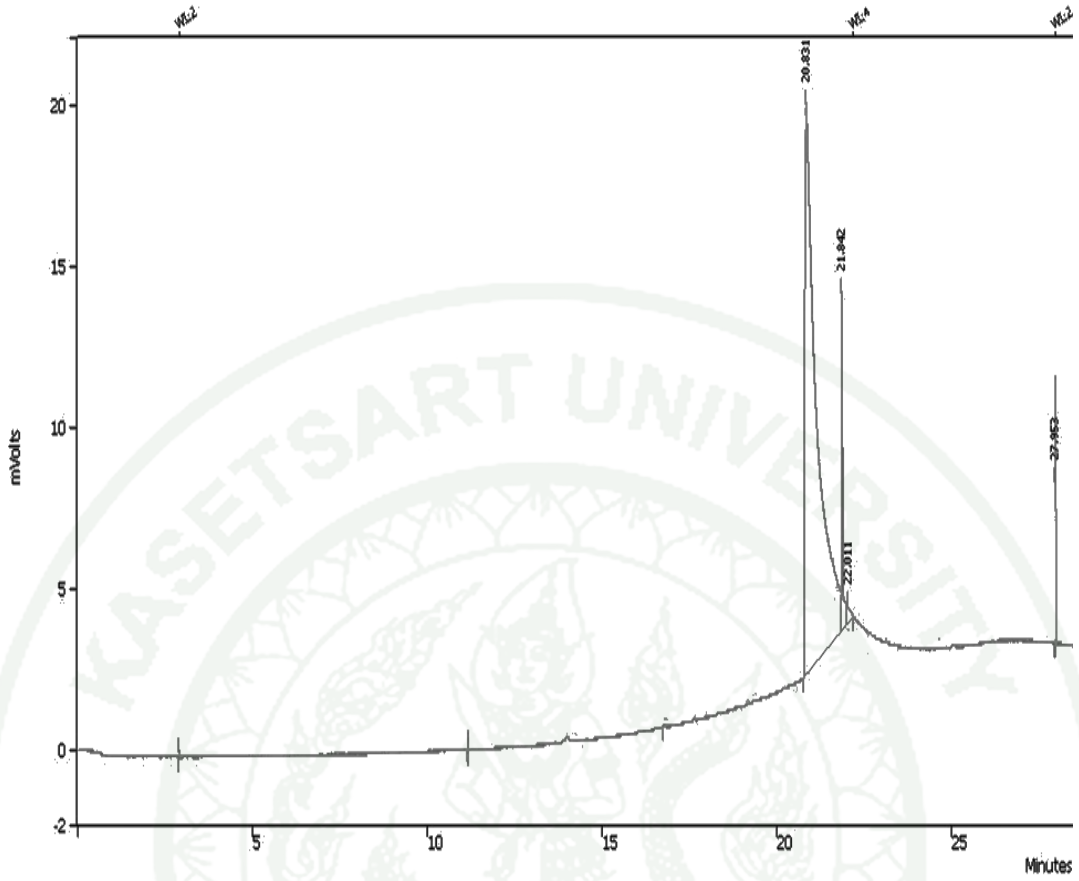

Appendix Figure A8 Chromatogram of 0.05M acetic acid

Appendix Table A8 Peak area and retention time of 0.05M acetic acid from chromatogram Appendix Figure A8

Peak No.	Result	Ret. Time (min)	Area (counts)	Width ½ (sec)
1	96.4354	20.831	411806	18.0
2	2.5420	21.842	10855	0.2
3	0.7562	22.011	3229	0.0
4	0.2664	27.953	1138	0.2
Total	100.0000		427028	

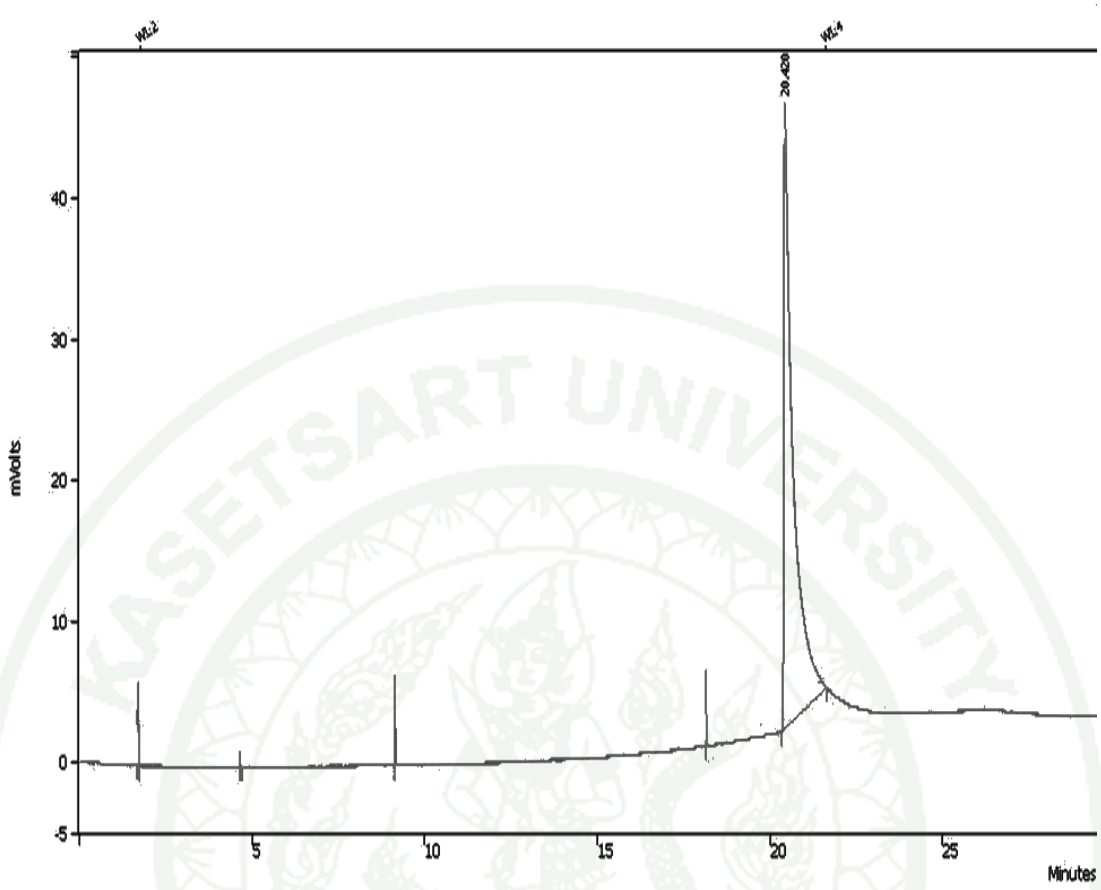

Appendix Figure A9 Chromatogram of 0.10M acetic acid

Appendix Table A9 Peak area and retention time of 0.10M acetic acid from chromatogram Appendix Figure A9

Peak No.	Result	Ret. Time (min)	Area (counts)	Width ½ (sec)
1	96.4354	20.831	411806	18.0
Total	100.0000		427028	

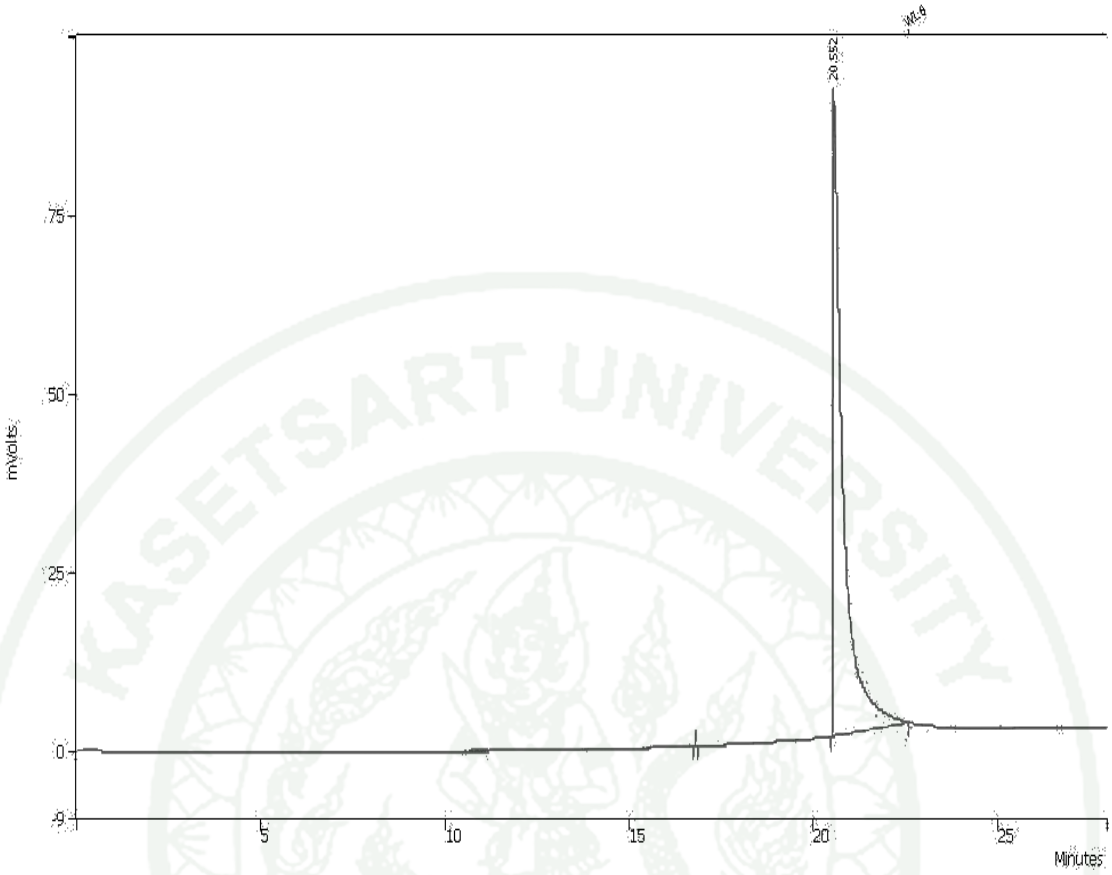

Appendix Figure A10 Chromatogram of 0.20M acetic acid

Appendix Table A10 Peak area and retention time of 0.20M acetic acid from chromatogram Appendix Figure A10

Peak No.	Result	Ret. Time (min)	Area (counts)	Width ½ (sec)
1	100.0000	20.552	1709081	13.2
Total	100.0000		1709081	

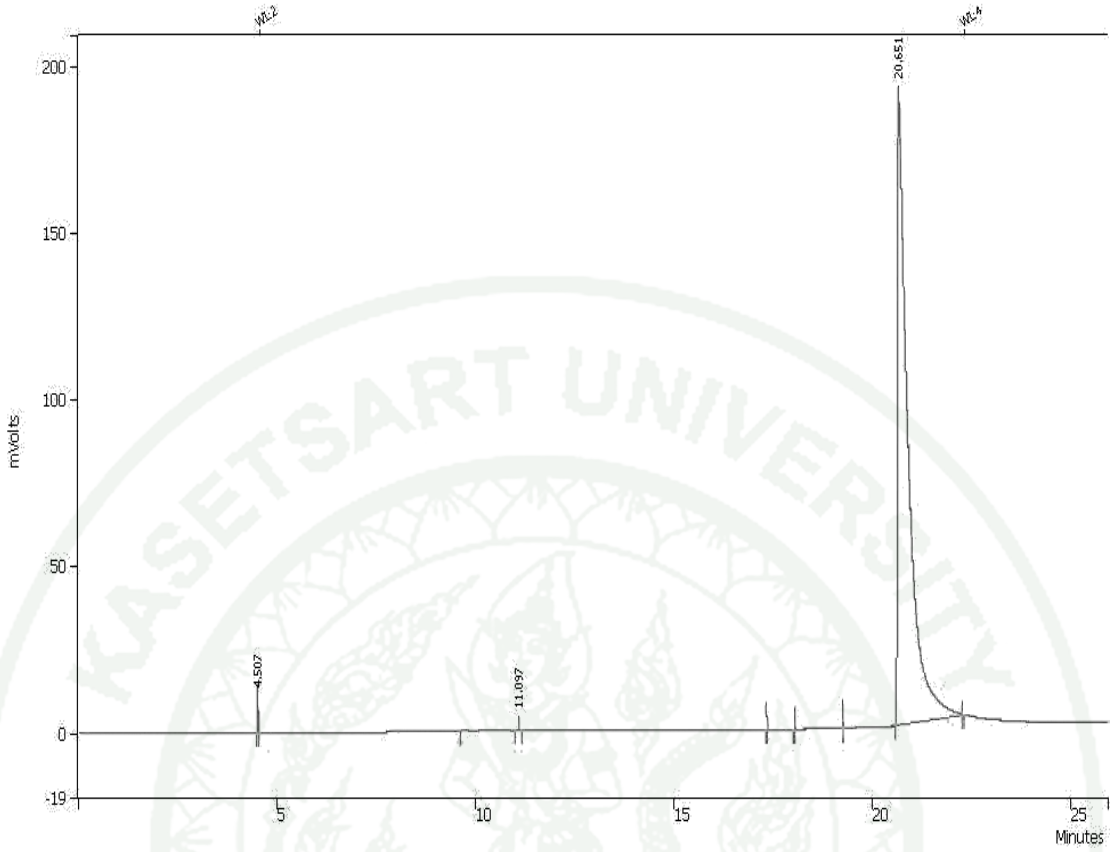

Appendix Figure A11 Chromatogram of 0.40M acetic acid

Appendix Table A11 Peak area and retention time of 0.40M acetic acid from chromatogram Appendix Figure A11

Peak No.	Result	Ret. Time (min)	Area (counts)	Width ½ (sec)
1	0.0775	4.507	2760	0.4
2	0.0355	11.097	1265	0.0
3	99.8869	20.651	3555205	14.9
Total	100.0000		3559230	

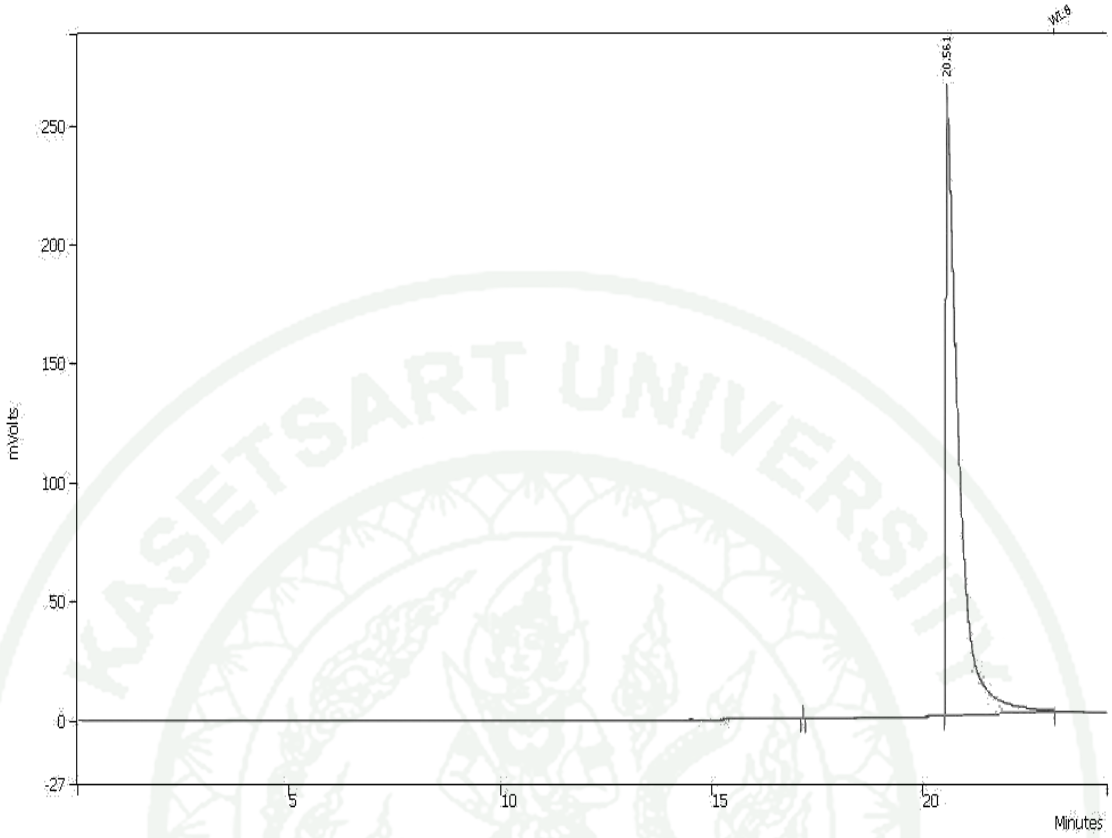

Appendix Figure A12 Chromatogram of 0.60M acetic acid

Appendix Table A12 Peak area and retention time of 0.60M acetic acid from chromatogram Appendix Figure A12

Peak No.	Result	Ret. Time (min)	Area (counts)	Width ½ (sec)
1	100.0000	20.561	5397550	16.4
Total	100.0000		5397550	

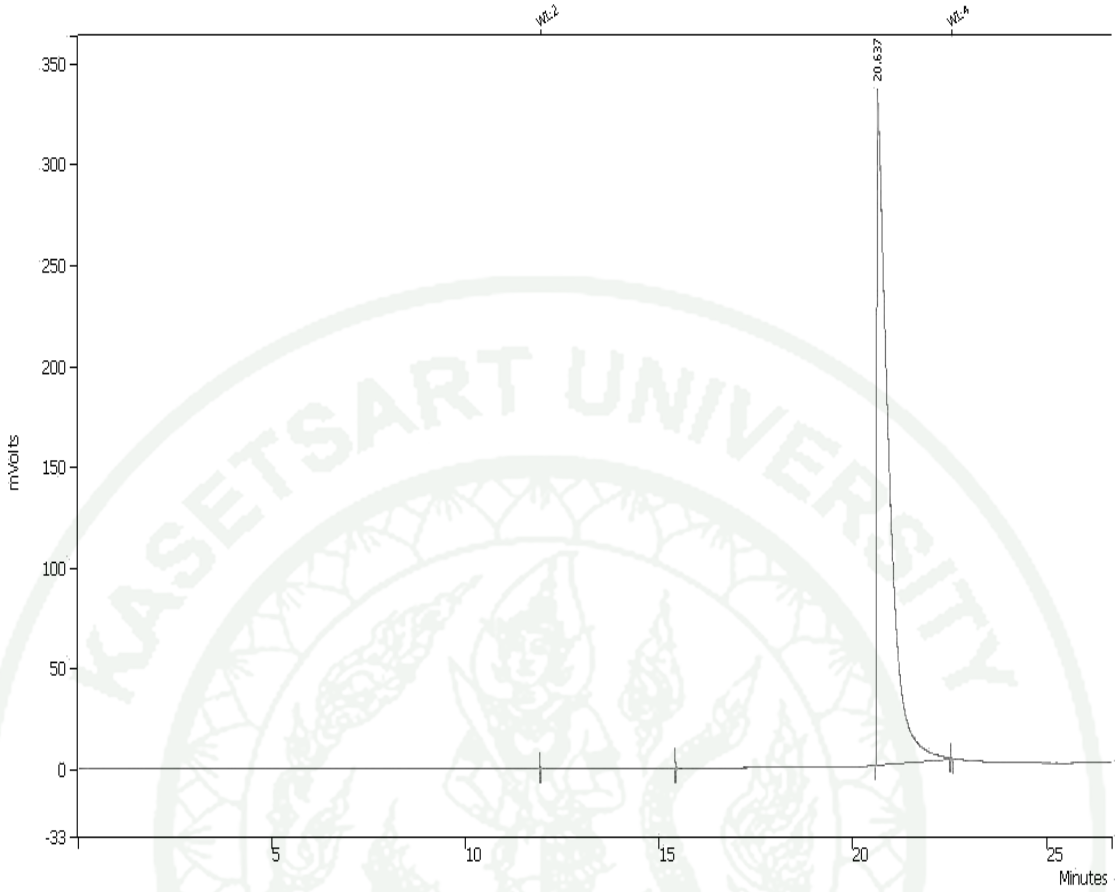

Appendix Figure A13 Chromatogram of 0.80M acetic acid

Appendix Table A13 Peak area and retention time of 0.80M acetic acid from chromatogram Appendix Figure A13

Peak No.	Result	Ret. Time (min)	Area (counts)	Width ½ (sec)
1	100.0000	20.637	7006908	17.8
Total	100.0000		7006908	

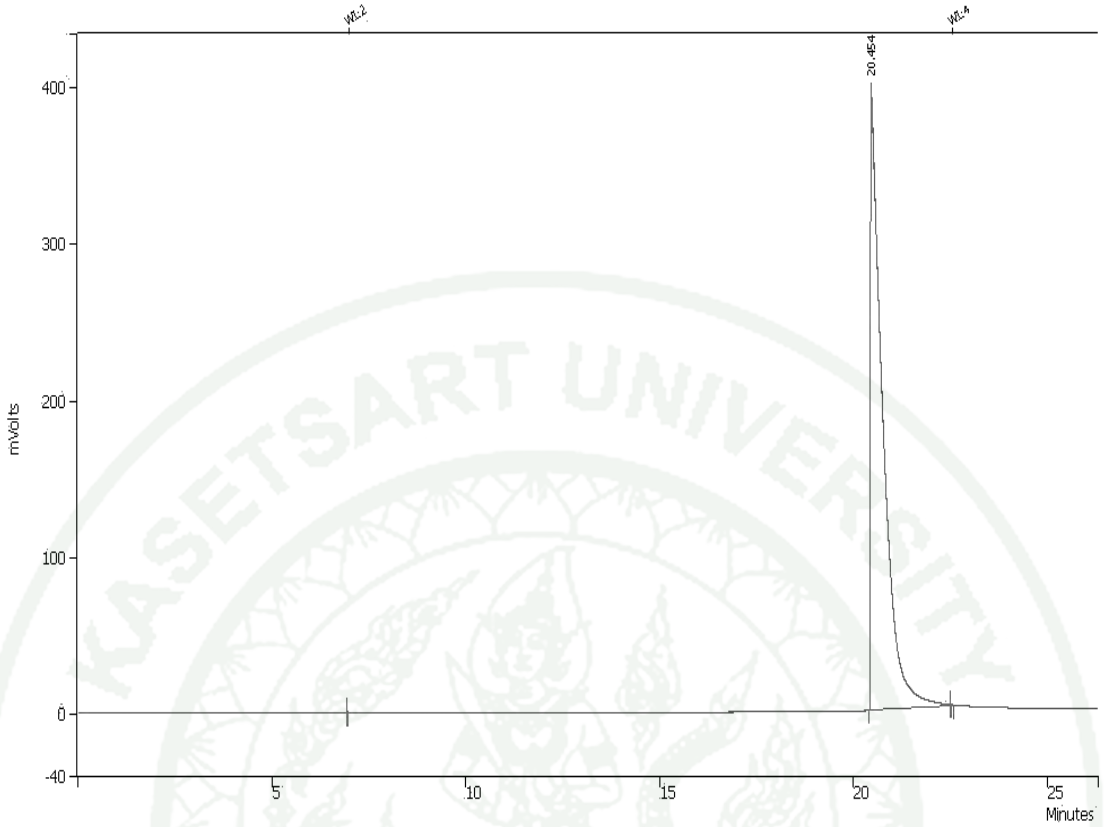

Appendix Figure A14 Chromatogram of 1.0M acetic acid

Appendix Table A14 Peak area and retention time of 1.0M acetic acid from chromatogram Appendix Figure A14

Peak No.	Result	Ret. Time (min)	Area (counts)	Width ½ (sec)
1	100.0000	20.454	8728758	18.7
Total	100.0000		8728758	

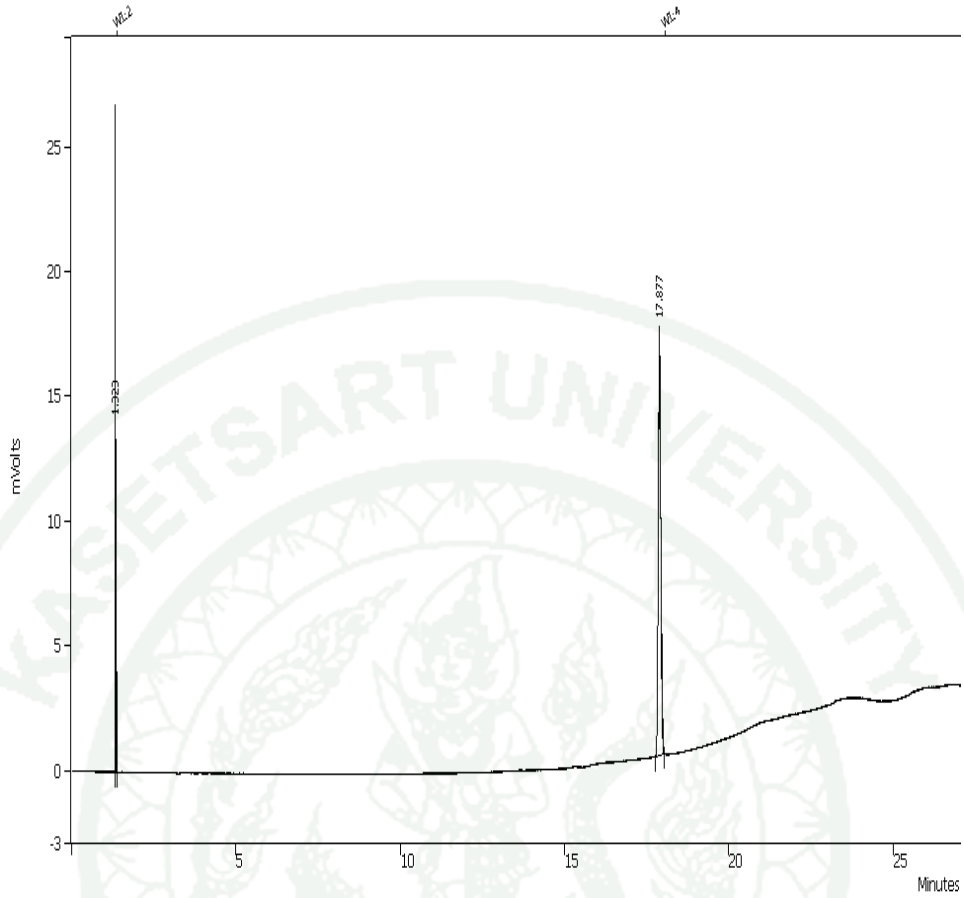

Appendix Figure A15 Chromatogram of 0.2M acetone

Appendix Table A15 Peak area and retention time of 0.2M acetone from chromatogram Appendix Figure A15

Peak No.	Result	Ret. Time (min)	Area (counts)	Width ½ (sec)
1	96.0551	17.877	88203	4.9
Total	100.0000		88203	

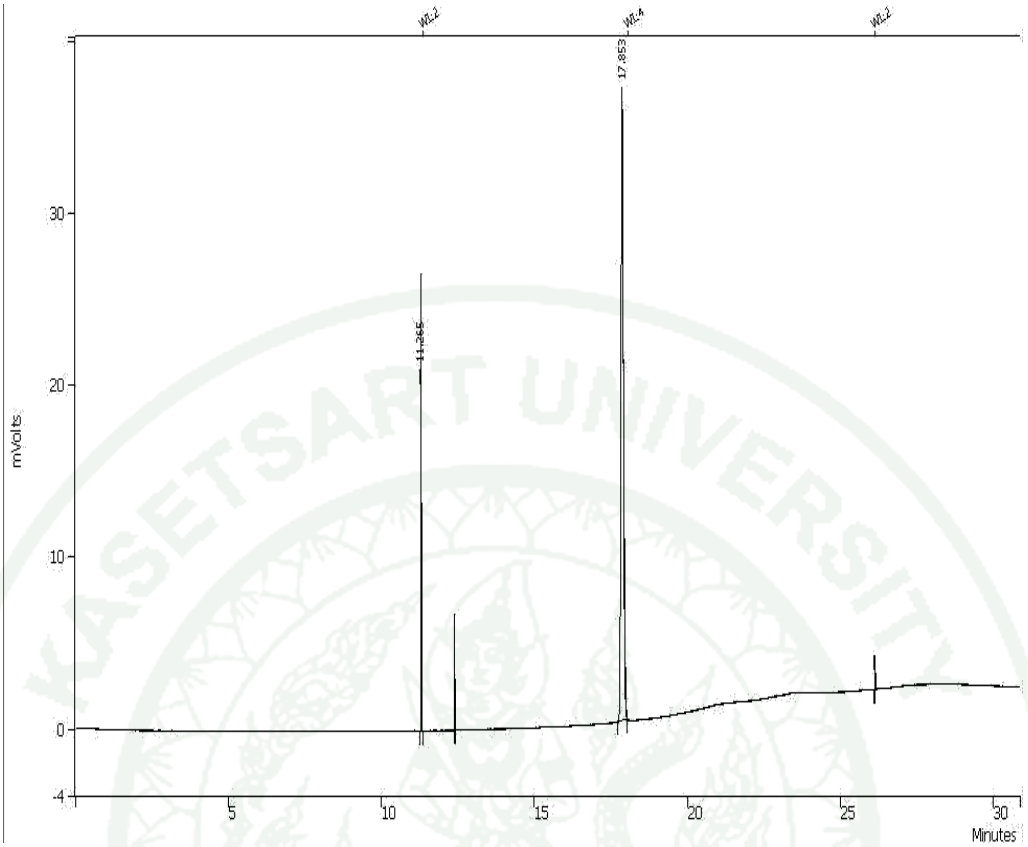

Appendix Figure A16 Chromatogram of 0.4M acetone

Appendix Table A16 Peak area and retention time of 0.4M acetone from chromatogram Appendix Figure A16

Peak No.	Result	Ret. Time (min)	Area (counts)	Width ½ (sec)
1	97.8488	17.853	198847	5.1
Total	100.0000		203219	

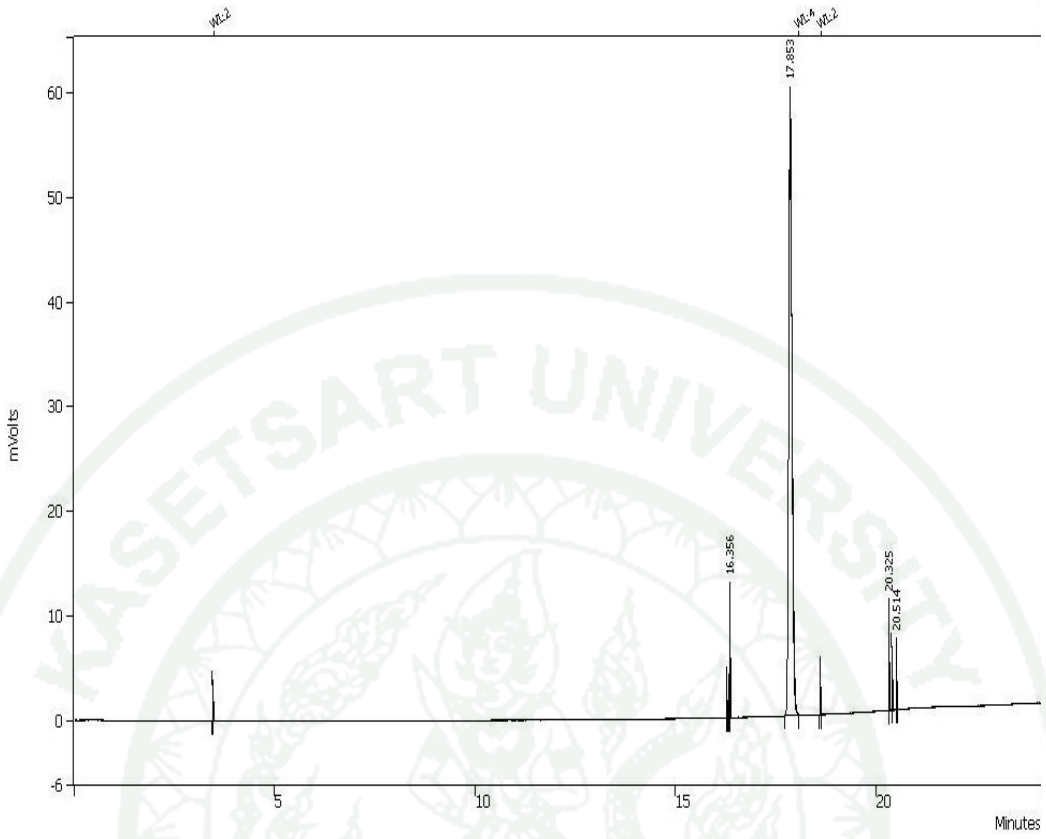

Appendix Figure A17 Chromatogram of 0.6M acetone

Appendix Table A17 Peak area and retention time of 0.6M acetone from chromatogram Appendix Figure A17

Peak No.	Result	Ret. Time (min)	Area (counts)	Width ½ (sec)
1	98.8263	17.853	331646	5.2
Total	100.0000		335584	

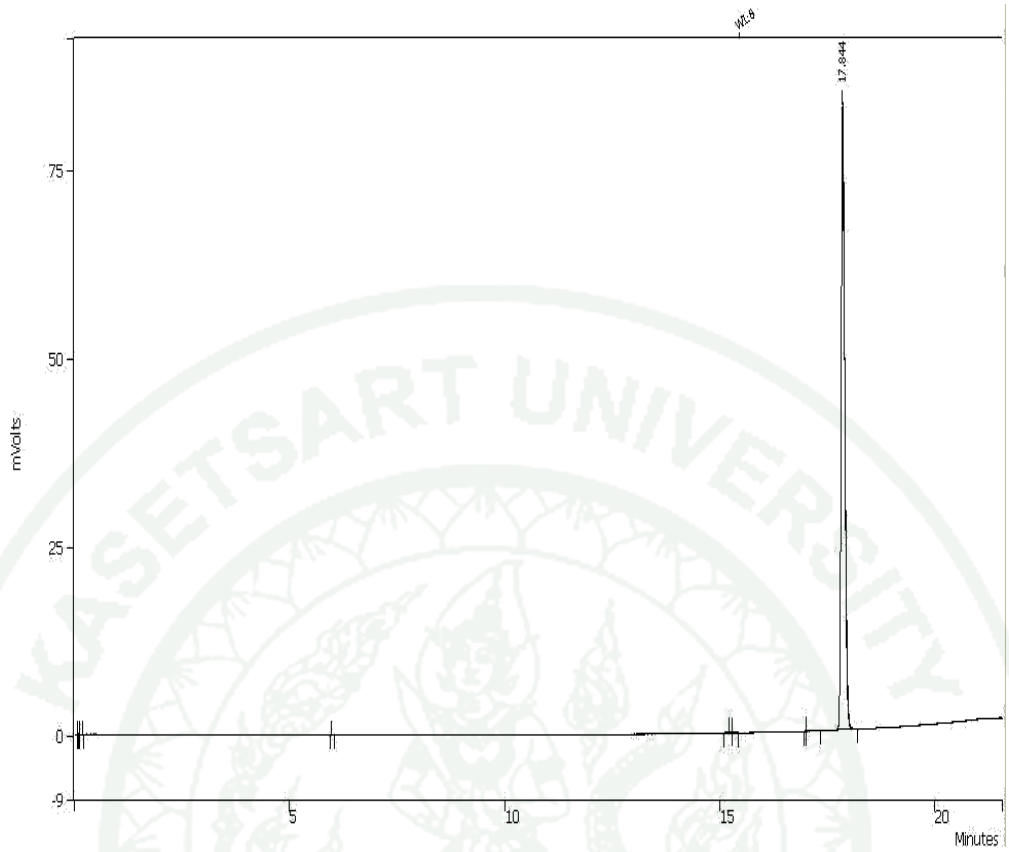

Appendix Figure A18 Chromatogram of 0.8M acetone

Appendix Table A18 Peak area and retention time of 0.8M acetone from chromatogram Appendix Figure A18

Peak No.	Result	Ret. Time (min)	Area (counts)	Width ½ (sec)
1	100.0000	17.844	480020	5.3
Total	100.0000		480020	

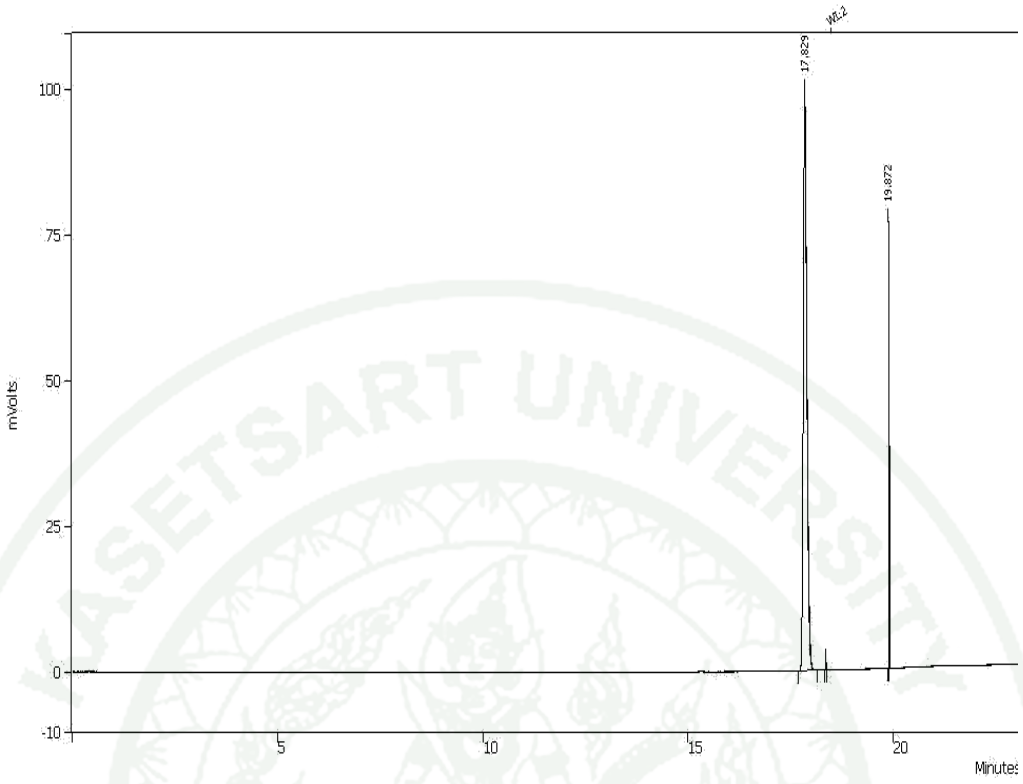

Appendix Figure A19 Chromatogram of 1.0M acetone

Appendix Table A19 Peak area and retention time of 1.0M acetone from chromatogram Appendix Figure A19

Peak No.	Result	Ret. Time (min)	Area (counts)	Width ½ (sec)
1	98.3205	17.829	591666	5.5
Total	100.0000		601773	

Appendix B

Standard calibration curves of gaseous products and liquid products

Appendix Table B1 Moles of gaseous standard calculation for various volumes

Volume (mL)	Gasses	RT(min.)	Peak area	total moles	moles of gases
0.1	H_2	2.345	433103	4.09×10^{-06}	1.006×10^{-06}
	CO	3.745	40390		1.064×10^{-06}
	CH_4	5.870	194242		1.007×10^{-06}
	CO_2	7.931	293588		1.012×10^{-06}
0.2	H_2	3.853	613424	8.18×10^{-06}	2.012×10^{-06}
	CO	3.706	19662		2.128×10^{-06}
	CH_4	5.905	111752		2.015×10^{-06}
	CO_2	8.054	262406		2.024×10^{-06}
0.4	H_2	3.882	754443	1.64×10^{-05}	4.024×10^{-06}
	CO	3.745	40390		4.256×10^{-06}
	CH_4	5.870	194242		4.029×10^{-06}
	CO_2	7.931	293588		4.049×10^{-06}
0.6	H_2	2.347	602289	2.45×10^{-05}	6.036×10^{-06}
	CO	3.740	64661		6.385×10^{-06}
	CH_4	5.831	308769		6.044×10^{-06}
	CO_2	7.911	331396		6.073×10^{-06}
0.8	H_2	2.474	1442335	3.27×10^{-05}	8.048×10^{-06}
	CO	3.882	75978		8.513×10^{-06}
	CH_4	5.972	373679		8.058×10^{-06}
	CO_2	8.094	403766		8.097×10^{-06}
1.0	H_2	3.970	2883328	4.09×10^{-05}	1.006×10^{-05}
	CO	3.703	96470		1.064×10^{-05}
	CH_4	5.796	441539		1.007×10^{-05}
	CO_2	7.847	429832		1.012×10^{-05}

Appendix Table B1 (continued)

Volume (mL)	Gasses	RT(min.)	Peak area	total moles	moles of gases
1.5	H_2	2.533	1495977	6.13×10^{-05}	1.509×10^{-05}
	CO	3.740	171588		1.596×10^{-05}
	CH_4	5.804	687378		1.511×10^{-05}
	CO_2	7.859	539638		1.518×10^{-05}
2.0	H_2	2.541	2028072	8.18×10^{-05}	2.012×10^{-05}
	CO	3.673	203488		2.128×10^{-05}
	CH_4	5.723	893584		2.015×10^{-05}
	CO_2	7.743	757792		2.024×10^{-05}

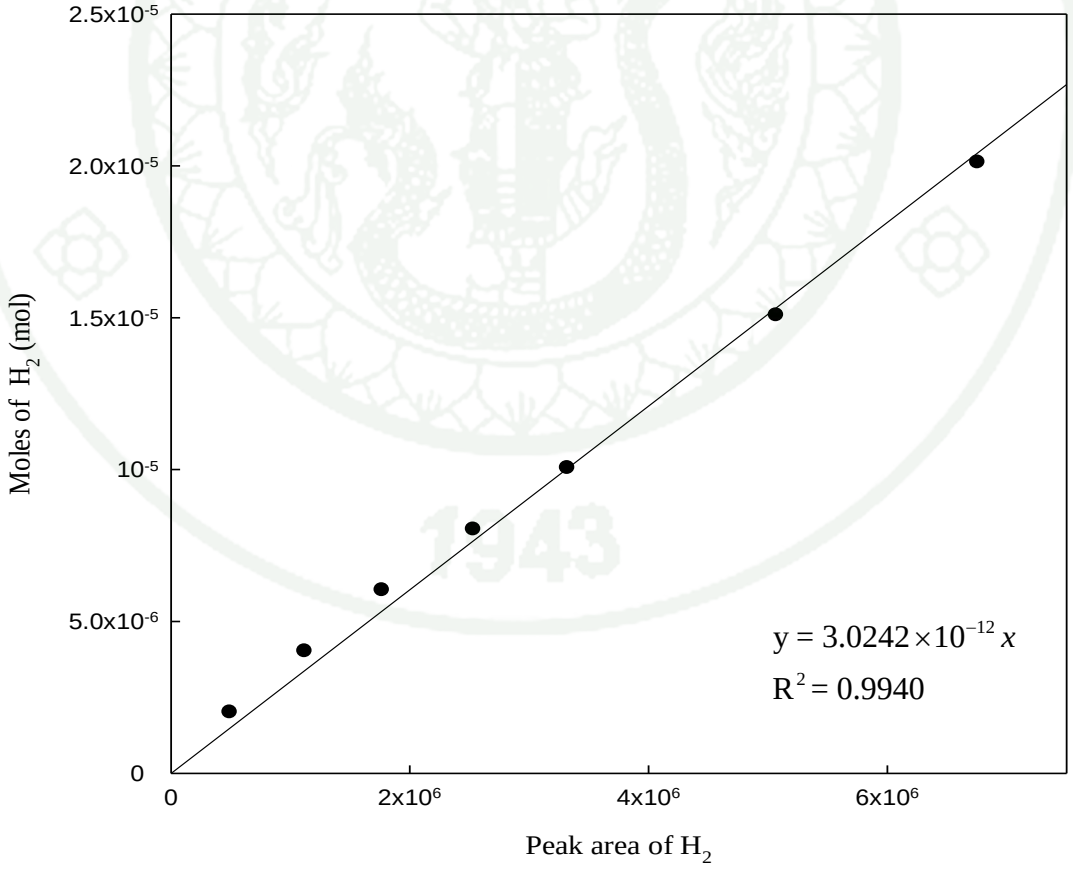

Appendix Figure B1 Standard calibration curve of hydrogen

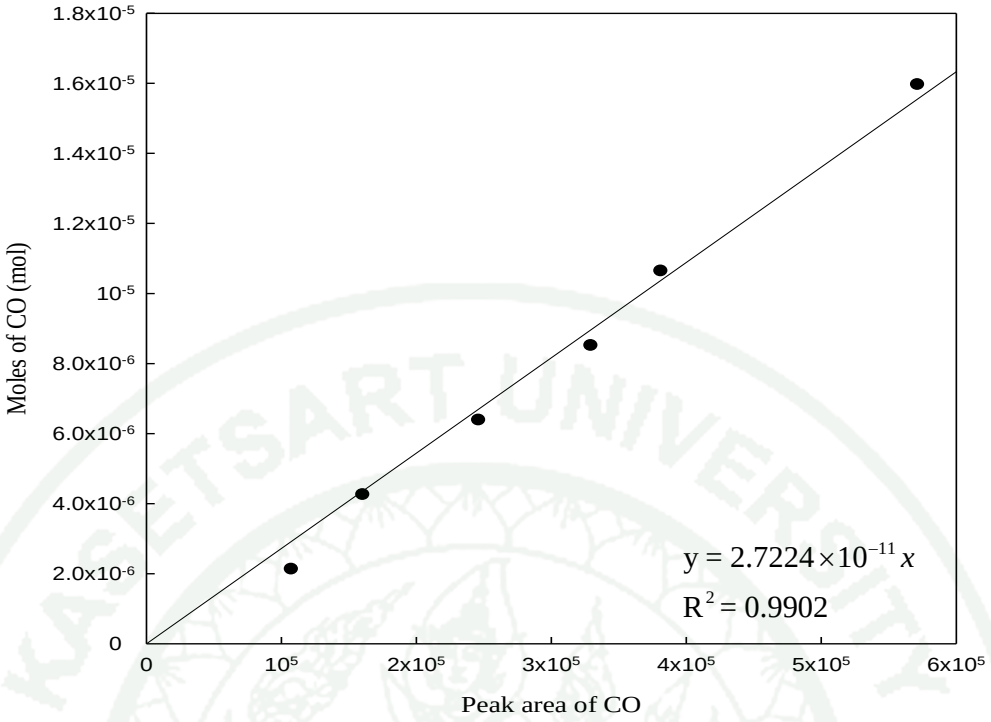

Appendix Figure B2 Standard calibration curve of carbonmonoxide

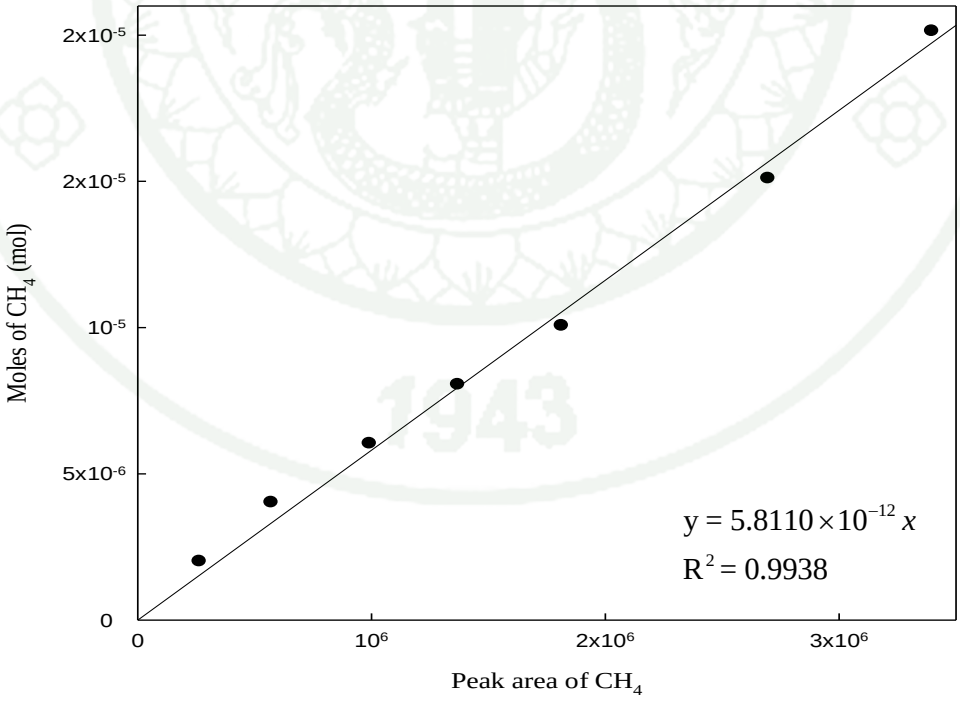

Appendix Figure B3 Standard calibration curve of methane

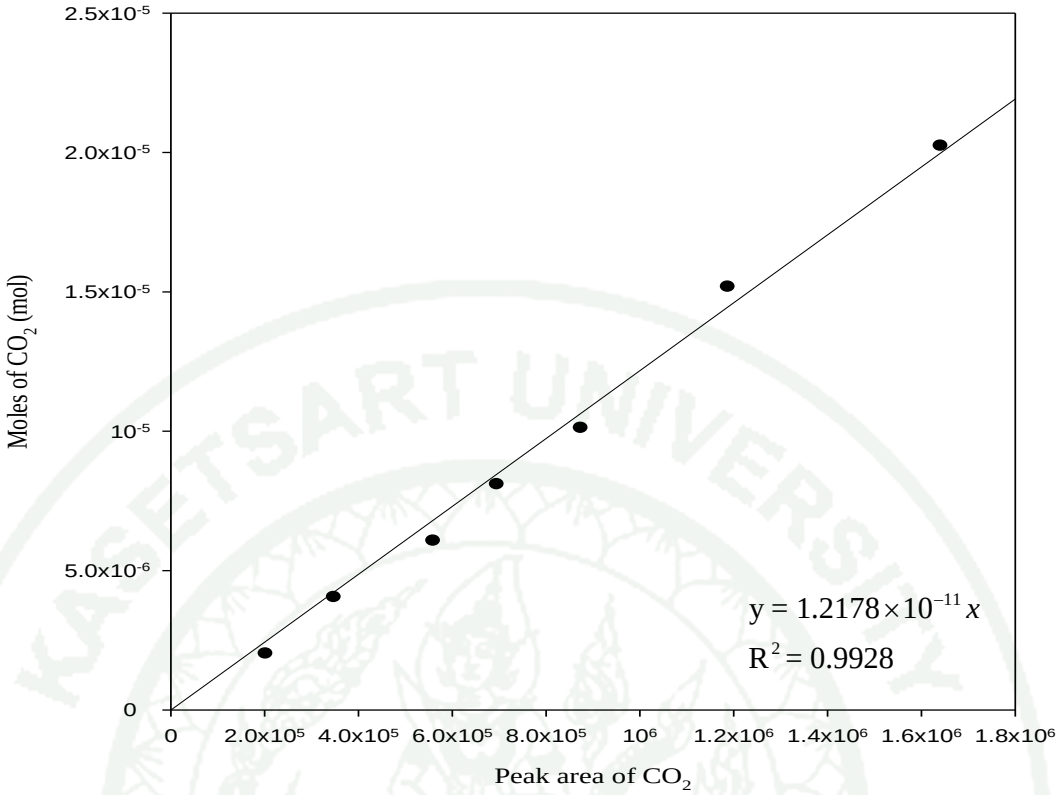

Appendix Figure B4 Standard calibration curve of carbondioxide

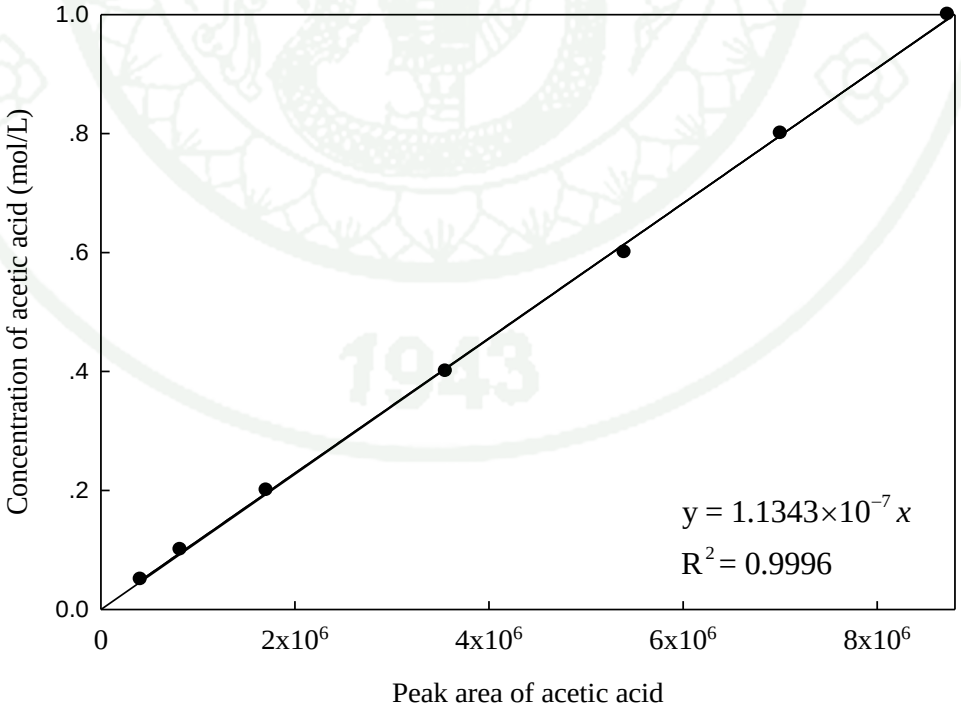

Appendix Figure B5 Standard calibration curve of acetic acid

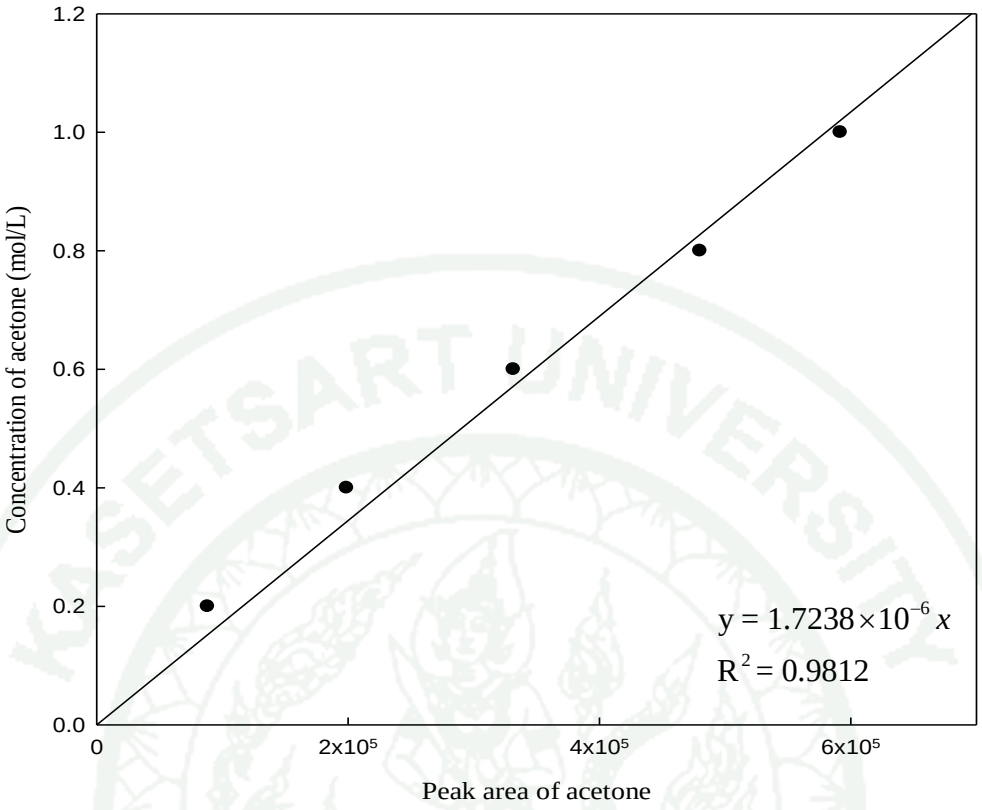

Appendix Figure B6 Standard calibration curve of acetone

Appendix C

Calculation method of hydrogen yields, conversion, and product distribution (in term of selectivity) obtained from GC

Calculation method of hydrogen yield

Hydrogen yield can be calculated as in Equation (C1).

$$\text{Hydrogen yield (\%)} = \frac{\text{moles of hydrogen produced}}{\left(2n+\frac{m}{2}-k\right)\times \text{moles of carbon in feed}} \times 100 \qquad \text{(C1)}$$

Where n, m, and k defined as moles of carbon, hydrogen, and oxygen in the feed ($C_nH_mO_k$), respectively.

Example for H_2 yield calculation is steam reforming of acetic acid which was performed by using the 15%Ni over 12C7A-CeO_2-TiO_2 (2:1:1) at 850^{o}C and S/C of 8 for 1 h. The gaseous products obtained from acetic acid reforming were collected by sampling bag (1,000 mL) and injected 1.0 mL of the product gases contained in sampling bag by a syringe to injection port of GC. The chromatogram of gaseous products, H_2, CO, CH_4, and CO_2, is shown in Appendix Figure C1, where peak area and retention time of each product are listed in Appendix Table C1.

From standard calibration curve of hydrogen (Appendix Figure B1)

$$y_1 = 3.0242\times10^{-12}x_1 \qquad \text{(C2)}$$

For carbonmonoxide (Appendix Figure B2); $y_2 = 2.7224\times10^{-11}x_2$ (C3)

For methane (Appendix Figure B3); $y_3 = 5.8110\times10^{-12}x_3$ (C4)

For carbondioxide (Appendix Figure B4); $y_4 = 1.2178\times10^{-11}x_4$ (C5)

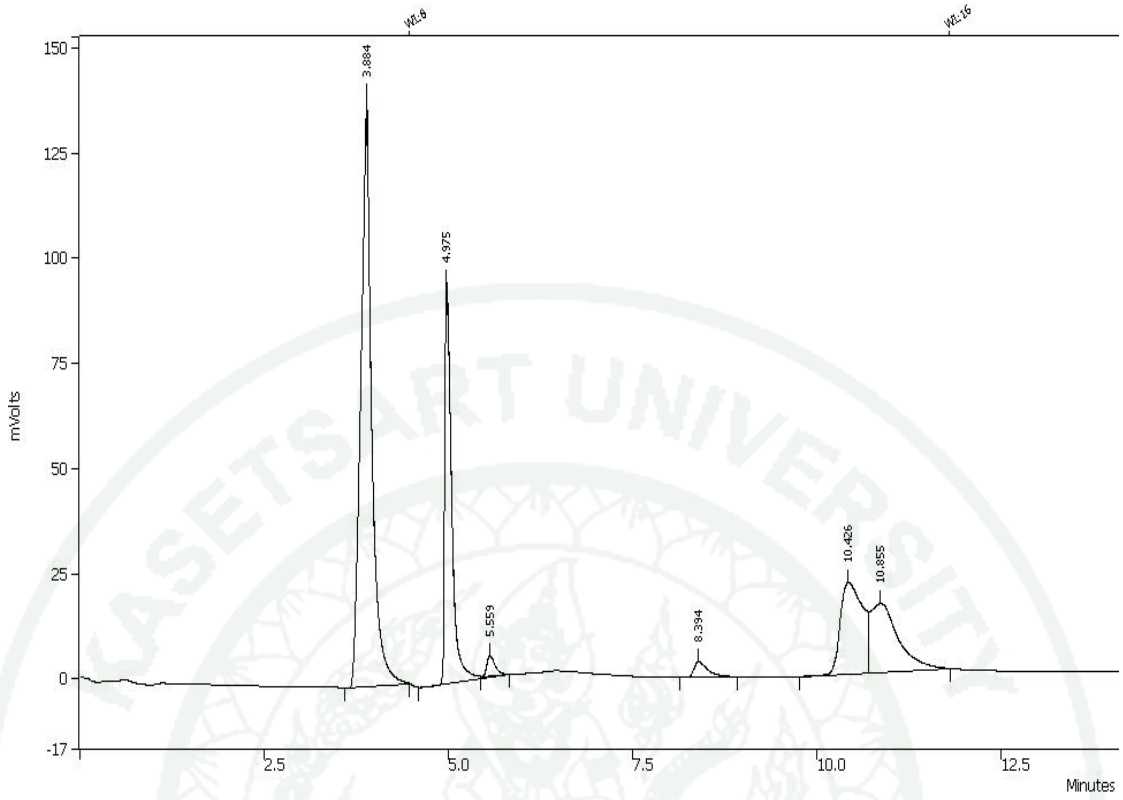

Appendix Figure C1 Chromatogram of gaseous products of acetic reforming at 850°C, S/C of 8, 1 h, using 15%Ni/12C7A-CeO_2-TiO_2 as a catalyst.

Appendix Table C1 Peak area and retention time of gaseous products of acetic acid reforming from chromatogram Appendix Figure C1

Peak No.	Gases	Ret. Time (min)	Area (counts)	Width ½ (sec)
1	H_2	3.884	2237986	8.5
2	N_2	4.975	623360	5.6
3	CO	5.559	366798	0.0
4	CH_4	8.394	46837	11.4
5	CO_2	10.426	465753	15.3
		10.855	431133	38.7
Total			4171867	

From Appendix Table C1, moles of gaseous product can be calculated by using the equations obtained from standard calibration curves for each gas (Equations C2 to C5) and listed in Appendix Table C2.

Appendix Table C2 Moles of gaseous products

i	Gaseous product	Peak area (x_i)	Moles of gaseous product (y_i)	Actual moles of gaseous product (mol)
1	H_2	2237986	6.768×10^{-6}	0.006768
2	CO	36679	9.986×10^{-6}	0.0009985
3	CH_4	46837	2.722×10^{-7}	0.0002722
4	CO_2	465753	5.672×10^{-6}	0.005672

The amount of mole (y_i) listed in Appendix Table C2 refers to mole of product gas, which contains in 1 mL of injected sample. The actual mole of the gaseous products was collected by 1,000 mL of the sampling bag for 5 min. Thus, the amount of mole calculated from standard calibration curve (y_i) should be multiplied by 1,000 in order to obtain the actual mole of product gas contained in the gas sampling bag as shown in Appendix Figure C2.

The moles of carbon in feed in Equation (C1) are determined by following Equations (C6) and (C7).

$$\text{moles HAc in feed} = \frac{\text{conc.}_{\text{HAc}} \left|\frac{\text{g}_{\text{HAc}}}{\text{mL}}\right| \times \text{flow rate} \left|\frac{\text{mL}}{\text{h}}\right| \times \text{time} \left|\text{h}\right|}{\text{molecular weight of HAc} \left|\frac{\text{g}}{\text{mol}}\right|_{\text{HAc}}} \quad \text{(C6)}$$

$$\text{moles of carbon in feed} = 2\times\text{mole}_{\text{HAc}} \quad \text{(C7)}$$

Where, Feed rate of acetic acid solution = 9.86 mL/h.

Concentration of acetic acid solution = 0.1647 g_{HAc}/mL (for S/C of 8)

Time (collection time) = 5 min.

Molecular weight of acetic acid = 60 g/mol

Substitute the determined parameters into Equation (C6);

$$\text{moles HAc in feed} = \frac{0.1647\left|\frac{g_{HAc}}{mL}\right|\times 9.86\left|\frac{mL}{h}\right|\times 5.0\left|\text{min.}\right|\times\left|\frac{1\text{ h.}}{60\text{ min.}}\right|}{60\left|\frac{g}{mol}\right|_{HAc}}$$

$$\text{moles HAc in feed} = 2.255\times10^{-3}\text{mol}_{HAc}$$

So that, $$\text{moles}_C = 2\times2.255\times10^{-3}$$

$$= 4.511\times10^{-3}\text{mol}_C$$

For acetic acid ($C_2H_4O_2$), the term $(2n+\frac{m}{2}-k)$ is reduced to a constant value of 4, whereas the value of "moles of hydrogen produced" is obtained from the value of "the actual moles of hydrogen" in Appendix Table C2.

From Equation (C1), all parameters are substituted to obtain a hydrogen yield as following

$$\text{Hydrogen yield (\%)} = \frac{0.006768}{4\times0.004511}\times100$$

$$= 37.51\%$$

Calculation method for selectivity for the gaseous products

Gaseous products distribution is reported in term of selectivity which can be calculated as following Equation

$$\text{Selectivity of gaseous product}_i = \frac{\text{moles of gaseous product}_i}{\sum_{i=1}^{n} \text{moles of gaseous products}} \quad \text{(C8)}$$

The data from Appendix Table C2, the actual mole of gaseous products, are used to calculate the selectivity as expressed below

$$\text{Selectivity of } H_2 = \frac{\text{moles}_{H_2}}{\text{moles}_{H_2} + \text{moles}_{CO} + \text{moles}_{CH_4} + \text{moles}_{CO_2}}$$

$$= \frac{0.006768}{0.006768 + 0.0009986 + 0.0002722 + 0.005672}$$

$$= 0.4936$$

The selectivities of other gaseous products are summarized in Appendix Table C3

Appendix Table C3 The selectivity of the gaseous products obtained from acetic acid reforming by using 15%Ni/12C7A–CeO_2–TiO_2 at 850°C, S/C of 8, and 1 h

i	Gaseous product	Actual moles of product (mol)	Selectivity_i
1	H_2	0.006768	0.4936
2	CO	0.0009985	0.07287
3	CH_4	0.0002722	0.01986
4	CO_2	0.005672	0.4139

Calculation method for conversion of feed stock

Conversion of the reactant can be calculated as Equation (C9)

$$\text{Conversion of reactant (\%)} = \frac{\text{moles of reactant}_{in} - \text{moles of reactant}_{out}}{\text{moles of reactant}_{in}} \times 100 \quad \text{(C9)}$$

Example for reactant conversion calculation is steam reforming of acetic acid which was performed by using the 15%Ni over 12C7A-CeO_2-TiO_2 (2:1:1) at 850^{o}C, S/C of 8, and 1 h. The liquid product obtained from acetic acid reforming was injected in an amount of 10.0 µL by a syringe to injection port of GC. The chromato-gram of liquid product, acetic acid, is shown in Appendix Figure C2, where peak area and retention time of the product is listed in Appendix Table C4.

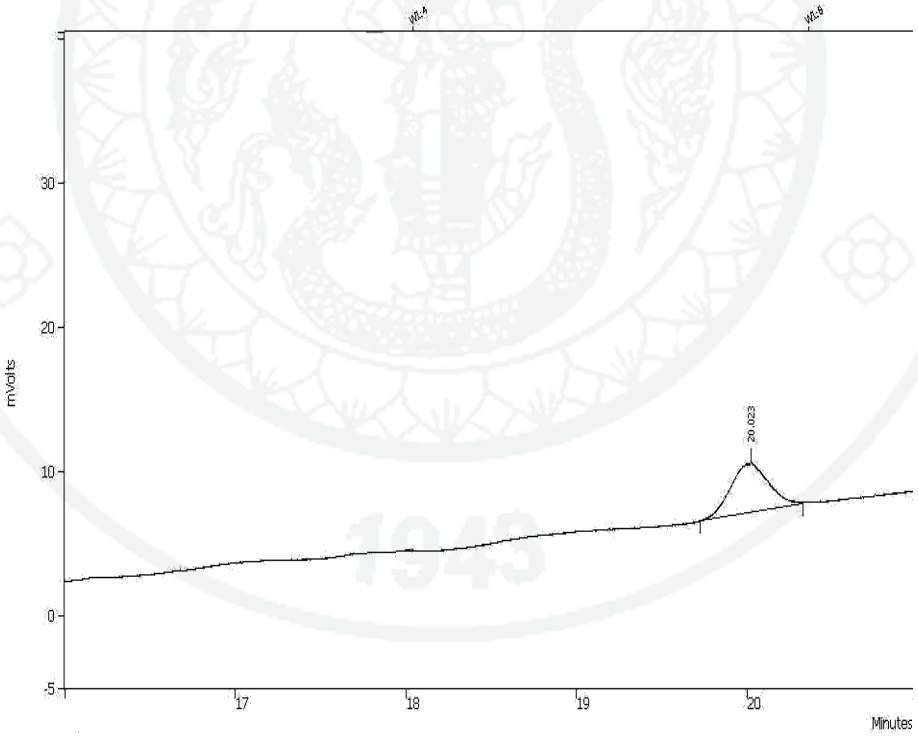

Appendix Figure C2 Chromatogram of liquid product of acetic reforming at 850^{o}C, S/C of 8, 1 h, using 15%Ni/12C7A-CeO_2-TiO_2 as a catalyst.

Appendix Table C4 Peak area and retention time of liquid product of acetic acid reforming from chromatogram Appendix Figure C2

Peak No.	Liquid product	Ret. Time (min)	Area (counts)	Width ½ (sec)
1	acetic acid	20.023	52179	16.4
Total			52179	

From standard calibration curve of acetic acid (Appendix Figure B5)

$$y = 1.1343\times10^{-7}x \qquad \text{(C10)}$$

Where: y = concentration of acetic acid per 10 µL of injected sample.
x = peak area of acetic acid (obtained from Appendix Table C4)

From Appendix Table C4, concentration of non reacted acetic acid can be calculated by using the equations obtained from standard calibration curves for acetic acid (Equation C10).

From Equation (C10); $y = 1.1343\times10^{-7}\times52{,}179$

concentration of non-reacted acetic acid = 5.919×10^{-3} mol/L

The amount of non-reacted acetic acid refers to mole of acetic acid outlet, which contains in 10.0 µL of injected sample. The total volume of collected liquid products was collected by 9.3 mL during reforming process for 1 h. Therefore, the amount of concentration calculated from standard calibration curve (y) should be adjusted in order to obtain the overall mole of liquid product.

The mole of acetic acid contained in the 10 µL (or 0.01 mL) of liquid product is equal to

$$\text{mole of HAc (0.01mL)} = 5.919\times10^{-3} \left|\frac{\text{mol}_{\text{HAc}}}{\text{L}}\right| \times 10.0 |\mu\text{L}| \times 1.0\times10^{-6} \left|\frac{\text{L}}{1\ \mu\text{L}}\right|$$

The amount of non-reacted acetic acid contains in 9.3 mL of the collected liquid product during reforming process for 1 h is shown below

$$\text{mole of HAc}_{out} = \frac{5.919\times10^{-3} \left|\frac{\text{mol}_{\text{HAc}}}{\text{L}}\right| \times 10 |\mu\text{L}| \times 1\times10^{-6} \left|\frac{\text{L}}{\mu\text{L}}\right| \times 9.3 |\text{mL}|}{0.01\ |\text{mL}|}$$

$$= 5.5047\times10^{-5}\ \text{mol}_{\text{HAc}}$$

The amount of mole for acetic acid inlet can be defined from Equation (C6) for 1 h.

$$\text{mole of HAc}_{in} = \frac{0.1647 \left|\frac{\text{g}_{\text{HAc}}}{\text{mL}}\right| \times 9.86 \left|\frac{\text{mL}}{\text{h}}\right| \times 60.0 |\text{min.}| \times \left|\frac{1\ \text{h.}}{60\ \text{min.}}\right|}{60 \left|\frac{\text{g}}{\text{mol}}\right|_{\text{HAc}}}$$

$$= 2.706\times10^{-2}\ \text{mol}_{\text{HAc}}$$

From Equation (C9), all parameters are substituted to obtain acetic acid conversion as following

$$\text{Conversion of HAc (\%)} = \frac{2.706\times10^{-2} - 5.505\times10^{-5}}{2.706\times10^{-2}} \times 100$$

$$= 99.80\%$$

Appendix D

Isotherm plots of prepared calcium aluminates

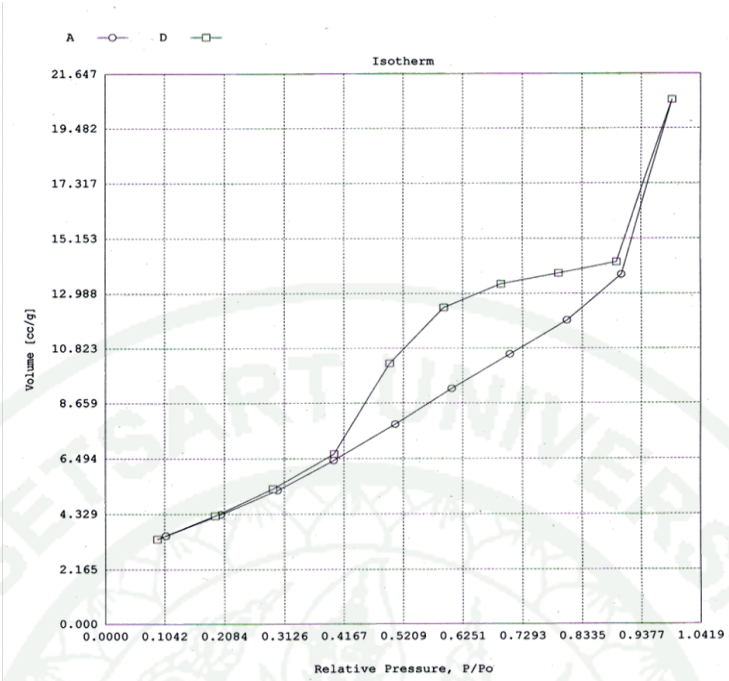

Appendix Figure D1 Isotherm plot of calcium aluminate prepared by solid-state reaction at 1,300^{o}C

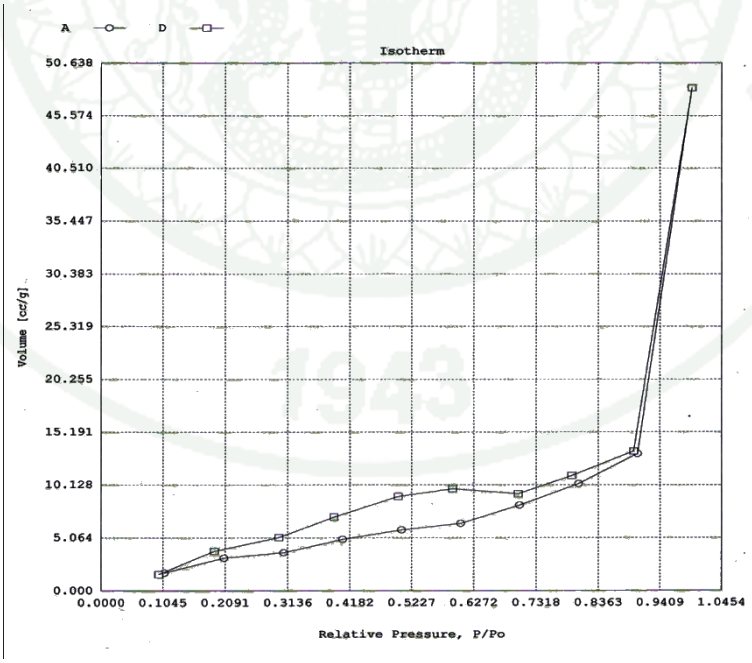

Appendix Figure D2 Isotherm plot of calcium aluminate prepared by CSD method at 900^{o}C

Appendix E

Coke formation on a surface of catalysts after steam reforming process by using TG-DTA technique

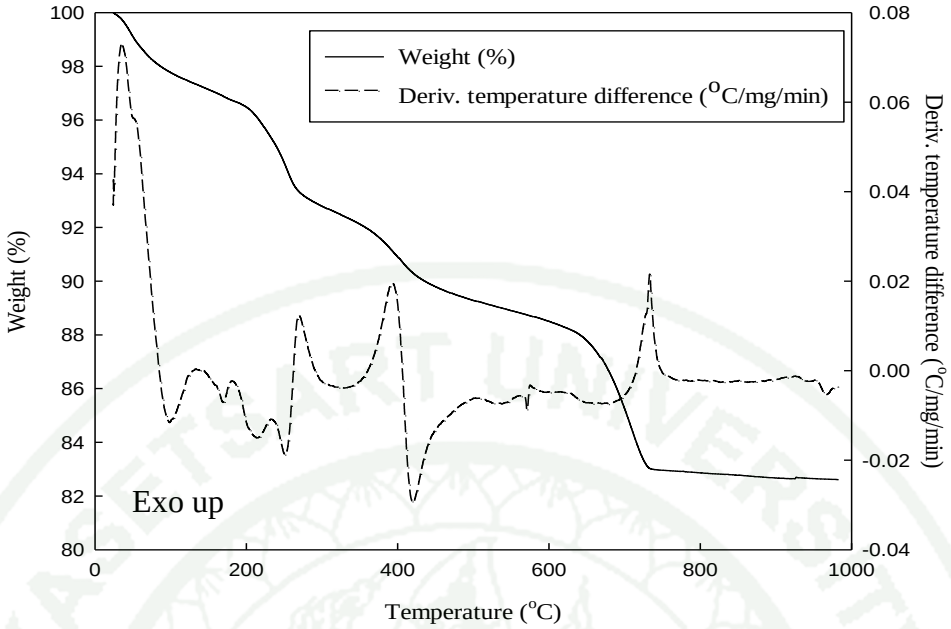

Appendix Figure E1 Thermogram of 12C7A after steam reforming reaction of acetic acid at 850°C, S/C of 8, and 1 h.

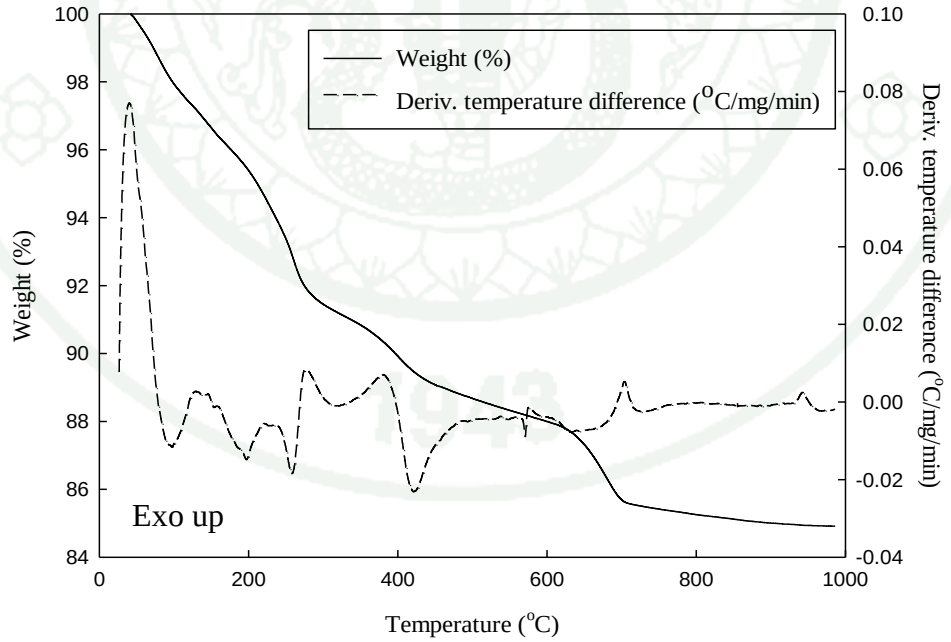

Appendix Figure E2 Thermogram of 12C7A-CeO_2 after steam reforming reaction of acetic acid at 850°C, S/C of 8, and 1 h.

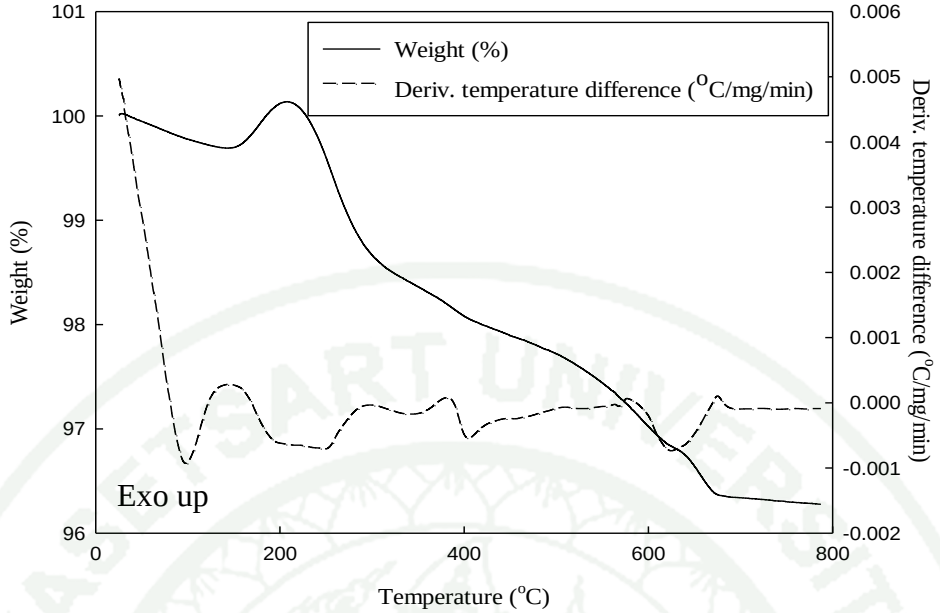

Appendix Figure E3 Thermogram of 12C7A-TiO_2 after steam reforming reaction of acetic acid at 850°C, S/C of 8, and 1 h.

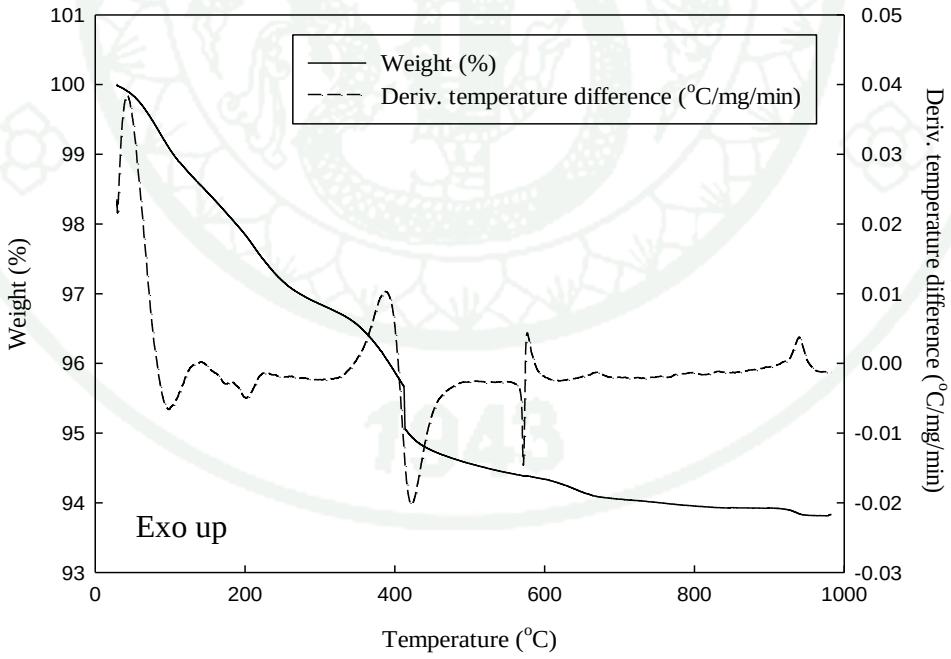

Appendix Figure E4 Thermogram of 12C7A-CeO_2-TiO_2 (2:1:1) after steam reforming reaction of acetic acid at 850°C, S/C of 8, and 1 h.

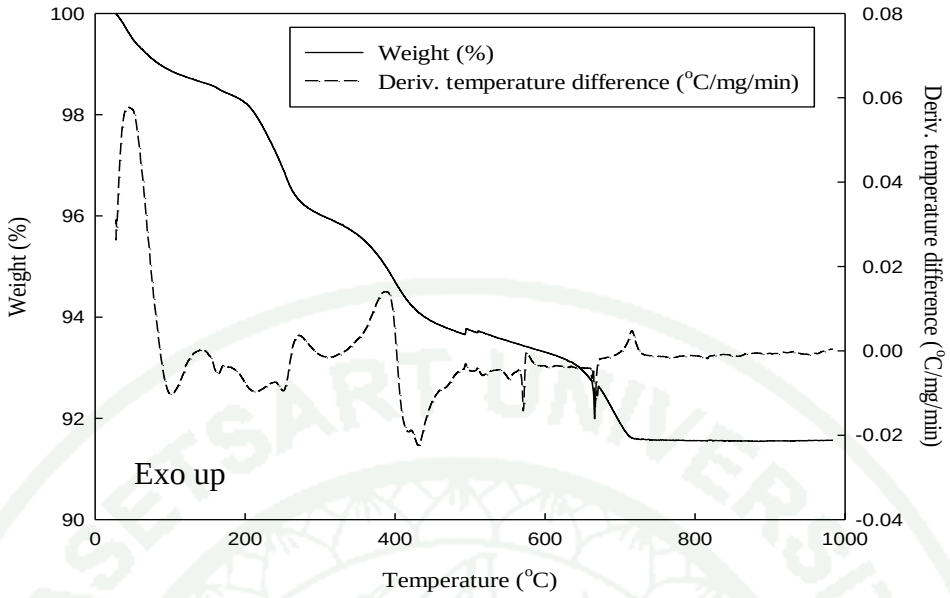

Appendix Figure E5 Thermogram of 12C7A-CeO_2-TiO_2 (1:1:1) after steam reforming reaction of acetic acid at 850°C, S/C of 8, and 1 h.

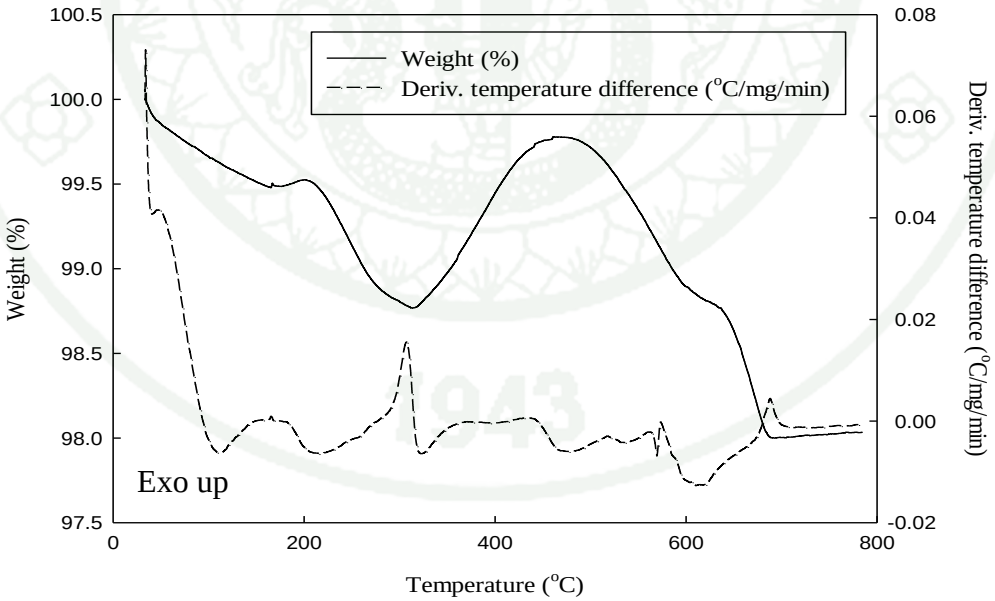

Appendix Figure E6 Thermogram of 15%Ni/12C7A-CeO_2-TiO_2 after steam reforming reaction of acetic acid at 850°C, S/C of 8, and 1 h.

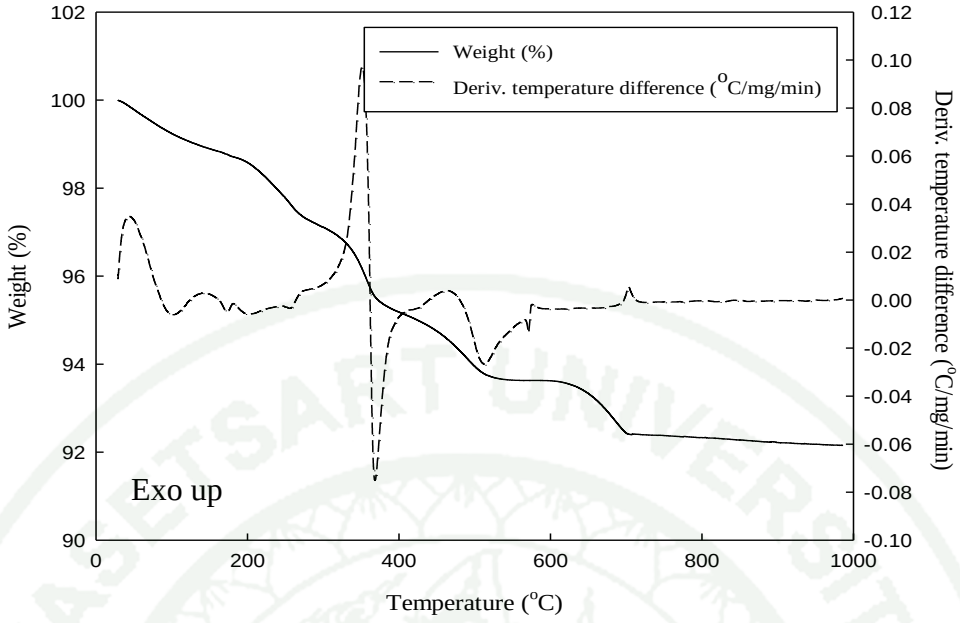

Appendix Figure E7 Thermogram of 15%Ni-5%Cu/12C7A-CeO_2-TiO_2 after steam reforming reaction of acetic acid at 850°C, S/C of 8, and 1 h.

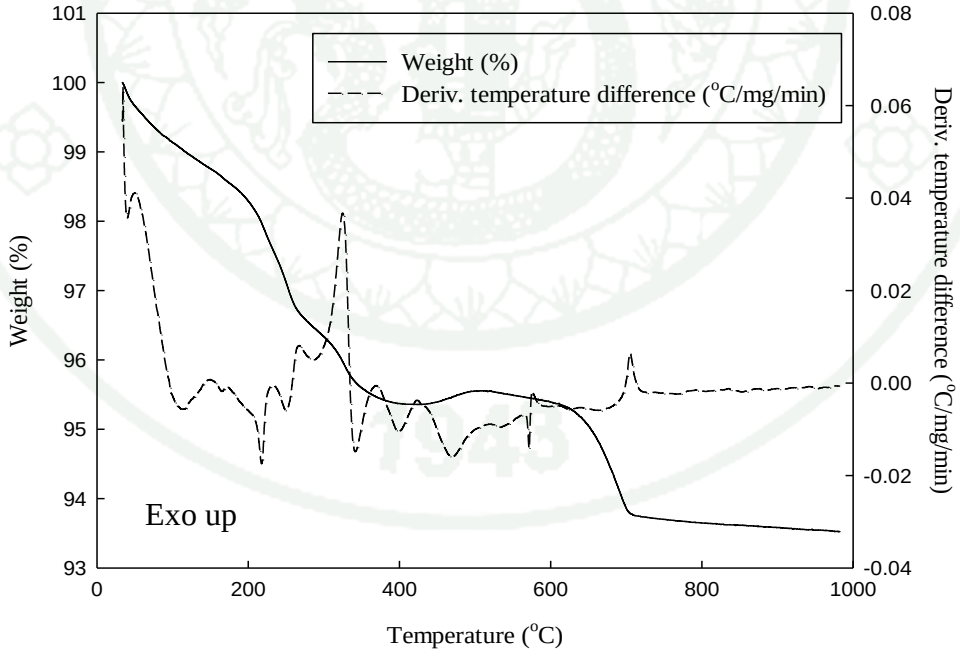

Appendix Figure E8 Thermogram of 15%Ni-5%Co/12C7A-CeO_2-TiO_2 after steam reforming reaction of acetic acid at 850°C, S/C of 8, and 1 h.

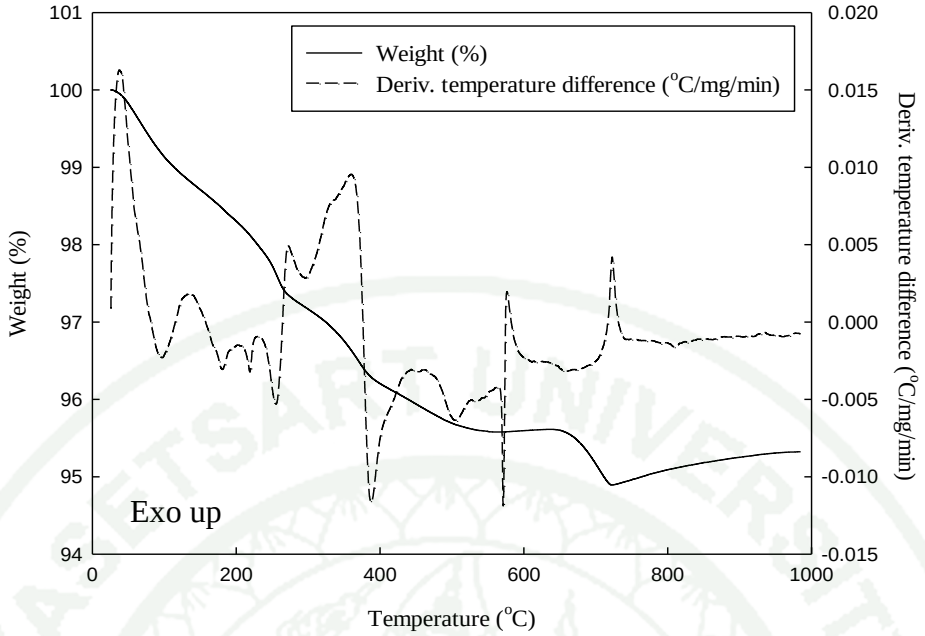

Appendix Figure E9 Thermogram of 15%Ni-5%Cr/12C7A-CeO_2-TiO_2 after steam reforming reaction of acetic acid at 850°C, S/C of 8, and 1 h.

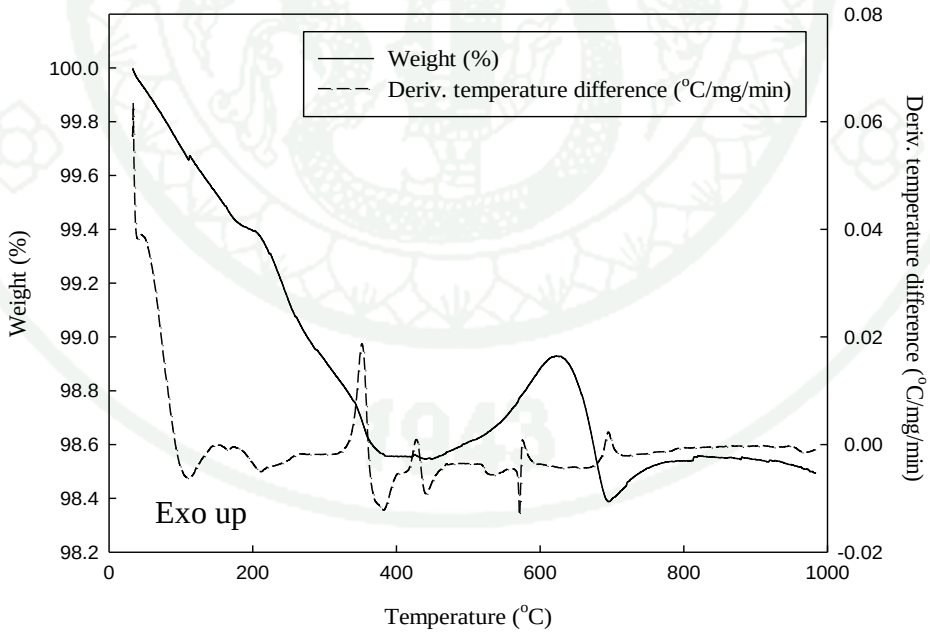

Appendix Figure E10 Thermogram of 15%Ni-5%Mg/12C7A-CeO_2-TiO_2 after steam reforming reaction of acetic acid at 850°C, S/C of 8, and 1 h.

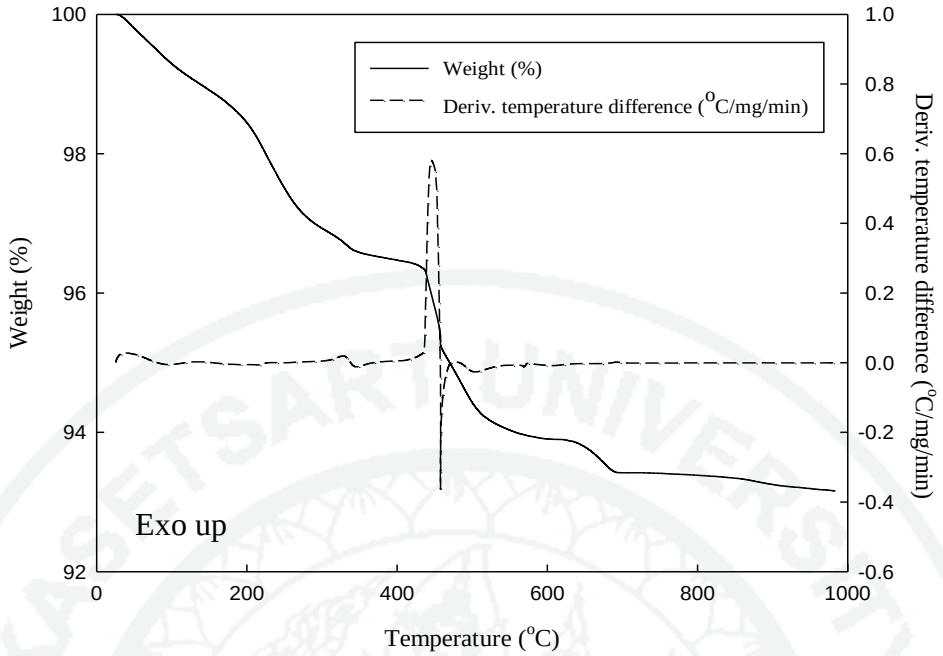

Appendix Figure E11 Thermogram of 15%Ni-5%Cu/12C7A-CeO_2-TiO_2 after steam reforming reaction of acetic acid at 850°C, S/C of 8, and 12 h.

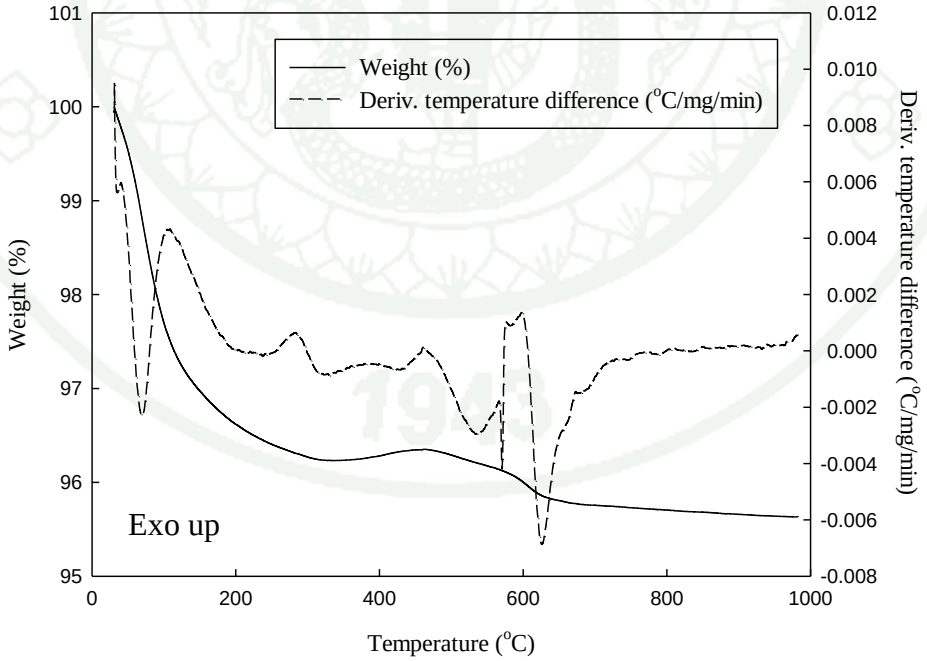

Appendix Figure E12 Thermogram of 15%Ni/Al_2O_3 after steam reforming reaction of acetic acid at 850°C, S/C of 8, and 1 h.

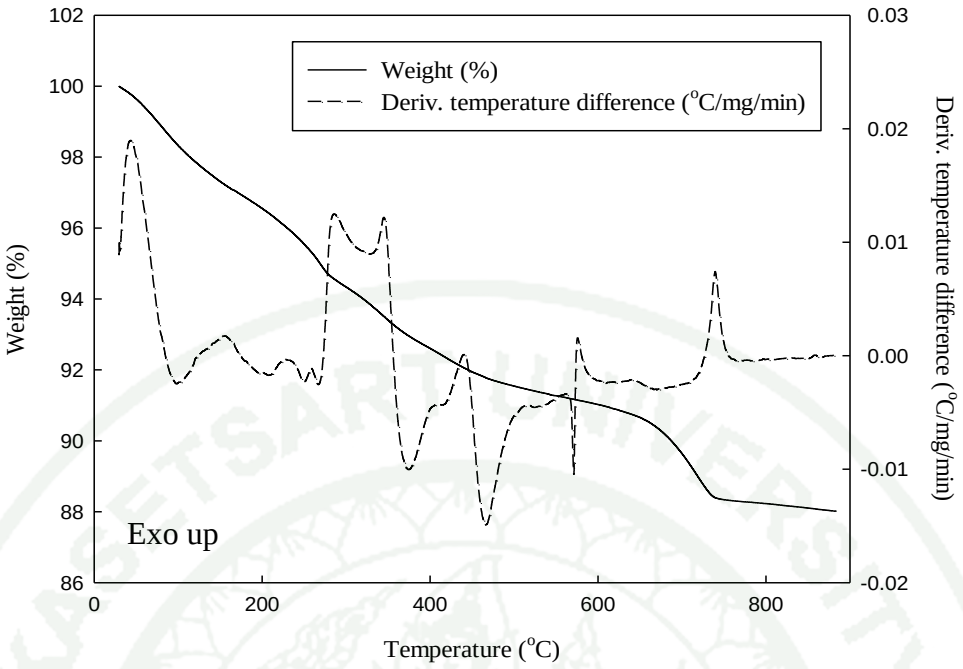

Appendix Figure E13 Thermogram of 15%Ni/12C7A-CeO_2-TiO_2 after steam reforming reaction of acetone at 850°C, S/C of 8, and 1 h.

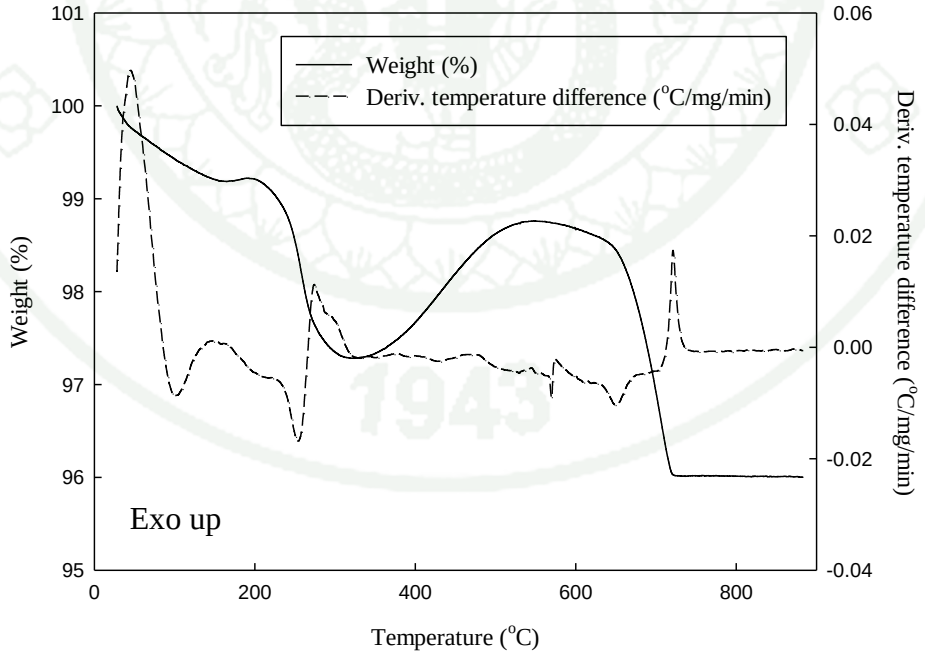

Appendix Figure E14 Thermogram of 15%Ni-5%Cu/12C7A-CeO_2-TiO_2 after steam reforming reaction of acetone at 850°C, S/C of 8, and 1 h.

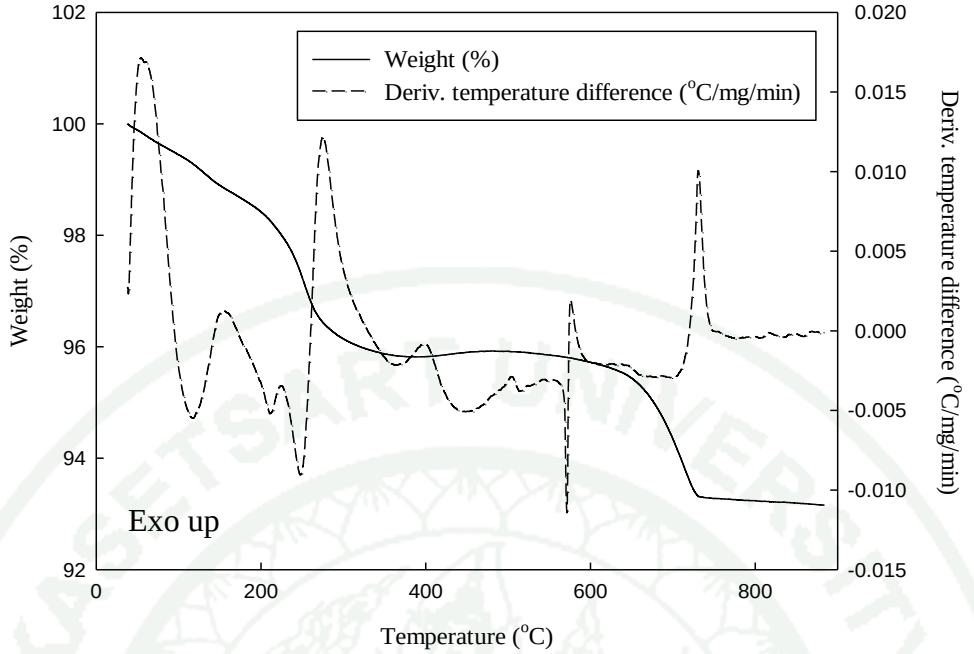

Appendix Figure E15 Thermogram of 15%Ni-5%Co/12C7A-CeO_2-TiO_2 after steam reforming reaction of acetone at 850°C, S/C of 8, and 1 h.

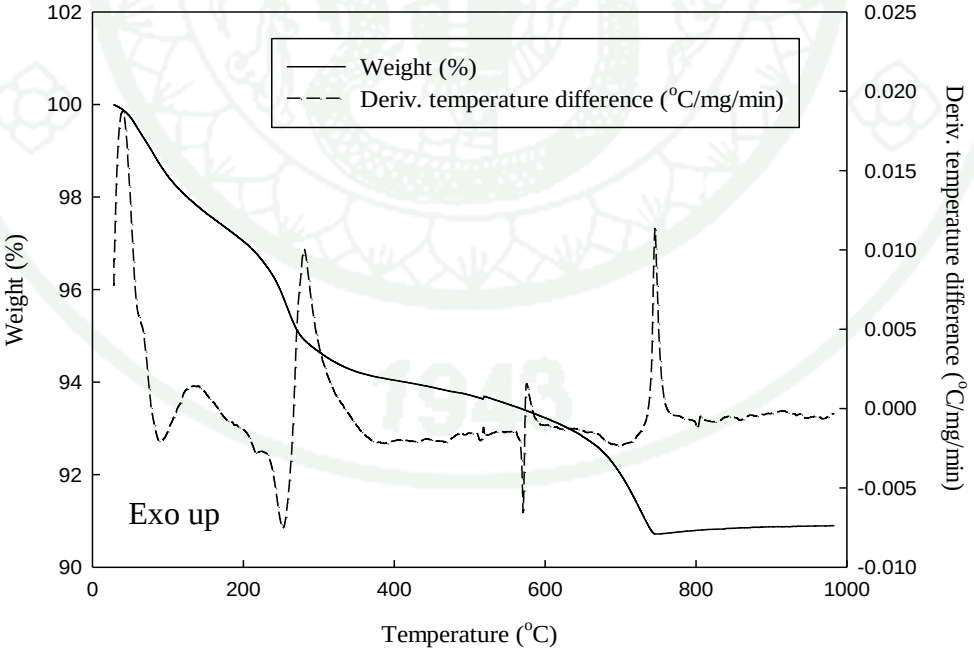

Appendix Figure E16 Thermogram of 15%Ni-5%Cr/12C7A-CeO_2-TiO_2 after steam reforming reaction of acetone at 850°C, S/C of 8, and 1 h.

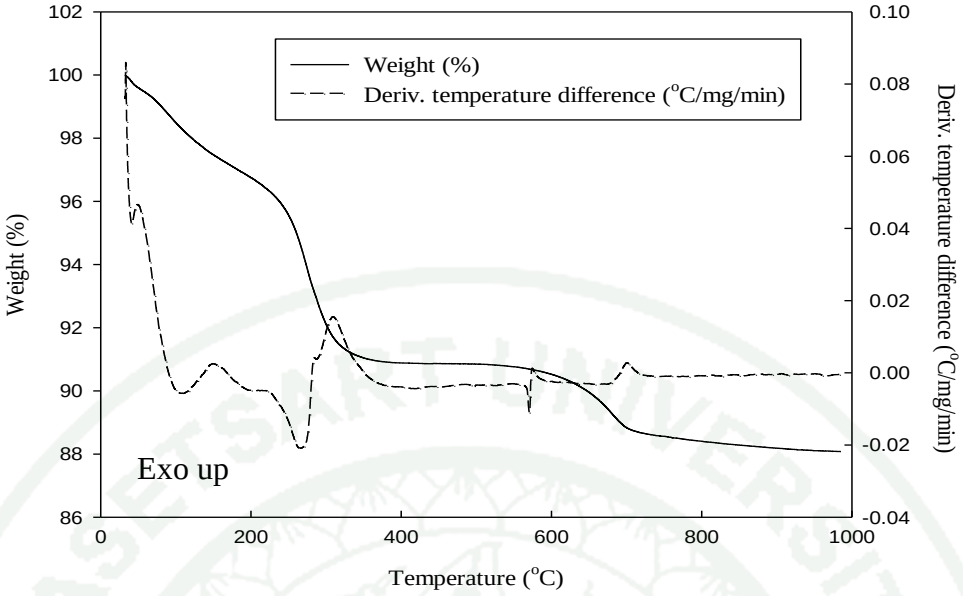

Appendix Figure E17 Thermogram of 15%Ni-5%Mg/12C7A-CeO_2-TiO_2 after steam reforming reaction of acetone at 850°C, S/C of 8, and 1 h.

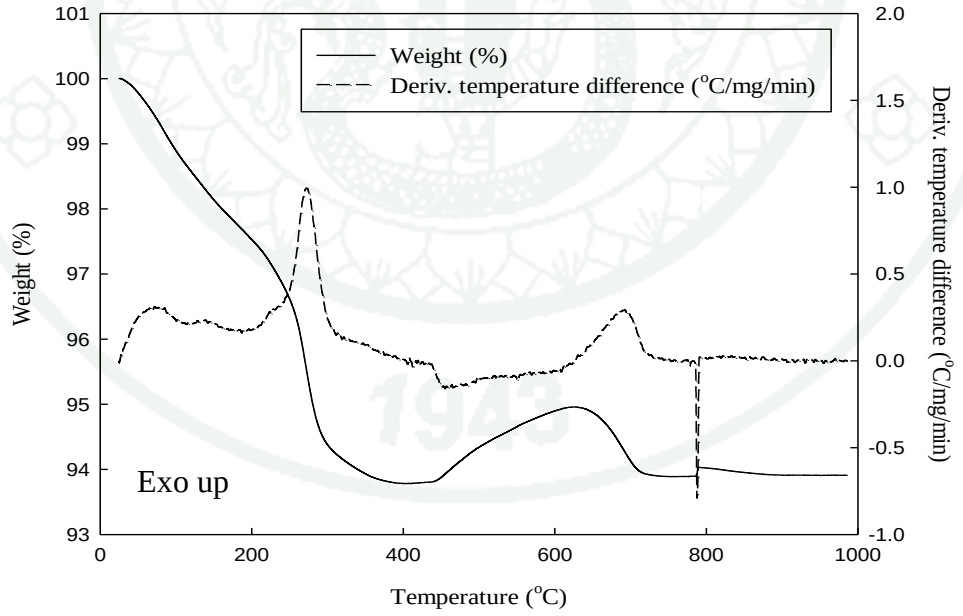

Appendix Figure E17 Thermogram of 15%Ni-5%Cu/12C7A-CeO_2-TiO_2 after steam reforming reaction of bio-oil's aqueous phase at 850°C, S/C of 8, and 1 h.

Appendix Table E1 The supporting materials affect on coke formation during steam reforming of acetic acid at 850°C, S/C of 8, and 1 h.

Catalysts	Coke formation rate ($mg_C/g_{Cat.}/h$)
12C7A	130.9
12C7A-CeO_2	87.25
12C7A-TiO_2	30.90
12C7A-CeO_2-TiO_2 (2:1:1)	41.58
12C7A-CeO_2-TiO_2 (1:1:1)	62.11

Appendix Table E2 Coke formation during steam reforming of acetic acid at 850°C, S/C of 8, and 1 h.

Catalysts	Coke formation rate ($mg_C/g_{Cat.}/h$)
15%Ni/12C7A-CeO_2-TiO_2	63.48
15%Ni/Al_2O_3	5.019
15%Ni-5%Cu/12C7A-CeO_2-TiO_2	30.90
15%Ni-5%Cr/12C7A-CeO_2-TiO_2	15.53
15%Ni-5%Co/12C7A-CeO_2-TiO_2	53.64
15%Ni-5%Mg/12C7A-CeO_2-TiO_2	14.44

Appendix Table E3 Coke formation during steam reforming of acetone at 850°C, S/C of 8, and 1 h.

Catalysts	Coke formation rate ($mg_C/g_{Cat.}/h$)
15%Ni/12C7A-CeO_2-TiO_2	51.92
15%Ni-5%Cu/12C7A-CeO_2-TiO_2	19.32
15%Ni-5%Cr/12C7A-CeO_2-TiO_2	41.46
15%Ni-5%Co/12C7A-CeO_2-TiO_2	27.16
15%Ni-5%Mg/12C7A-CeO_2-TiO_2	41.04

Appendix F

Chemical compositions of the aqueous phase of bio-oil from pyrolysis process of coffee bean residue characterized by GC-MS technique

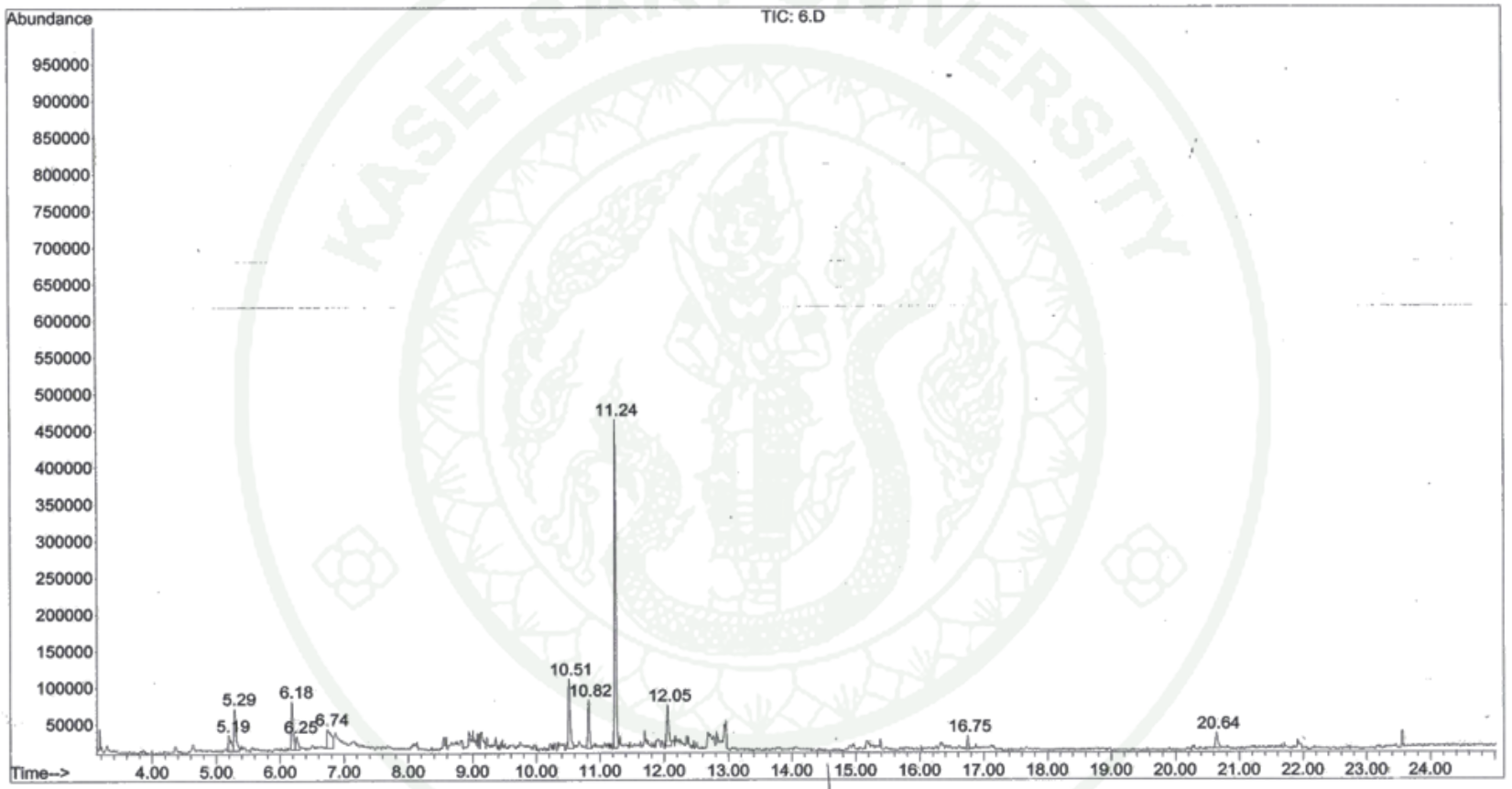

Appendix Figure F1 Chromatogram obtained from GC-MS technique of the aqueous phase of bio-oil

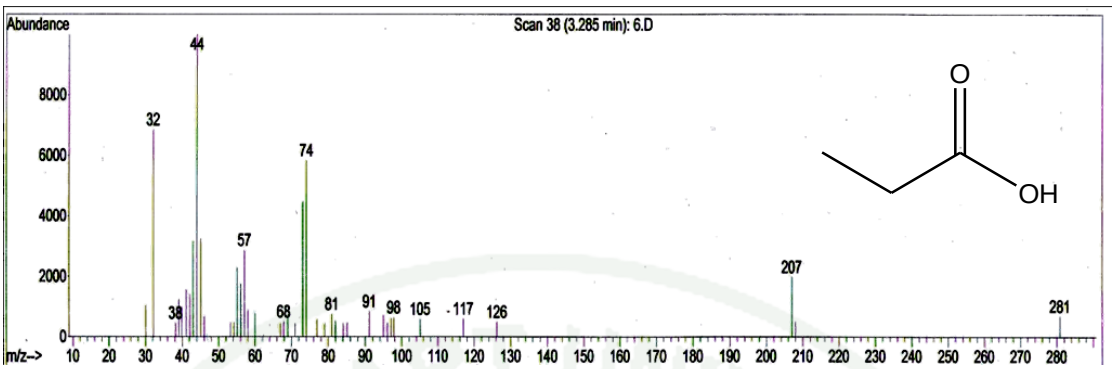

Appendix Figure F2 Mass spectrum of propanoic acid at retention time of 3.285 min.

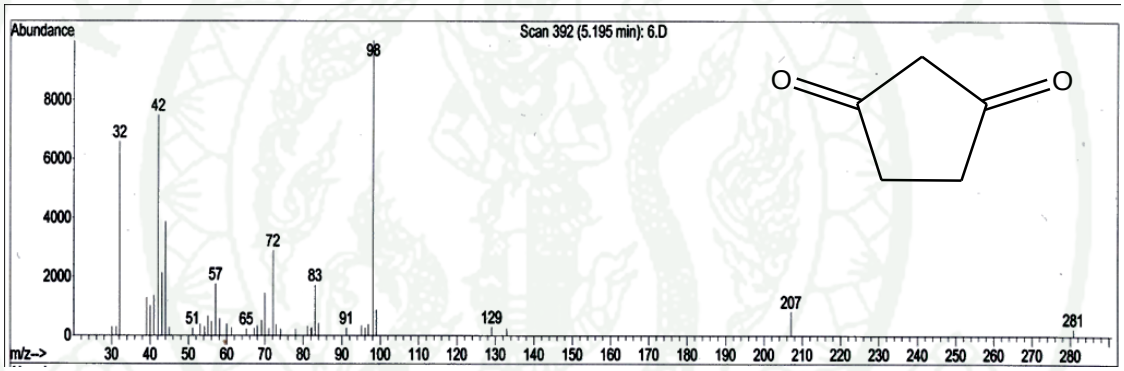

Appendix Figure F3 Mass spectrum of 1,3-Cyclopentanedione at retention time of 5.195 min.

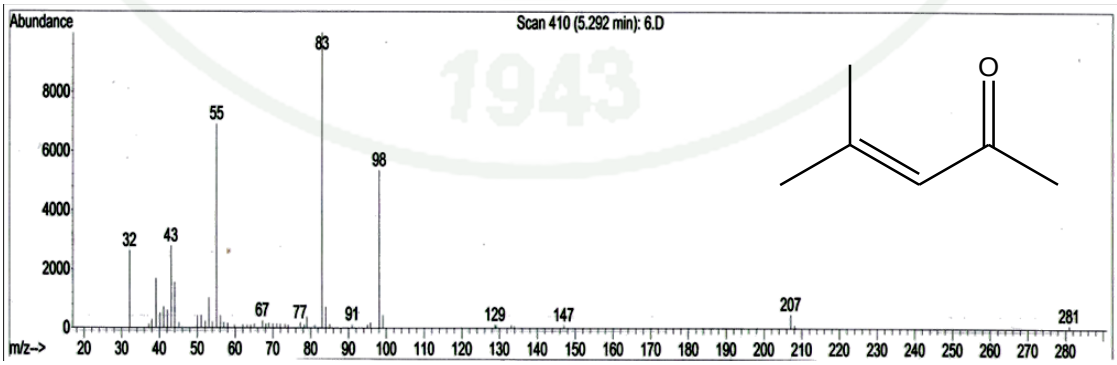

Appendix Figure F4 Mass spectrum of 3-Penten-2-one, 4-methyl- at retention time of 5.292 min.

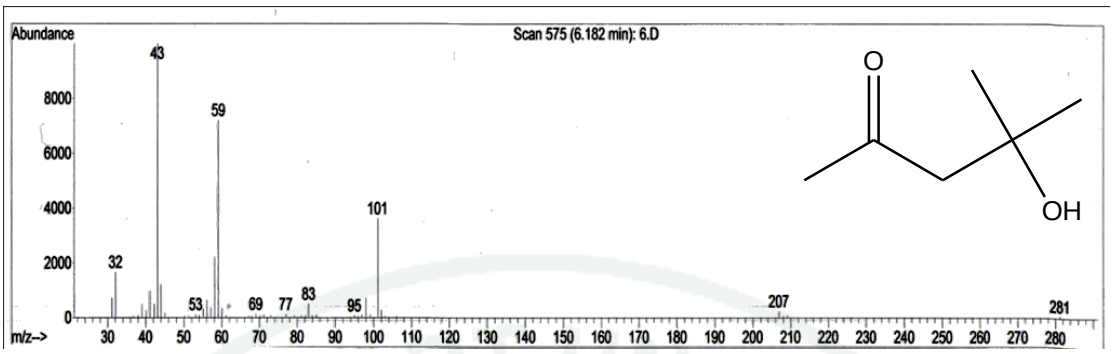

Appendix Figure F5 Mass spectrum of 2-Pentanone, 4-hydroxy-4-methyl- at retention time of 6.182 min.

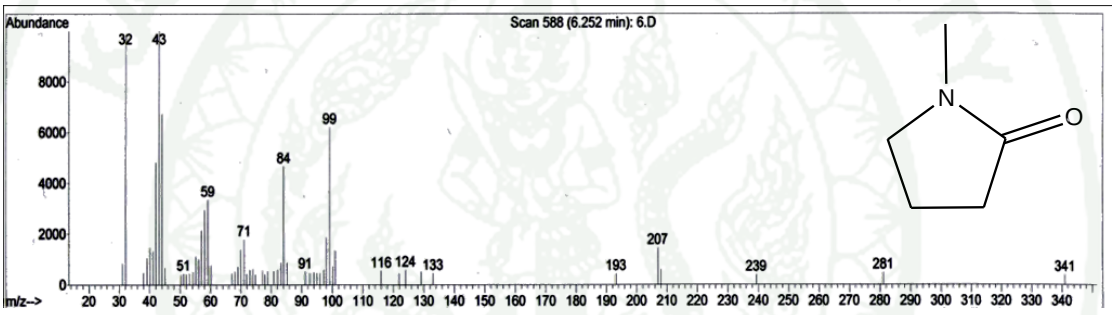

Appendix Figure F6 Mass spectrum of 2-Pyrrolidinone,1-methyl- at retention time of 6.252 min.

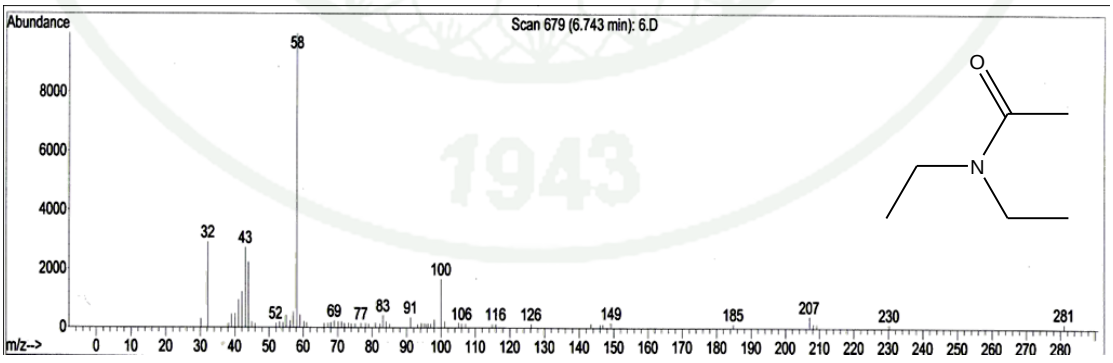

Appendix Figure F7 Mass spectrum of N,N-Diethylacetamide at retention time of 6.743 min.

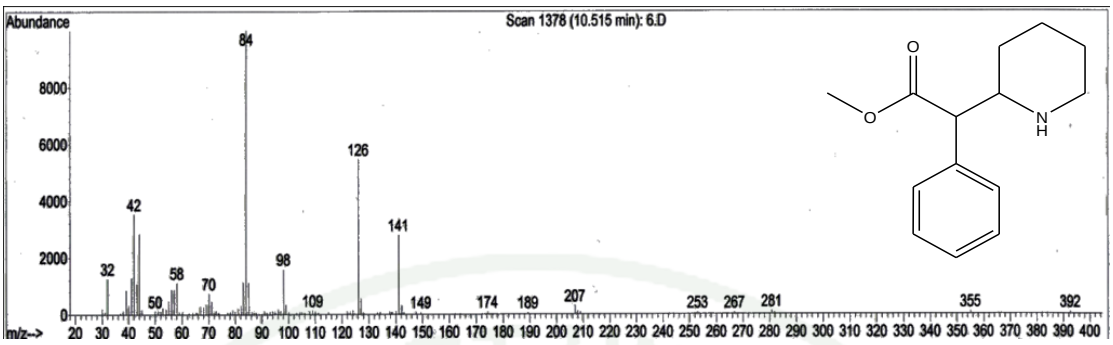

Appendix Figure F8 Mass spectrum of methyl 2-phenyl-2-(piperidin-2-yl)acetate at retention time of 10.515 min.

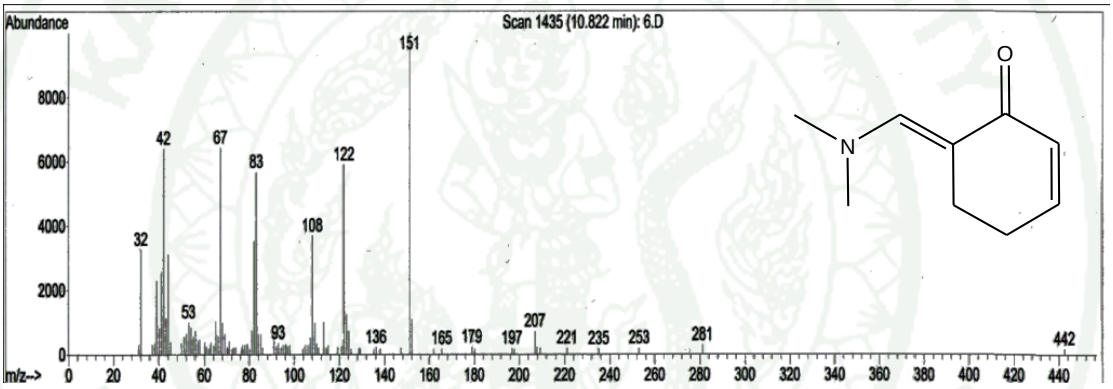

Appendix Figure F9 Mass spectrum of 2-Cyclohexen-1-one, 6-[(dimethylamino) methylene]- at retention time of 10.822 min.

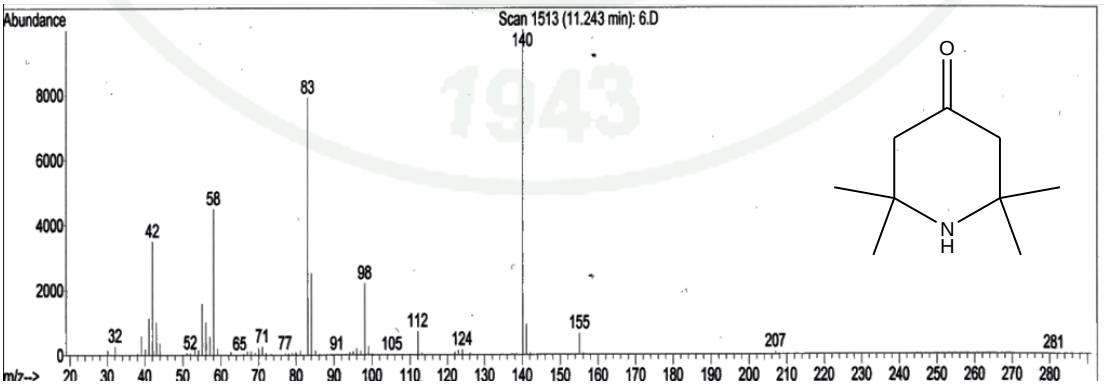

Appendix Figure F10 Mass spectrum of 4-piperidinone, 2, 2, 6, 6-tetramethyl- at retention time of 11.243 min.

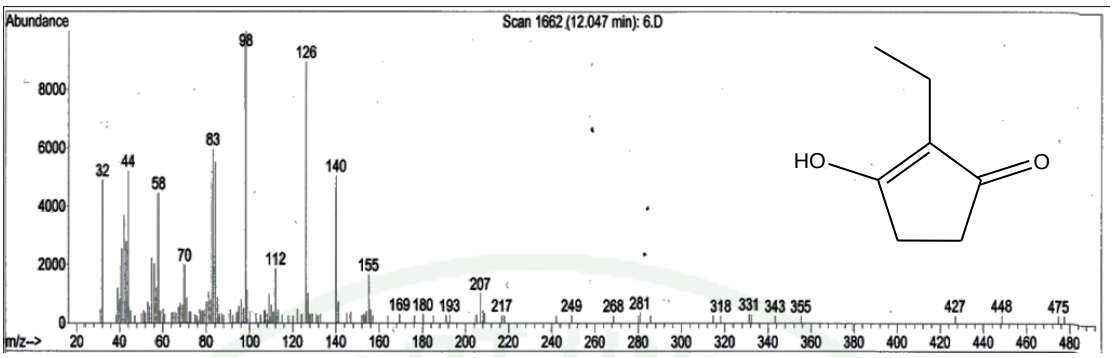

Appendix Figure F11 Mass spectrum of ethylcyclopentenolone at retention time of 12.047 min.

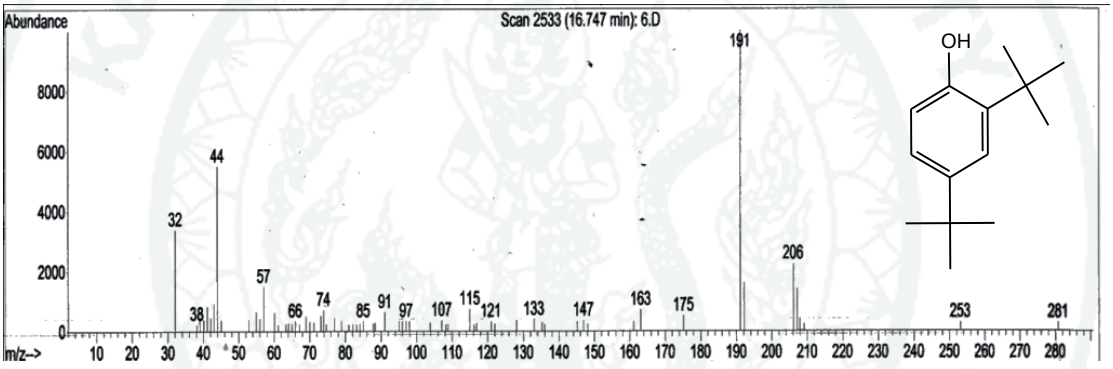

Appendix Figure F12 Mass spectrum of phenol,2,4-bis(1,1-dimethylethyl)-at retention time of 16.747 min.

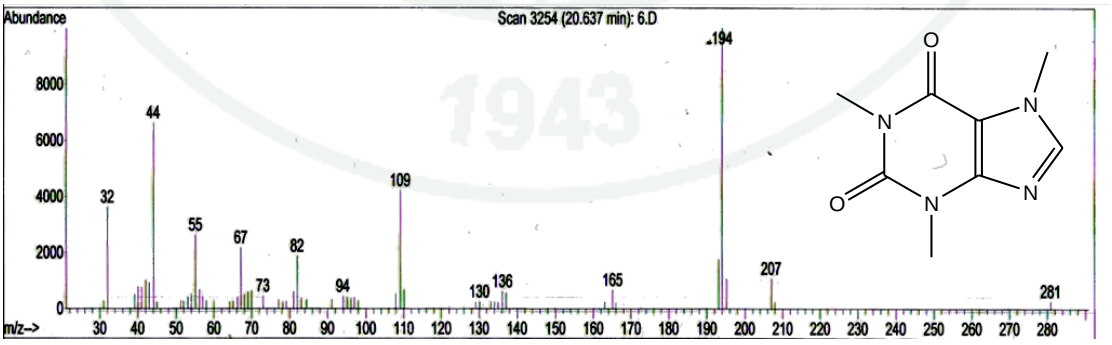

Appendix Figure F13 Mass spectrum of caffeine at retention time of 20.637 min.

CIRRICULUM VITAE

NAME : Mr. Phusit Saechia

BIRTH DATE : November 6, 1985

BIRTH PLACE : Bangkok, Thailand

EDUCATION :

YEAR	**INSTITUTE**	**DEGREE/DIPLOMA**
2007	Kasetsart Univ.	B.S. (Chemistry)

POSITION/TITLE : -

WORK PLACE : -

SCHOLARSHIP/AWARD : -